6 Chapter 6: Development, optimization, and characterization of fourth-generation ternary solid dispersion of standardized *Piper longum* fruit extract for melanoma therapy

6.1 Background

The study aimed to enhance the solubility, dissolution, and oral bioavailability of standardized PLFEE via fourth-generation ternary solid dispersion (SD) for melanoma therapy. With the use of the solvent evaporation method, the standardized PLFEE was formulated into SD, optimized using Box-Wilson's Central Composite Design (CCD) via Design-Expert® software. Multiple preliminary SD formulations were prepared as per the suggestion of software, and the saturation solubility was estimated by the validated HPLC method. The response surface methodology (RSM) and optimization tools were implemented to achieve highly efficient formulation with high saturation solubility. The software-suggested optimized formulation was prepared (n = 5), and the experimental outcome (saturation solubility) was verified to validate the predictability of the software. The optimized SD was characterized for percentage yield, drug content, content uniformity, moisture content, micromeritics properties (density, flow property), surface morphology (high resolution scanning electron microscopy (HRSEM)), crystallinity (X-ray diffraction (XRD) and polarization microscopy (PLM)), thermal behavior (differential scanning calorimetry (DSC) and thermogravimetric analysis (TGA)), drug-excipient compatibility (Attenuated total reflectance-Fourier transform infrared spectroscopy (ATR-FTIR) and High-Performance Thin Layer Chromatography (HPTLC)), *in-vitro* dissolution, stability (long term and accelerated), *in-vitro* cytotoxicity, *in-vitro* cell migration, *in-vivo* oral bioavailability, and *in-vitro* & *in-vivo* anticancer activity against melanoma (B16F10) bearing C57BL/6 mice.

6.2 Objectives

- Development of fourth-generation ternary SD of standardized PLFEE via solvent evaporation method, response surface analysis, and optimization using Central Composite Design (CCD) of Design-Expert® software.
- Pharmaceutical characterizations and stability study of optimized SD
- *In-vitro* anticancer activity and cellular migration studies
- *In-vivo* oral bioavailability study
- *In-vivo* anticancer activity study in melanoma (B16F10) bearing C57BL/6 mice.

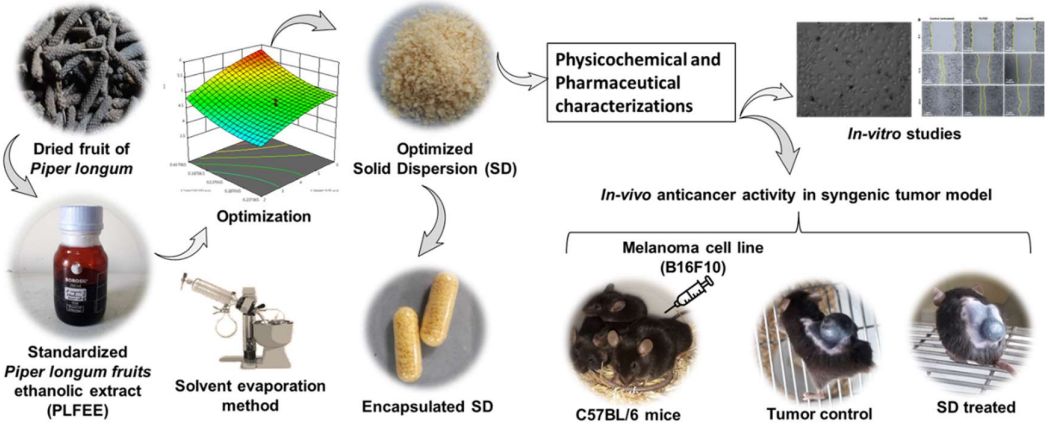

Figure 6. 1 Schematic representation of workflow of chapter 6.

6.3 Methodology

6.3.1 Screening of carrier matrix (CM) by phase solubility experiment

To choose the most suitable CM for SD formulation, the phase solubility of standardized PLFEE (mainly the PIP) was checked in an aqueous solution of different carriers using the protocol described by Higuchi and Connors [84]. Polymers (Kolliphor P 188, Hydroxypropyl cellulose, Poloxamer 407, Soluplus®, PEG-4000, PEG-9000, PVP k30) and surfactants (Gelucire® 44/14, Kolliphor® RH 40, Tween® 20, Tween® 80) were screened. An excess quantity of PLFEE (100 mg) was added to 1.5 mL of the aqueous solution of CM at multiple concentrations (i.e., 2, 4, and 8% w/v) in microcentrifuge tubes and vortexed for 5 min in a vertex mixture (SPINIX™

Vertex shaker, Tarsons Products Pvt. Ltd., Kolkata, India). All tubes were tightly closed, sealed to avoid solvent loss, and shaken for 48 h in a shaking water bath (Hindustan Apparatus Mfg., Mumbai, India) maintained at 37 ± 0.5°C. Then, the samples were centrifuged (Remi CM 12 PLUS, Mumbai, India) at 10,000 rpm for 15 min. The supernatant was filtered through a 0.22 µm syringe filter, diluted suitably with HPLC grade methanol, and the concentrations of PIP were assayed by the validated HPLC method at 342 nm. All phase solubility tests were carried out in triplicate, and the data were presented as the average of three measurements. The Gibbs free energy equation (Equation 6.1) was used to estimate the free energy transfer (ΔG_t°) of PIP from pure water to an aqueous polymeric or surfactant solution as follows [85-87]:

$$\Delta G_t^0 = -2.303RT \log \frac{S_c}{S_0} \qquad (6.1)$$

Where S_c/S_0 is the solubility ratio of PIP with aqueous polymeric or surfactant solution to that of neat water (without any polymer or surfactant). R is the universal gas constant, and T is the absolute temperature in Kelvin.

6.3.2 Formulation of SD

Different SDs of standardized PLFEE were formulated by solvent evaporation method employing a rotary evaporator using Soluplus® and Tween® 80 as CMs. Briefly, a specified amount of PLFEE and CMs were solubilized in 2 mL ethanol and 10 mL of acetone, respectively. For complete solubilization, both solutions were sonicated in an ultrasonic bath (AN-SS-6L, GT SONIC®, at ultrasonic frequency: 40 kH, and power: 150 W) for 10 min. Then, the solutions were mixed in a round bottom flask (100 mL) and sonicated at 25 ± 0.2°C for definite periods (as per the software-suggested formula) for the interaction of extract and CMs at a molecular level. Solvent

evaporation was performed at 70 rpm using a rotary vacuum evaporator equipped with a vacuum pump and water bath at 50°C temperature. The film of SD was scrapped and dried in a vacuum desiccator for 24 h for the removal of residual solvent. The dried formulation was ground gently by a glass mortar and pestle and shifted through sieve # 60 to obtain uniform particle size. The obtained SD was kept in well-closed glass vials and stored in an anhydrous calcium chloride desiccator at room temperature. A physical mixture containing the composition of SD was prepared by simple intensive mixing of a definite quantity of PLFEE and CMs followed by gentle grinding with mortar and pestle until the formation of a homogenous product. Subsequently, the resultant mixture was sieved through mesh # 60 and kept in a well-closed glass container at room temperature for further characterization.

6.3.3 Quality by design (QbD) and optimization

6.3.3.1 Response surface methodology (RSM)

In the present investigation, RSM was used to analyze the influence of critical material attributes (CMA), such as Soluplus® to PLFEE ratio (X_1, w:w), Tween® 80 to PLFEE ratio (X_2, w:w), and critical process parameters (CPP), such as sonication time (X_3, min) on critical quality attributes (CQA), such as saturation solubility of PIP (Y_1) by applying a Quality by design (QbD) based approach using 3-factor, 5 levels rotatable (α value of 1.681) Box-Wilson central composite design (CCD) via a Trial version of Design-Expert® software (Version-12, Stat-Ease Inc., Minneapolis, MN, USA). A total of 20 runs (trial batches), including 6 replications of central points with 8 factorial points (cube points) and 6 axial points (star points), were produced by the software. The results of CQAs of 20 batches were fed into the software and analyzed by the inbuilt analysis of variance (ANOVA) tool to examine model adequacy and significance ($P<0.005$) by comparing certain statistical constraints, such as correlation

coefficient (R^2), model F-value, model p-value, lack of fit F-value, lack of fit p-value, the difference between predicted and adjusted R^2 value, and signal to noise ratio (adequate precision). To envisage the best SD, the statistical model was fitted to linear, two-factor (2F) interactions, quadratic, and cubic models. The software-generated mathematical polynomial equations were used to study multiple factors-response relationships. The interaction effect of the CMAs and CPP on the CQAs was also visualized using 3D response surface graphs and corresponding 2D contour plots. The factor-responses relationship was estimated using a statistical polynomial Equation 6.2 [88, 89].

$$Y = b_0 + b_1X_1 + b_2X_2 + b_3X_3 + b_{11}X_1^2 + b_{22}X_2^2 + b_{33}X_3^2 + b_{12}X_1X_2 + b_{23}X_2X_3 + b_{13}X_1X_3 \quad (6.2)$$

where, Y is the response or dependent variable, X_1, X_2, and X_3 three different factors (independent variables), b_0 is Y intercept (a constant), and b_1, b_2, and b_3 are the linear or first order coefficients for the factor X_1, X_2 & X_3 respectively. The terms b_{11}, b_{22}, and b_{33} are the quadratic or second-order coefficients of squared terms, such as $X_1^{\ 2}$, $X_2^{\ 2}$, and $X_3^{\ 2}$. The interactive polynomial coefficients b_{12}, b_{23} & b_{13} are associated with the interaction of multiple factors (X_1X_2, X_2X_3, and X_1X_3) during simultaneous analysis.

6.3.3.2 Optimization

Optimum CMAs and CPP required for the formulation of desired SD were acquired by numerical and graphical optimization techniques available in the software based on a set constrained condition of enhancing the saturation solubility of PIP (Y_1).

6.3.3.3 Check point analysis (validation of method)

The predictability/validity of the rotatable CCD model was verified by formulating a checkpoint batch (n = 5) of optimized formula under optimum circumstances as suggested by Design-Expert software and evaluating the corresponding CQAs (saturation solubility). Quantitative assessment between the software-based theoretical prediction and obtained experimental results was done by estimating the percentage prediction error (% Bias) by Equation 6.3 [87, 89, 90].

$$\%\ prediction\ error = \frac{Experimental\ value - predicted\ value}{Predicted\ value} \times 100 \qquad (6.3)$$

6.3.4 Characterizations of optimized SD

6.3.4.1 Saturation solubility

The saturation solubility test was performed to evaluate the increase in the aqueous solubility of PIP in the formulated SD. Briefly, a surplus amount of standardized PLFEE (100 mg) and each SD (containing 100 mg standardized PLFEE) was mixed with 1.5 mL of water in a volumetric flask (10 mL). Samples were placed in triplicate on a thermostatically controlled oscillating water bath at 37 ± 0.5°C for 48 h. Then, the samples were centrifuged at 10,000 rpm for 15 min, filtered through a 0.22 µm syringe filter, appropriately diluted with HPLC grade methanol, and investigated by the developed HPLC method at 342 nm. The results of saturation solubility were used for formulation optimization. Further, all the characterizations were done for optimized SD.

6.3.4.2 Drug content and content uniformity

The optimized SD equivalent to 100 mg of PLFEE was mixed with 10 mL of ethanol in a volumetric flask and sonicated for 10 min for complete solubilization. The

solubilized sample was centrifuged (10,000 rpm for 15 min) and filtered (0.45 μm PVDF membrane filter). After suitable dilution, the drug content for PIP was estimated by HPLC. The % PIP content in the optimized SD was compared with that of an equivalent quantity of standardized PLFEE, considering its PIP content as 100%. The content uniformity was estimated by sampling from three different locations of optimized SD powder and estimating the variation in the PIP content. Each sample was analyzed in triplicate, and the average was reported.

6.3.4.3 Percentage Yield

The yield of optimized SD was evaluated to ascertain the efficiency of the solvent evaporation technique by comparing the mass of optimized SD obtained to that of the initial weight of both standardized PLFEE and CMs using Equation 6.4. The experiment was repeated in triplicate, and the average was reported.

$$\%\, Yield = \frac{Weight\ of\ prepared\ SD}{Weight\ of\ PLFEE+CM} \times 100 \qquad (6.4)$$

6.3.4.4 Micromeritics Property

Micromeritic properties, like tapped density, bulk density, Carr's index, angle of repose, and Hausner's ratio, were investigated for the optimized SD [91, 92]. Each of the experiments was carried out in triplicate, and the average was reported.

6.3.4.4.1 Angle of repose (Θ)

A precisely weighed amount of SD was taken in a funnel and permitted to flow through it freely onto a flat surface to form a cone-shaped granular pile. The θ was estimated using Equation 6.5.

$$Angle\ of\ repose\ (\theta) = tan^{-1}\frac{h}{r} \qquad (6.5)$$

Where h is the height of the cone and r is the radius of the cone base

6.3.4.4.2 Carr's compressibility index (CI) and Hausner ratio (HR)

A definite quantity of optimized SD was kept in a measuring cylinder of a digital tapped density apparatus (IKON Instruments, Delhi, India) to estimate tapped density. The cylinder was allowed to tap, and the volume was noted at intervals of 10 taps. The tapped volume was considered when there was no alteration in volume after 3 consecutive readings. The bulk density was estimated by dividing the weight (g) by the bulk volume or volume without tapping (mL). The CI was calculated by using Equation 6.6.

$$CI = \frac{Tapped\ Density - Bulk\ Density}{Tapped\ Density} \times 100 \quad (6.6)$$

The HR was calculated using Equation 6.7.

$$Hausner\ ratio\ (HR) = \frac{Tapped\ Density}{Bulk\ Density} \quad (6.7)$$

6.3.4.5 X-ray diffraction (XRD)

The crystallinity of PLFEE, CMs, physical mixture (PM), and optimized SD were analyzed by a powder X-ray diffractometer (Rigaku Miniflex 600 Desktop System; Tokyo, Japan) using Ni-filtered Cu Kα radiation (λ = 1.5406 A°) at 40 kV voltage and 15 mA current. The diffraction pattern was recorded using MiniFlex Guidance software (Version 2.0.2.1) over a range of 2 Theta from 10° to 70° with a step size of 0.02°/step at a scan speed of 7°/min at 25°C. Since Tween® 80 is viscus in nature, the drop cast technique was used to examine its XRD diffraction pattern by making a thin film on a glass plate via dropping and drying at 40°C.

6.3.4.6 Differential scanning calorimetry (DSC)

Thermal analysis of PLFEE, CMs, PM, and optimized SD was executed using DSC equipment (DSC 60 Plus, Shimadzu, Japan) furnished with TA-60WS Collection

software (Version 2.21). Approximately 5 mg of each sample was kept in a pierced aluminum pan and placed in the thermal chamber. The study was performed from 20 to 300°C at a linear heating rate of 10°C/min in a nitrogen atmosphere at a flow rate of 100 mL/min. An empty pan was treated as the blank and the instrument was calibrated with indium having a melting point of 156.6°C.

6.3.4.7 Thermogravimetric analysis (TGA)

TGA analysis of PLFEE, CMs, PM, and the optimized SD was carried out using TGA apparatus (Shimadzu TGA-50 analyzer, Shimadzu, Japan) equipped with TA-60WS Collection software (Version 2.21). The analysis was conducted under a nitrogen atmosphere (flow rate of 100 mL/min) by linearly heating the samples (~7-10 mg) in a platinum pan from 10 to 800°C at a heating rate of 10°C/min.

6.3.4.8 Attenuated total reflectance-Fourier transform infrared spectroscopy (ATR-FTIR)

Infrared analysis of PLFEE, CMs, PM, and optimized SD was performed to predict the possible interaction between PLFEE and CMs using an ATR-FTIR spectrophotometer (Bruker Alpha II, Bruker Optics, Ettlingen, Germany). Data were acquired using OPUS software (OPUS software version 7.0). Each spectrum was recorded from 4000 to 400 cm^{-1} with 4 cm^{-1} spectral resolution and 40 spectral scans.

6.3.4.9 High-Performance Thin Layer Chromatography (HPTLC)

The compatibility of PLFEE with the formulation excipients was further verified by HPTLC analysis. The integrity of PIP and PLGN in the PLFEE, PM, and SD was investigated by qualitative fingerprinting analysis with the HPTLC instrument (CAMAG, Switzerland) equipped with WinCATS software (Version: 1.4.7.2018). Analysis was carried out on 20 × 10 cm silica gel 60 F254 precoated aluminum plates (E. Merck, Darmstadt, Germany). The pure PIP, PLGN, PLFEE, PM, and optimized

SD formulations were dissolved in ethanol centrifuged, and the supernatant was collected for HPTLC analysis. Accurately, 5 µL of each sample was applied (dosage speed was 100 nL/sec) in triplicate with a bandwidth of 8 mm by Linomat V sample applicator (CAMAG, Switzerland) fitted with 100 µL CAMAG syringe at an initial distance of 15 mm from the left side and 8 mm from the bottom of the pre-coated aluminum plate. Out of various reported mobile phase systems, toluene: ethyl acetate (6:4 v/v) was selected due to its better band resolving capacity and higher resolution. After sample application, the plate was developed in a pre-saturated twin trough glass chamber (CAMAG, 20 x 10 cm) up to 90 mm distance using 20 mL of the mobile phase. The developed plate was dried by hair drier (Philips, India), the slit dimension was positioned at 6.00 × 0.45 mm micro and scanned by HPTLC scanner (CAMAG TLC Scanner IV) at a scanning speed of 20 mm/sec at 340 and 342 nm. The retardation factor (R_f) values of the bands of the samples and pure phytoconstituents were compared to determine the drug-excipient compatibility [93]. The fingerprint of the developed plate was observed in CAMAG TLC Visualizer 2, and photographs were captured by the embedded charge-coupled device (CCD) camera (SONY, Super HAD, HDR).

6.3.4.10 Contact angle

Contact angle (θ) of PLFEE and optimized SD was measured via image analysis method utilizing sessile-drop goniometry with the help of a calibrated drop shape analyzer (DSA25S, KRÜSS GmbH, Hamburg, Germany) equipped with a digital camera (ALLIED Vision Technologies, Stadtroda, Germany) and KRUSS advance software (1.6.2.0). The equipment was calibrated (object size 0.5 mm and magnification factor 141.2 Px/mm) before the measurements and analysis were performed at 20° C. The thin dried films of samples were prepared by spreading the

PLFEE or SD methanolic solution (0.5 g/mL) uniformly on microscope slides in an area of 4 cm^2 and allowing the solvent to evaporate in a vacuum oven at 40°C to produce a uniform film. Water was loaded in 1 mL of a disposable syringe, and 2 µL was dropped at a rate of 2.666 µL/sec on the plain film of PLFEE or optimized SD on a microscope slide. The digital images of the drop were captured by a camera, and the image of the water drop was processed by KRUSS advance software to obtain the contact angle. A least of 10 images were captured to obtain the left contact angle (θ_L), right contact angle (θ_R), and mean contact angle (θ_M). The experiment was carried out in triplicate, and the average was reported.

6.3.4.11 High-resolution scanning electron microscopy (HRSEM)

Representative HRSEM photomicrographs of PLFEE, CMs, PM, and optimized SD were captured using a high-resolution scanning electron microscope (FEI Nova™ Nano SEM 450, FEI, USA) equipped with Everhart–Thornley detector (ETD) and xT Microscope control software (version 1.0) at a voltage of 15 kV. Further, to study the crystal property, samples (PIP, PLFEE, and SD) were solubilized in methanol, dropped on a glass slide, dried overnight, and the produced films were subjected to HRSEM analysis. The samples were prepared by mounting on aluminum stubs using double-sided carbon tape followed by sputter coating by a desk sputter coater (DSR 1, Nanostructured Coating Co., Iran) with gold and palladium (at a ratio of 60:40 w/w) for 120 sec.

6.3.4.12 Polarized Light Microscopy (PLM)

PLM of PLFEE, CMs, PM, and the optimized SD was performed at 10X magnification using a polarizing microscope (Radical RXLr-5, New Delhi, India) equipped with a digital camera (5 MP, Microscopic Procam Camera) and Radical ProCam software (version 3.7) under the crossed polarizer analyzer arrangement at room temperature.

Samples were sprinkled on a microscopic glass slide and examined at various angles by rotating the analyzer slider fitted at the top.

6.3.4.13 Moisture content analysis

The moisture content of the optimized SD was evaluated by a moisture analyzer (AXIS, Poland) at 70°C using a halogen radiator for a short duration (30 s). The moisture content was determined in triplicate, and the average was reported.

6.3.4.14 *In-vitro* dissolution and release kinetics

In-vitro dissolution was performed using a USP Type-I dissolution apparatus (Electrolab Trust-E08, Mumbai, India), at 37 ± 0.5°C with basket rotation of 100 rpm, using 900 mL of 0.1 N HCl (pH: 1.2) as dissolution media. Accurately 50 mg standardized PLFEE (equivalent to 18.85 mg of PIP), an equivalent amount of PM, and optimized SD were encapsulated in empty hard gelatin capsules (Size 00) and used for dissolution study. At predetermined time intervals (i.e., 0.083, 0.25, 0.5, 0.75, 1, 1.5, 2, 2.5, 3, 4, 5, 6, 8, 10, 12, 14, 16, 18, 20, 22, and 24 h), 2 mL of aliquots of medium were withdrawn and replenished with an equal volume of fresh media for maintaining sink condition. The withdrawn samples were centrifuged (10,000 rpm for 15 min) and filtered (0.45 µm PVDF membrane filter), re-extracted to HPLC grade methanol, and quantified for PIP content by the validated HPLC method. The analysis was executed in triplicate, and the average cumulative % of drugs released was plotted against time to study the pattern of release.

The mathematical model-dependent method was utilized to know the release kinetics of PIP from the optimized SD. The data of *in-vitro* dissolution were fitted to different kinetic models (first-order, zero-order, Korsmeyer-Peppas, Hixson-Crowell cube-root model, and Higuchi model) by using regression analysis to evaluate the release

kinetics of PIP. The linear regression analysis was carried out, and the coefficient of correlation (R^2) in each case was determined [94]. Furthermore, to understand the mechanism of PIP release from the SD, the first 60% of the release data were fitted to the Korsmeyer-Peppas model. The following models are considered for release kinetic analysis (Equation 6.8-6.12).

$$\textit{Zero-order kinetics}, C_0 - C_t = K_0 t \quad (6.8)$$

Where C_0 is the initial drug concentration at zero time (t = 0), C_t is the quantity of drug released at time t, and K_0 is the zero-order release constant.

$$\textit{First-order kinetics}, LogC = LogC_0 - \frac{K_1 t}{2.303} \quad (6.9)$$

Where C is the percent of drug remaining at time t, C_0 is the initial concentration of the drug, and K_1 is the first-order rate constant.

$$\textit{Higuchi}, Q = K_H t^{1/2} \quad (6.10)$$

Where Q is the amount of drug released in time t, and K_H is the Higuchi dissolution constant.

$$\textit{Korsmeyer-Peppas}, \frac{M_t}{M_\infty} = k_{kp} t^n \quad (6.11)$$

Where M_t is the amount of drug released in time t, M_∞ is the amount of drug released after time ∞, M_t / M_∞ is the fraction of drug released at time t, k_{kp} is the Korsmeyer release rate constant, and n is the drug release exponent or diffusional exponent.

$$\textit{Hixson-crowel}, \sqrt[3]{W_0} - \sqrt[3]{W_t} = K_{HC} t \quad (6.12)$$

Where W_0 is the quantity of drug remaining at time 0 (initial quantity of the drug), W_t is the quantity of drug remaining to be released at time t, and K_{HC} is the Hixson-Crowell rate constant.

6.3.4.15 Hydrodynamic particle size, size distribution, and zeta potential of the optimized SD in dissolution media

The hydrodynamic size (Z_{avg}), polydispersity index (PDI), and zeta potential (ζ) were estimated to investigate the size, homogeneity, and electrokinetic potential of the particles produced during the dissolution of SD in dissolution media (pH 1.2). During the dissolution study, 500 µL of aliquot was withdrawn from the dissolution vessel after 1 h, diluted 10 times with HPLC grade water, and filtered through a 0.2 µm syringe filter. The Z_{avg}, PDI, and ζ were measured by dynamic light scattering (DLS) [95] using a particle size analyzer (Zetasizer Pro, Malvern Panalytical Ltd., UK) equipped with ZS Xplorer software (version 2.3.1). The Z_{avg} and PDI were measured at 25°C with a refractive index of 1.333 using a DTS 0012 polystyrene disposable cuvette at a backscatter angle of 173°, whereas the zeta potential was evaluated using a ZEN1002 universal dip cell having palladium electrodes with 2 mm spacing. The experiments were carried out in triplicate, and the average was reported.

6.3.4.16 High-Resolution Transmission Electron Microscopy (HRTEM) and selected area electron diffraction (SAED) analysis

The HRTEM and SAED analysis of the dissolution sample was carried out to investigate their particulate morphology and crystallinity. The analysis was performed using a high-resolution transmission electron microscope (FEI, TECNAI G2 F20 TWIN, USA) equipped with a high-angle annular dark field (HAADF) detector and Gatan's Digital Micrograph software (version 3.7.4) at 200 kV using a carbon-coated copper grid (400 Mesh, 3.05 mm diameter, Ted Pella). The aliquot from dissolution was diluted two times with HPLC grade water, filtered through a 0.2 µm syringe filter,

and 20 µL was dropped onto the TEM grid and dried overnight at room temperature. The TEM photomicrographs were analyzed using ImageJ software (National Institutes of Health (NIH), Bethesda, Maryland), version 1.53e, Java 1.8.0_172), and the average size was calculated.

6.3.4.17 Stability Study

The optimized SD (n = 3) was filled in hard gelatin capsules (Size 00), sealed in double aluminum foil, and exposed to accelerated stability conditions (40 ± 2°C and 75 ± 5% RH) for up to 6 months. The sampling was done at 0, 3, and 6 months, and the stability was evaluated in terms of appearance, drug content, saturation solubility, crystallinity, thermal behavior, and chemical composition (by functional groups). The drug content and saturation solubility of the optimized formulation were estimated by the validated HPLC. The changes in crystallinity were assessed by XRD and DSC. The changes in thermal behavior were investigated using DSC and TGA analysis. Moreover, the alteration in the important functional groups was investigated through ATR-FTIR spectroscopy.

6.3.5 *In-vitro* cytotoxicity assay

The MTT assay was performed against the melanoma cell line (B16F10) and human embryonic kidney 293 cells (HEK 293) as per our reported method with certain modifications [96]. The cytotoxicity of the optimized SDs was evaluated and compared with PLFEE suspension (simple dispersion in media) and PLFEE solution (dissolved in 0.2% DMSO). The B16F10 and HEK 293 cell lines were obtained from the National Centre for Cell Science (NCCS), Pune, India. The cells were seeded at a concentration of 1×10^6 cells/well in a microtiter plate containing DMEM/F-12 medium with 10% FBS, 50 unit/mL penicillin, and streptomycin and incubated in a 5% CO_2 atmosphere for 24 h at 37°C to attain 70% of confluency. After the attainment

of confluency, the medium was discarded, washed thrice with phosphate-buffered saline (PBS, 10 mM, pH 7.4), and further incubated with serum-free fresh media containing various concentrations (20-200 µg/mL) of test substances (optimized SDs, PLFEE suspension, and PLFEE solution) and negative control (placebo of optimized SDs and 0.2% DMSO) for 24 h. A standard anticancer drug, DTIC (2.5-80 µg/mL) was used as a positive control. The SDs were immediately dispersed in culture media before treatment. Due to the hydrophobic nature of PLFEE, it was solubilized in 0.2% DMSO for treatments. Also, the suspension of PLFEE was made by simple dispersion with the media for comparison purposes. Then the sample solutions were substituted with serum-free media containing 200 µL of MTT solution (5 mg/mL), and cells were further incubated for 4 h at 37°C. The previous medium was removed, and the cells were washed thrice with PBS. The formazan crystals generated from MTT reduction by viable cells were dissolved by the addition of 150 µL of DMSO. Then, the absorbance of the solution was measured at 570 nm in a microtiter plate reader (Bio-Rad Laboratories, Munchen, Germany). The percentage cell viability was calculated using the formula in Equation 6.13. The experiments were repeated in triplicate, and the average value was reported.

$$\%\ cell\ viability = \frac{Abs_{(t)}}{Abs_{(C)}} \times 100 \qquad (6.13)$$

where $Abs_{(t)}$ and $Abs_{(c)}$ are the absorbances of the plate with the treated sample and the absorbance of the control (without any treatment), respectively. The concentration required for 50 % inhibition of cell viability (IC_{50} value) was estimated using nonlinear regression analysis of log (concentration) vs. response data by GraphPad Prism 5 Software (GraphPad Software, Inc., San Diego, California). The obtained average IC_{50} values of each sample were compared statistically using a one-way analysis of

variance (ANOVA) followed by Tukey's test. The statistical significance was considered at $p<0.05$.

6.3.6 Cell migration assay (*in-vitro* wound healing assay)

In-vitro cell migration assay was carried out using 2-well inserts (ibidi®, Munich, Germany) placed in 6-well plates as per the previously described method with certain modifications [95, 97]. Briefly, B16F10 cells were suspended in culture media (1×10^5 cells/mL), and 100 µL of the cell suspension was added to each of the 2 wells in the cell inserts placed in 6-well plates. Then, the cells were incubated for 24 h to adhere the cells at the bottom of the wells, and cell-free gaps (wounds) were made by removing the culture inserts with the help of sterile forceps. Cellular debris and floating cells were washed off using sterile PBS. Then, the cells were treated with sterile fresh media containing standardized PLFEE (in 0.2% DMSO) and optimized SD each at a concentration of 50 µg/mL and incubated for 24 h. One additional plate seeded with cell suspension without any treatment was served as a control. The cell-free wound areas were observed and photomicrographed using an inverted microscope (Victory Plus, Dewinter, New Delhi, India) at 0, 12, and 24 h. At each time point, 5 microphotographs were captured, and the wound areas were analyzed quantitatively using Image J software. The % area occupied by the cell-free gaps (wounds) due to the migration of cells was calculated using Equation 6.14, considering the initial scrapped area as 100 %.

$$\%\ area\ occupied\ = \frac{Cell\ free\ area\ _{(0)} - Cell\ free\ area\ _{(t)}}{Cell\ free\ area_{(0)}} \times 100 \qquad (6.14)$$

Where, the cell-free area $_{(0)}$ and the cell-free area $_{(t)}$ are the wound areas obtained initially and after certain time (12 and 24 h), respectively.

6.3.7 Approved protocol for standard experimental animals' conditions

The experiment was carried out following an approved protocol from the Institutional Animal Ethics Committee (IAEC Approval Number: IIT(BHU)/IAEC/2023/056). The "Committee for the Purpose of Control and Supervision of Experiments on Animals" (CPCSEA) guidelines were followed for the care and experimentation of laboratory animals. The animals (female Sprague-Dawley (SD) rats: 12-13 weeks old, 280 ± 18.345 g and female C57BL/6 mice: 7-8 weeks old, 18 ± 1.784 g body weight) were housed in cages with open access to water and standard food (Laboratory animal feeds, VRK Nutritional Solutions, Maharashtra, India), maintained in a room at 25 ± 1°C, 55 ± 5% RH with 12 h of dark/light cycle, and acclimatized to the laboratory environment over 1 week before experiments.

6.3.8 *In-vivo* oral Bioavailability study

The bioavailability study includes the (i) quantitative estimation of one of the major bioactive constituents (PIP) of standardized PLFEE in plasma by validated bioanalytical HPLC method and (ii) bioavailability study of optimized SD and its comparison with neat extract and physical mixture.

6.3.8.1 Bioanalytical HPLC method for quantitative estimation of Piperine (PIP) in plasma

Chromatographic separation and analysis were performed by an Agilent HPLC system (Agilent 1260 Infinity II, Agilent, USA) equipped with a quaternary pump (1260 Quat Pump VL)), diode array detector (1260 DAD WR), automatic sampler (1260 Vial Sampler), column (Quasar^{TM} C18 LC column, PerkinElmer, 250 × 4.6 mm with 5 µm particle size), a standard flow cell (10 mm, 13 µL, and 120 bar) and Open LAB CDS EZChrom Workstation VL software. The isocratic elution was carried out at a flow rate of 1.00 mL/min using a mobile phase comprised of methanol (HPLC &

spectroscopy grade, Finar Limited, India) and HPLC grade water (Finar Limited, India) at a ratio of 80:20 v/v with a run time of 10 min. Quantification of PIP in plasma sample was carried out by the developed HPLC method at 342 nm using p-dimethylaminobenzaldehyde (p-DMAB, 99% Purity, Spectrochem Pvt. Ltd., Mumbai, India) as internal standard (IS) [98].

6.3.8.1.1 Blood sample collection and separation of plasma

Female SD rats were chosen for the bioavailability experiment. Animals without administration of PLFEE or formulation were chosen for the collection of blank plasma. Briefly, a blood sample (2.5 mL) was obtained from the retroorbital plexus into a heparinized tube, and plasma was collected by centrifugation of blood at 10000 rpm for 10 min in a refrigerated centrifuge (4°C). The supernatant plasma was decanted and used for the preparation of the calibration curve of PIP in plasma.

6.3.8.1.2 Preparation of primary stock solution and primary working standard solution

A primary stock solution of PIP (1 mg/mL) was prepared by diluting the pure PIP (>97% Purity, Sigma Aldrich) with HPLC-grade methanol. Further, the primary working standard solutions (0.5 to 256 µg/mL) were prepared from primary stock solution by diluting with HPLC-grade methanol. Similarly, the primary stock solution (1 mg/mL) of IS (p-DMAB) was prepared in HPLC grade methanol and used for the preparation of primary working standard solution (100 µg/mL) by suitable dilution.

6.3.8.1.3 Spiking of plasma samples, extraction, and processing

Plasma standards of both PIP with p-DMAB were made by spiking blank plasma with the primary working standard solution of PIP (0.5 to 256 µg/mL) and IS (100 µg/mL) to obtain the required concentrations. Accurately, 100 µL of blank plasma samples were spiked with 100 µL of various primary working standard solutions (0.5 to 256

μg/mL) and 10 μL of IS (100 μg/mL) and incubated for 20 min. After incubation, the plasma protein precipitation and extraction of PIP and IS from plasma was carried out by adding 0.790 mL of HPLC grade methanol to produce secondary working standard solutions (0.05 to 25.6 μg/mL) containing a constant amount of IS (1 μg/mL). The samples were vortexed for 5 min at 2400 rpm (SPINIX^{TM} Vertex shaker, Tarsons Products Pvt. Ltd., Kolkata, India) and sonicated for 10 min at 40 kHz ultrasonic frequency (GT Sonic Ultrasonic Cleaner, Guang Dong GT Ultrasonic Co., Ltd., China, Ultrasonic power: 150 W) for obtaining maximum recovery. Further, the samples were centrifuged (Remi CM 12 PLUS, Mumbai, India) at 10,000 rpm for 10 min at 4°C and filtered through 0.22 μm PVDF membrane filter (AXIVA Sichem Pvt. Ltd., New Delhi, India) to obtain a clear organic layer. Then, accurately 1 mL of each organic layer was evaporated in a vacuum under a nitrogen stream, reconstituted with 1 mL of HPLC grade methanol, filtered through 0.22 μm PVDF membrane filter, kept in 1.5 mL of screw top amber colored autosampler HPLC vials (Agilent) prior to the HPLC analysis.

Three quality control (QC) samples (0.1, 1.6, and 25.6 μg/mL) were made analogously by spiking in blank plasma followed by drug extraction and reconstitution in an organic solvent. Additionally, three QC standards (0.1, 1.6, and 25.6 μg/mL) were prepared by adding 100 μL of primary working standard solutions (1, 16, and 256 μg/mL) and 10 μL of IS (100 μg/mL) and diluting up to 1 mL with HPLC grade methanol. Twenty microliters of secondary working standard solutions were injected by autosampler for quantification of PIP and IS at 342 nm by DAD detector. The analysis was performed in triplicate, and the calibration curve was made by plotting the ratio of the peak area of each analyte to IS on the y-axis versus the concentration of the analyte on the x-axis.

6.3.8.2 Validation of bioanalytical HPLC method

The developed HPLC method for quantification of PIP in plasma was validated for linearity, range, selectivity, accuracy (relative error), precision (repeatability and intermediate precision: intra-day and inter-day), sensitivity (lower limit of detection (LLOD), lower limit of quantification (LLOQ)), % recovery, robustness, system suitability, and stability test as per US Food Drug Administration (US-FDA) bioanalytical method validation guidance (Bioanalytical Method Validation Guidance for Industry, U.S. Department of Health and Human Services, FDA, Center for Drug Evaluation and Research (CDER), Center for Veterinary Medicine (CVM)) [99].

6.3.8.2.1 Linearity & range

The linearity of the method was examined by observing the correlation coefficients obtained from the calibration curves PIP. The range of linearity was verified by fitting the calibration data (n = 3) to the linear equation and determining the concentration range that follows the linearity.

6.3.8.2.2 Selectivity

The selectivity of the method to the analyte (PIP) and IS in the plasma sample was investigated through the comparison of HPLC chromatogram of six batches of blank plasma extracted with methanol with that of blank plasma spiked with standard solutions (i.e., plasma sample spiked with IS, plasma sample spiked with PIP, and plasma sample spiked with IS with PIP).

6.3.8.2.3 Accuracy

The accuracy of the HPLC method was investigated from the percentage relative error (% RE) from the replicate analysis of QC samples (0.1, 1.6, and 25.6 µg/mL). The QC

samples were injected into the HPLC system, and the concentrations were measured from the calibration curve. The % RE was estimated by Equation 6.13.

$$\% RE = \frac{Observed\ value - Expected\ or\ actual\ value}{Expected\ value} \times 100 \qquad (6.13)$$

6.3.8.2.4 Precision

The precision of the developed HPLC method was ascertained by repeatability and intermediate precision study. Six replicates of the QC sample (1.6 µg/mL) were chromatographed by the HPLC method, and the repeatability of the method was assessed by determining the percent relative standard deviation (% RSD) of the obtained area ratio. The intermediate precisions (intra-day and inter-day) were assessed by analyzing the chromatographic area of three QC samples (0.1, 1.6, and 25.6 µg/mL) and calculating the % RSD.

6.3.8.2.5 Sensitivity: Lower Limit of Detection (LLOD) and Lower Limit of Quantification (LLOQ)

The LLOD and LLOQ of the HPLC method were estimated by the standard deviation of the response and the slope method using Equation 6.14 and Equation 6.15, respectively.

$$LLOD = \frac{3.3\ SD}{S} \qquad (6.14)$$

$$LLOQ = \frac{10\ SD}{S} \qquad (6.15)$$

Where SD is the standard deviation of response (y-intercept) and S is the average slope of calibration curves.

6.3.8.2.6 Percent extraction recovery (PER)

The PER was of PIP, and IS was estimated by comparison of the peak areas of plasma extracted QC samples to that of un-extracted QC standards containing an equivalent quantity of each tested sample (i.e., to represent 100 % recovery).

6.3.8.2.7 Robustness

The robustness of the developed HPLC method was studied by intentional changes in different chromatographic circumstances, such as various wavelengths (340, 342, and 344 nm), various run times (8, 10, and 12 min), flow rates (0.8, 1, and 1.2 mL/min), mobile phase composition (78:22, 80:20, and 82:18 v/v of methanol: water), and analyzing the changes in the ratio of peak area and retention time (Rt) of PIP at a concentration of 1.6 µg/mL.

6.3.8.2.8 System Suitability

The consistency in the performance of the HPLC method was studied by system suitability constraints. Six replicates of secondary working standard solution (1.6 µg/mL) of PIP were injected, and parameters like % RSD of peak area ratio, % RSD retention time (Rt), the number of theoretical plates, peak purity, capacity factor, tailing factor were considered for system suitability analysis.

6.3.8.2.9 Stability test

The stability test was performed to investigate the changes in the concentration of the studied analyte after each storage condition, and it was interrelated with the initial concentration (freshly prepared/immediately processed samples). Stability tests were conducted at three QC levels (0.1, 1.6, and 25.6 µg/mL) under different storage conditions: long-term (i.e., -20°C for 30 days) and accelerated condition (after completion of 3 freeze-thaw cycles, i.e., -20°C for 12 h and 25°C for 12 h).

6.3.8.3 *In-vivo* oral bioavailability study

Female SD rats (n = 15), weighing 286 ± 20.531 g, were randomly divided into three groups (5 rats/group): a plain standardized PLFEE group, PM group, and SD group. Before oral dosing, they fasted for 12 h with free access to water. Samples (PLFEE, PM, and SD) were suspended in 1 mL of 0.5% w/v of sodium carboxymethylcellulose (Na-CMC), mixed by vortex mixture, and used immediately for dosing. A single dose (166.67 mg/kg) of standardized PLFEE (equivalent to 62.83 mg/kg of PIP), an equivalent amount of PM, and SD were administered to rats by oral gavage (stainless steel, Gauge 14). After dosing, 250 µL of blood samples were withdrawn from retro-orbital plexus at 0.25, 0.5, 1, 2, 4, 6, 8, 12, and 24 h and immediately transferred into pre-heparinized (40 IU/mL blood) micro-centrifuge tubes (Eppendorf AG, Hamburg, Germany). Collected blood samples were centrifuged at 10,000 rpm for 10 minutes, at refrigerated condition (4° C) to separate plasma, and supernatant plasma samples were stored at -20° C until analysis. Accurately, 100 µL of each plasma sample was mixed with 10 µL (100 µg/mL) of p-dimethylaminobenzaldehyde (p-DMAB) as internal standard (IS) in a 1.5 mL of microcentrifuge tube. Then, the plasma protein precipitation and extraction of PIP and IS were carried out by adding 0.890 mL of HPLC grade methanol, followed by vertexing vigorously for 5 min and sonicating for 10 min at 40 kHz ultrasonic frequency for maximum extraction. The samples were centrifuged at 10,000 rpm for 10 min at 4° C, and the supernatant was filtered through a 0.22 µm PVDF membrane filter to obtain a clear organic layer. Then, the organic layer was evaporated in a vacuum under a gentle stream of nitrogen, reconstituted with 1 mL of HPLC grade methanol, filtered through 0.22 µm PVDF membrane filter, kept in 1.5 mL of screw top amber colored autosampler HPLC vials (Agilent, USA), before the HPLC analysis. The detailed HPLC methodology for the estimation of PIP in rat

plasma with complete validation is provided in the supplementary file (section 1.5). The PK parameters of SD were estimated through PK Solver software (version 2.0) [100] and compared with PM and PLFEE. Maximum plasma concentration (C_{max}), time to reach maximum concentration (T_{max}), the area under the curve ($AUC_{0–24h}$ or $AUC_{0-\infty}$), elimination half-life ($t_{1/2}$), and mean residence time (MRT) were obtained by non-compartmental analysis based on plasma drug concentration-time curve. The relative bioavailabilities (F_{rel}) of SD (test) to that of neat PLFEE (Reference 1) or PM (Reference 2) were calculated using Equation 5.16.

$$F_{rel} = \frac{AUC_{test}}{AUC_{Reference}} \times 100 \qquad (5.16)$$

6.3.9 Acute oral toxicity study (LD_{50})

Acute oral toxicity was carried out using healthy nulliparous and non-pregnant female C57BL/6 mice as per Organization for Economic Co-operation and Development (OECD) guidelines 425 using up-and-down procedure (UDP) [101]. Before starting the experiment, the C57BL/6 mice were housed in a cage with free access to standard food and water and were maintained on a 12 h dark/light cycle in a room at 25 ± 1°C and 55 ± 5% RH. The animals were familiarized with the laboratory environment for 1 week prior to carrying out the *in-vivo* study. Before administration of the dose, the animals were kept fasted (food withdrawn for 3h with easy access to water), and the body weight was recorded. Due to the lack of evidence on the toxicity profile of standardized PLFEE, as per the guideline, the main test was carried out with a starting recommended dose of 175 mg/kg by gavage using a stomach tube (stainless steel, size: 18). The required amount of PLFEE was suspended in 0.5% w/v Na-CMC and administered as a single dose (not exceeding 200 µL Na-CMC solution). The neat 0.5% w/v Na-CMC was administered at a volume of 200 µL/dose to healthy mice (n

= 4) and considered as vehicle control for comparison purposes. After administration, the mice were deprived of food for 2 h. Individually, the animals were observed after the first 30 min, with special attention at first 4 h, periodically during the first 24 h, and daily afterward for 14 days. Every animal was watched at least twice a day to observe any toxicity, survival or behavioral alteration, and change in body weight. The AOT425STATPgm software (United State Environmental Protection Agency/ US EPA) was utilized for obtaining a testing sequence and LD_{50} (dose that causes toxicity to 50% of the animal population) [102]. The survival or death result of the animal after 48 h (short-term outcome) was subjected to the software, and the experiment was continued as per the software's instruction with the administration of the recommended next dose in up-and-down fashion up to the attainment of "stop dosing" instruction (based upon 5 reversals in 6 tests) and through observation. The surviving mice (observed from the short-term outcome) were further observed for 14 days. After 14 days, the health of the animals (mice treated with 550 mg/kg of standardized PLFEE (n = 4) and healthy mice (n = 4) administered with 0.5% w/v Na-CMC) was thoroughly observed, weighed, anesthetized by isoflurane, and blood was withdrawn by cardiac puncture for hematological and biochemical analysis as per the manufacturer's instructions. The animals (4 animals from each group) were humanly killed, and the vital organs (heart, kidney, liver, lungs, and spleen) were carefully collected, washed with ice-cold saline, and fixed in 10% aqueous formalin for 12 h for histopathological observations. Approximately 4 μm thick paraffin organ sections (n = 6) were cut and stained with hematoxylin and eosin and mounted in a non-aqueous mounting medium (Dibutylphthalate Polystyrene Xylene (DPX)). The sections were optically examined under the light microscope (Magnus MLX Plus, Olympus Opto Systems India Pvt. Ltd., Uttar Pradesh, India) equipped with a 5.1 MP digital

microscopic camera (Magcam DC 5) and Magvision software (version x36, 3.7.6820) at 10x magnification.

6.3.10 *In-vivo* anticancer activity in melanoma (B16F10) bearing C57BL/6 mice

The *in-vivo* anticancer activity of standardized PLFEE, optimized SD, standard marketed drug (Dacarbazine) was evaluated against B16F10 melanoma-bearing C57BL/6 female mice (8-9 weeks old, 20 ± 1.547 g body weight (b.wt.)). The animals were kept in cages, with free access to food and water, and kept under controlled environmental conditions on a 12 h dark/light cycle in a room at 25 ± 1°C and 55 ± 5% RH. Before tumor induction, the hair at the dorsal side was carefully removed with an electric clipper. The B16F10 murine melanoma cell line was procured from the National Center for Cell Science (NCCS, Pune, India). The cell line was grown in DMEM/F-12 media supplemented with 10% fetal bovine serum (FBS) and antibiotics (streptomycin- penicillin solution, 50 unit/mL) at 37°C in a humidified atmosphere containing 5% CO_2. The cells were cultured up to 90% confluency in T75 Flasks and harvested for *in-vivo* study by trypsinization followed by centrifugation (5000 rpm), washing, and pellet dispersion in phosphate-buffered saline (PBS, pH 7.4). The syngeneic transplantation model was used to develop a solid tumor in C57BL/6 mice. For *in-vivo* experiments, the harvested cells were adjusted to 1×10^6 cells/0.1 mL in PBS, and 100 µL of the cell suspension was subcutaneously injected into C57BL/6 mice. After 7 to 8 days of injection, mice bearing palpable tumors (volume: 35 ± 3 mm^3) were grouped into seven groups as per the experimental design. Standardized PLFEE (200 mg/kg b.wt, based on preliminary study) or an equivalent amount of optimized SD (with 0.5% Na-CMC) were administered orally (p.o.) by gavage daily for up to 30 days. Standard anticancer drug dacarbazine (DTIC) was injected at a dose of 5 mg/kg intraperitoneally (i.p.) after every 2 days up to 30 days [103]. Tumor

volume and body weight were measured every alternate day throughout the treatment period.

6.3.10.1 Experimental design

A total of 70 adult female C57BL/6 mice were divided into 7 groups as follows:

Group-I (Normal control): Non-tumor bearing mice, receiving vehicle (0.5% Na-CMC) at a dose of 10 mL/kg body weight (b. wt.) p.o. daily

Group-II (Tumor control): Tumor-bearing mice, receiving vehicle (0.5% Na-CMC) at a dose of 10 mL/kg b.wt. p.o. daily.

Group-III (Standard drug/ DTIC group): Tumor-bearing mice, receiving DTIC (5 mg/kg) i.p. every 2 days.

Group-IV (PLFEE group): Tumor-bearing mice, receiving standardized PLFEE (200 mg/kg b.wt. daily) p.o. daily.

Group-V (SD group): Tumor-bearing mice, receiving optimized SD (29.552 mg of SD, equivalent to 200 mg of PLFEE per kg b.wt. daily) p.o. daily.

Group-VI (DTIC + PLFEE group): Tumor-bearing mice, receiving standardized PLFEE (200 mg/kg b.wt.) p.o. daily, and DTIC (5 mg/kg b.wt.) i.p. every 2 days.

Group-VII (DTIC + SD group): Tumor-bearing mice, receiving SD (29.552 mg of SD, equivalent to 200 mg of PLFEE per kg b.wt.) p.o. daily, and DTIC (5 mg/kg b.wt.) i.p. every 2 days.

6.3.10.1.1 Tumor regression studies

The tumor regression studies were carried out as per the reported protocol [104].

6.3.10.1.1.1 Tumor volume (TV):

The size of the solid tumor was measured during the treatment using digital Vernier calipers (ZHART, CT-ZT-VERNIER, India), and the tumor volume was estimated by using Equation 6.17.

$$TV = \frac{length \times width^2}{2} \qquad (6.17)$$

6.3.10.1.1.2 Volume doubling time (VDT):

It is the time required for the solid tumor to achieve double the initial volume.

6.3.10.1.1.3 Tumor growth inhibition (% TGI):

It was estimated at the end of the study using Equation 6.18.

$$\%\, TGI = \frac{1 - (\frac{T_t}{T_0} \times \frac{C_0}{C_t})}{1 - \frac{C_0}{C_t}} \times 100 \qquad (6.18)$$

where T_t and T_0 are the median tumor volume treated at time t, and time 0, respectively. C_t and C_0 are the median tumor volume of control at time t, and time 0, respectively. Tumor growth inhibition greater than 50% is considered meaningful.

6.3.10.1.1.4 Percentage increase in life span (% ILS)

After completion of various treatments (i.e., after 30 days), 5 mice from each group were allowed to study the % ILS. The mean survival time (MST) in days was estimated, and the % ILS was calculated using Equation 6.19.

$$\%\, ILS = \frac{MST\ of\ treated\ group - MST\ of\ control\ group}{MST\ of\ control\ group} \times 100 \qquad (6.19)$$

6.3.10.1.1.5 Tumor weight and Histopathology

At the end of the study, 5 mice from each group were sacrificed by cervical dislocation for tumor weight and histopathology studies. Tumors from various groups were

collected, weighed, fixed in 10% buffered formalin for 12 h, and similarly processed for histopathology as described in the acute toxicity study [104].

6.3.11 Statistical analysis

The mean and standard deviation (SD) for all experiments were calculated and expressed as mean ± SD. Statistical analysis was performed by one-way analysis of variance (ANOVA) followed by Tukey's test (for 3 groups or more) or student's t-test (between two groups) at $P<0.05$ using GraphPad Prism 5 (GraphPad Software, Inc., San Diego, California).

6.4 Result and Discussions

6.4.1 Phase solubility study

Various hydrophilic polymers and surfactants were screened out by phase solubility study to select the most suitable carrier matrix for the preparation of SD. The solubility results of PIP (in PLFEE) tested in 2, 4, and 8% w/v aqueous solution of each CMs are shown in Figure 6. 2a-e. The solubility values depend on the slope values of the plot of CM concentrations v/s solubility. The higher the slope value, the superior the solubilization power of that CM (Figure 6. 2a, Table 6. 1) [105]. The Soluplus® showed the highest slope value (0.284) among the polymers, and Tween® 80 showed the highest slope value (0.5) among the surfactants, signifying the best capacity to solubilize PIP. Thus, among the polymers, the Soluplus® showed the highest PIP solubility (Figure 6. 2b), and among the surfactants, the Tween® 80 showed the highest PIP solubility (Figure 6. 2c). Other polymers and surfactants also showed a considerable rise in the solubility of PIP than the solubility in pure water. In most of the cases, the solubility was found to be improved with a rise in the concentration of polymers or surfactants. Similar results have been testified for many poorly soluble drugs/ phytoconstituents using hydrophilic carriers due to the formation of water-

soluble complexes between the drug and the CMs [92, 105-107]. The estimated Gibbs free energy transfer (ΔG_t°) values, obtained from the phase solubility study, which is a critical thermodynamic factor associated with the solubility of PIP or PIP with polymeric/surfactant aqueous solution are presented in Table 6. 1. Change in ΔG_t° values is an indication of the change in solubility from PIP to PIP-polymeric or surfactant solution [86]. All the obtained ΔG_t° values were found to be negative. The negative values of ΔG_t° reflect the spontaneous solubilization of PIP in those aqueous polymeric or surfactant solutions, and the solubilization process is energetically favorable [85, 86]. The lowest ΔG_t° values are obtained with the highest polymer or surfactant concentrations. This revealed that the solubilization process is more favorable at higher polymeric or surfactant concentrations [85-87].

Phase solubility study in Soluplus® displayed an improvement in solubility of PIP with increasing the concentration of polymer, with r^2 value equal to 0.985, giving A_N type of phase diagram (Figure 6. 2d), where "A" represents the polymer-drug combination is soluble in media and the subscript "N" represents a negative deviation from linearity [84, 92, 108]. This finding is consistent with previously reported solubility results regarding the increased aqueous solubility of BCS class-II drug carvedilol by Soluplus® with such type of phase diagram [92]. Solubility of PIP in 8% w/v of Soluplus® was found to be 2.693 ± 0.022 mg/mL compared to PIP (PLFEE) in water (0.224 ± 0.005), corresponding to a 12.022-fold increase, demonstrating excellent affinity between PIP and Soluplus®. Similarly, the phase solubility study in Tween® 80 presented an increase in PIP solubility with increasing the concentration of surfactant, with r^2 value of 0.999, giving A_L type of phase diagram (Figure 6. 2e), where "A" represents the polymer-drug combination is soluble in media and the subscript "L" represents the linearity [84, 108]. Solubility of PIP in 8% w/v of Tween®

80 was found to be 3.858 ± 0.023 mg/mL as compared to PIP in PLFEE (0.224 ± 0.005 mg/mL), corresponding to a 17.223-fold increase, indicating excellent affinity between PIP and Tween® 80.

The increase in solubility can be explained by micellar solubilization [92]. The self-micellization behavior of Soluplus® increases wettability, reduces the interfacial tension between the drug and the aqueous solution, and ultimately increases the saturation solubility. The micellization of Soluplus® in water was reported to be a spontaneous endothermic process above the critical micelle concentration (CMC) and critical micelle temperature (CMT) in the presence or absence of drug candidates [109]. Soluplus® is a free-flowing white to slightly yellowish triblock graft copolymer comprising polyvinyl caprolactam (57%), polyvinyl acetate (30%), and polyethylene glycol (13%) having a molecular weight ranging from 90,000 to 140,000 g/mol, and HLB value ~14.0 [109-111]. The polymer possesses an amphiphilic chemical structure (Figure 6. 3a), having a massive number of hydroxyl groups that behave as an excellent solubilizer for poorly soluble drugs in water [92]. The PEG acts as the hydrophilic head group, and the polyvinyl acetate with polyvinyl caprolactam acts as the hydrophobic tail of the amphiphile [109, 111]. The hydrophobic part forms the core of the micelle, whereas the hydrophilic group is positioned towards the aqueous medium, which forms the outer part of the micelles (Figure 6. 3a) [109].

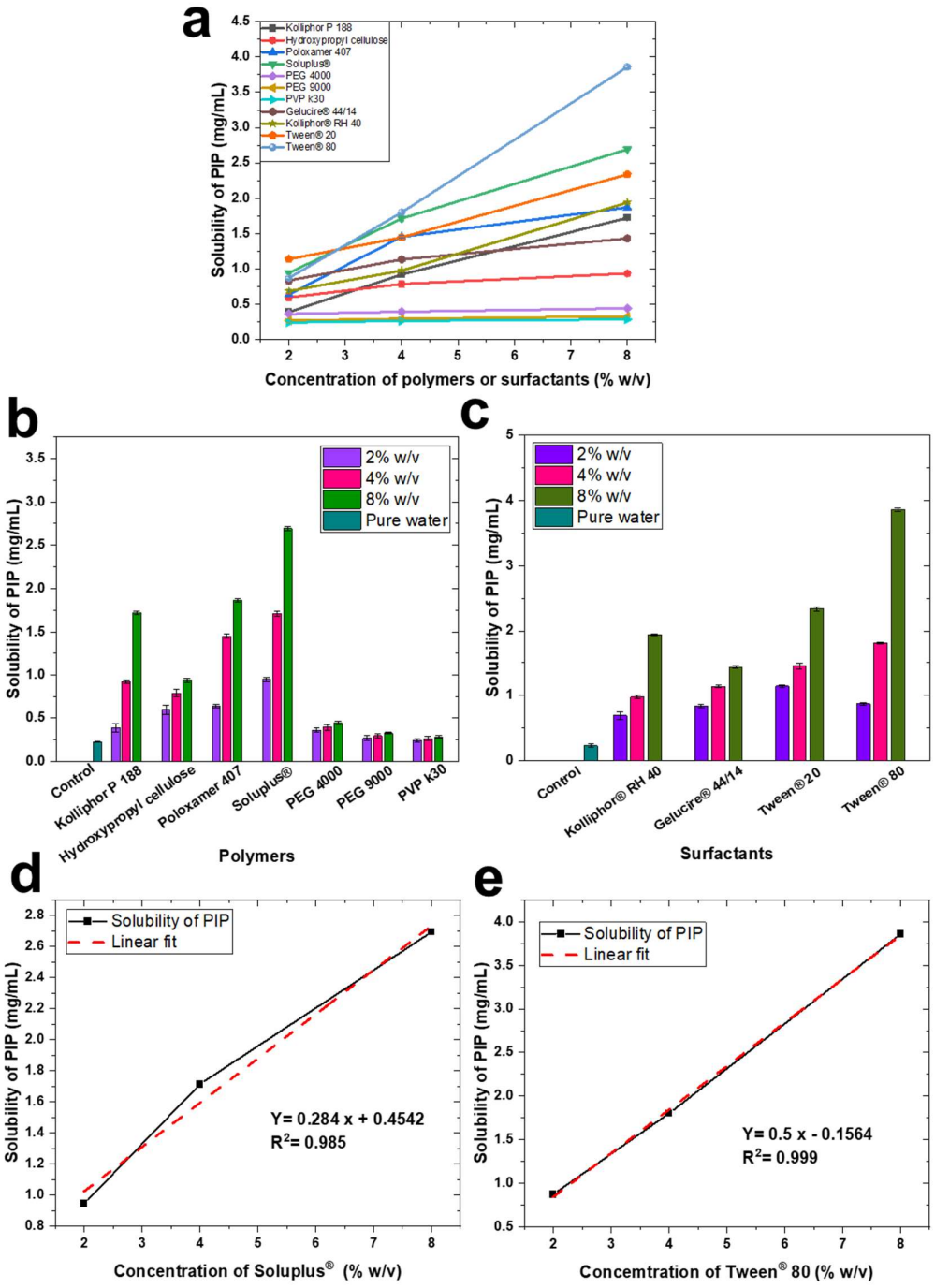

Figure 6. 2 Phase solubility of PIP from *Piper longum* fruits ethanolic extract (PLFEE) in various carrier matrices (CMs) (a) solubility of PIP in polymers and surfactants (b) solubility in polymers, (c) solubility in surfactants, (d) A_N type phase diagram of Soluplus®, and (e) A_L type phase diagram of Tween®80. Each value represents the solubility of PIP in 2, 4, and 8% (w/v) aqueous solution of carriers and is represented as mean ± S.D. (n = 3).

Tween® 80 (Polyoxyethylene (20) sorbitan monooleate) is a nonionic surfactant with low cost and low toxicity [112]. The amphiphilic Tween® 80, comprising of hydrophilic ethylene oxide (20) with sorbitol (1) groups, and the hydrophobic part comprising of oleic fatty acid (1) (Figure 6. 3b). At concentrations above the CMC, the surfactant monomers aggregate to form micelles to diminish the free energy of the system [112]. The micellar solubilization of hydrophobic candidates by Tween®80 was schematically represented in Figure 6. 3b. The amphiphilic nature of Tween® 80 solubilizes the PIP through micellar solubilization in which the hydrophilic head groups are toward the water medium and the hydrophobic tail forms the core of the micelle and are towards the hydrophobic PIP.

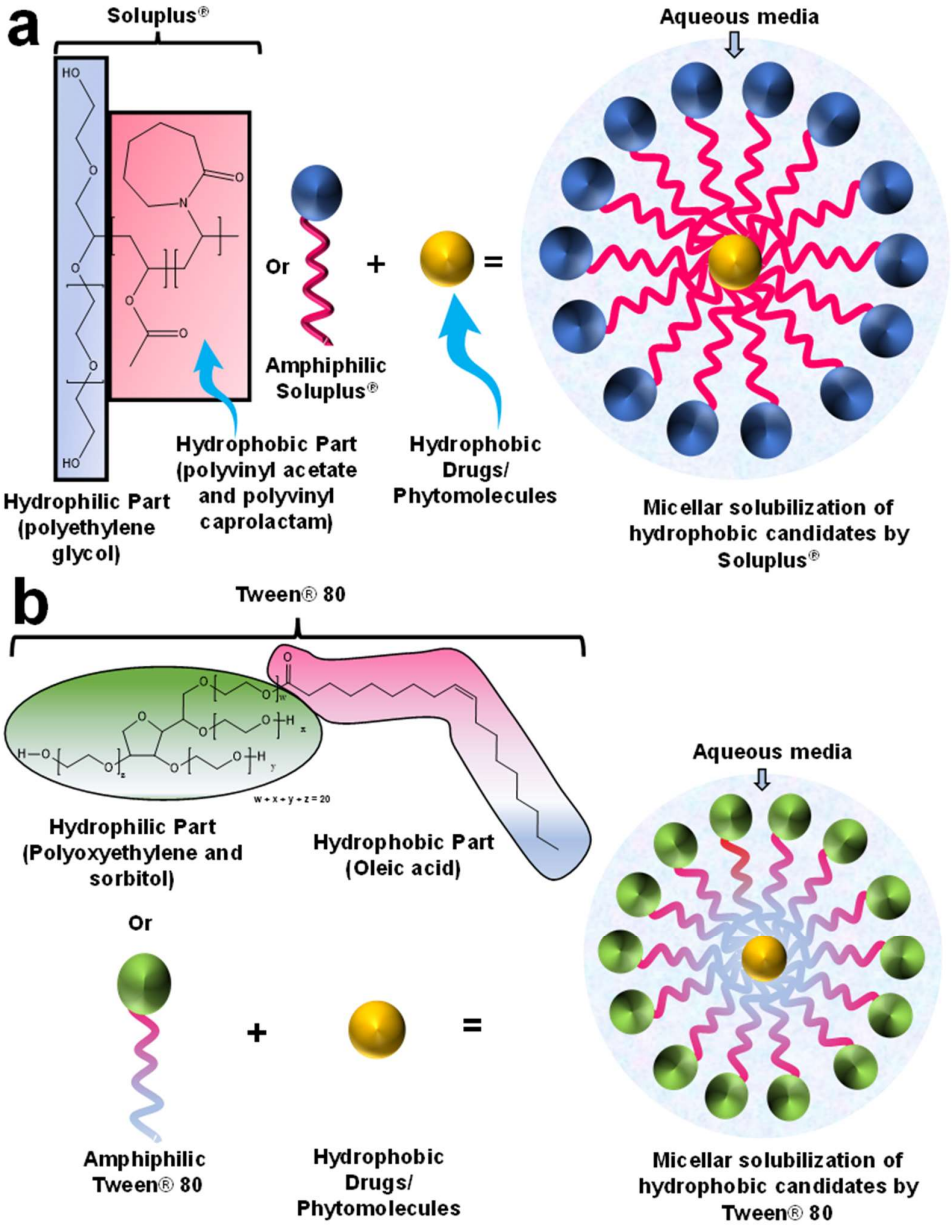

Figure 6. 3 Chemical structure and micellar solubilization properties of Soluplus® and Tween® 80 (a) the chemical structure and schematic illustration of the micellar solubilization of hydrophobic candidates by Soluplus® (b) the chemical structure and schematic illustration of the micellar solubilization of hydrophobic candidates by Tween®80

Table 6. 1 Gibbs free energy (ΔG_t°) transfer of PIP from pure water to an aqueous polymeric or surfactant solution

Name Polymer or Surfactant	Concentration of polymer or Surfactant (% w/v)	ΔG_t° Values (kJ/mol) at 37°C	Slope	Intercept	R^2
Kolliphor P 188	2%	-1.414	0.219	0.012	0.994
	4%	-3.632			
	8%	-5.251			
Hydroxypropyl cellulose	2%	-2.516	0.053	0.522	0.933
	4%	-3.23			
	8%	-3.676			
Poloxamer 407	2%	-2.695	0.1907	0.431	0.865
	4%	-4.814			
	8%	-5.463			
Soluplus®	2%	-3.699	0.284	0.454	0.985
	4%	-5.236			
	8%	-6.402			
PEG 4000	2%	-1.235	0.013	0.339	0.994
	4%	-1.453			
	8%	-1.747			
PEG 9000	2%	-0.466	0.009	0.253	0.983
	4%	-0.712			
	8%	-0.986			
PVP k30	2%	-0.195	0.006	0.232	0.941
	4%	-0.437			
	8%	-0.620			
Gelucire® 44/14	2%	-3.388	0.095	0.688	0.964
	4%	-4.172			
	8%	-4.773			
Kolliphor® RH 40	2%	-2.878	0.213	0.205	0.987
	4%	-3.785			
	8%	-5.556			
Tween® 20	2%	-4.18	0.203	0.691	0.993
	4%	-4.78			
	8%	-6.038			
Tween® 80	2%	-3.496	0.5	0.156	0.999
	4%	-5.364			
	8%	-7.33			

6.4.2 Formulation of SD

The best hydrophilic polymer and surfactant that confirmed the maximum solubility of PIP among the tested CMs were chosen for the development of SD. The phase solubility result justified the selection of Soluplus® and Tween®80 as the most

appropriate CMs for the development of SD. Various steps involved in the development of PLFEE containing SD and its incorporation into a hard gelatin capsule (size 00) are represented in Figure 6. 4a. Solvent evaporation by rotatory vacuum evaporation was widely exploited for the development of SD on a lab scale [90, 105, 113-115]. Soluplus® was initially established as a pharmaceutical additive for hot-melt extrusion and has been testified in various findings to form amorphous SD [92, 109, 116-119]. The amphiphilic nature of Soluplus® allows it to solubilize in aqueous and organic solvents. Its solubility in volatile organic solvents makes the solvent evaporation method suitable for the formulation of SD [111]. Soluplus® is categorized as a carrier for fourth-generation SD [92]. The nonionic surfactant Tween® 80 is also frequently reported as CM for the development of SDs [106, 107, 120]. The incorporation of surfactants into SD improves the solubility as well as permeability through the gastrointestinal membrane during oral administration. Since Tween® 80 is liquid, which may produce a sticky formulation, the maximum amount of Tween® 80 that can be incorporated into the SD without the development of a sticky product was chosen for the development of SDs. The Soluplus® also possesses surfactant-like behavior, which improves the solubility and permeability of drugs across a biological membrane. Thus, the 4th generation ternary SDs (PLFEE-SDs) were prepared using standardized PLFEE, Soluplus®, and Tween® 80.

Due to limited toxicity and excellent solubilizing ability, ethanol and acetone (class III solvents) were used for the preparation of SD. Initially, ethanol was used to dissolve PLFEE and CMs for the development of SD. However, a rubbery rigid film (Figure 6. 4b) and/or sticky product (Figure 6. 4c) were formed with discontinuous and/or continuous vacuum evaporation. Further, a low volume of ethanol (2 mL) was used to dissolve PLFEE, and acetone (10 mL) was used to solubilize CMs for the development

of SD with continuous vacuum evaporation. A white-colored, highly porous, dried, homogeneous thin film of SD was formed (Figure 6. 4d). Hence ethanol and acetone were used further for the formulation of PLFEE-loaded SD. Overnight vacuum drying of the SD removed the residual organic solvents. The high volatility of acetone compared to ethanol allowed the rapid evaporation of the solvent, leading to a porous solid film, which was easily scrapped by a spatula, grounded by mortar and pestle, and shifted through mesh # 60 for obtaining powdered SDs. Rapid solvent evaporation (70 rpm, 50° C) causes channeling in SDs, increasing the porosity, specific surface area, and ultimately the dissolution rate [19].

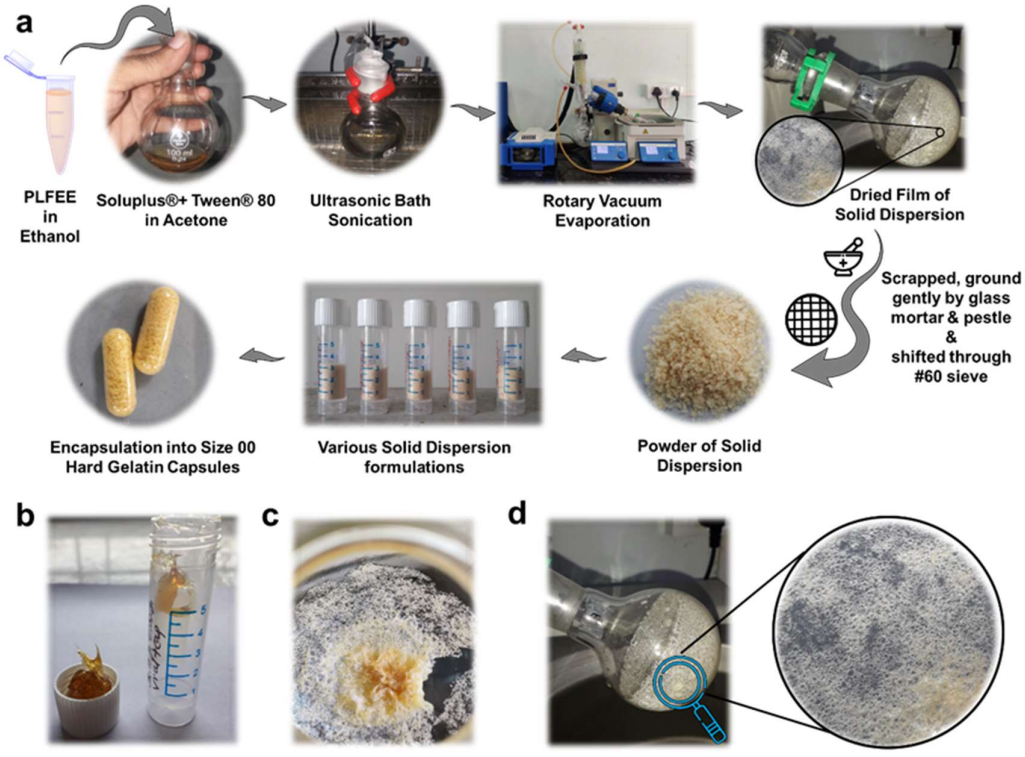

Figure 6. 4 Formulation development of SDs and formulation consequences (a) various steps involved during the development of PLFEE loaded SDs, (b) sticky product, (c) rubbery film type product, and (d) highly porous dried thin film of formulation.

6.4.3 Quality by design (QbD) and optimization

6.4.3.1 Response surface methodology (RSM)

RSM in formulation development permits understanding the changes in a particular response (Y) for the changes in the independent variables (X_1, X_2, and X_3). The study of the impact of various factors on the response by the one-factor-at-a-time (OFAT) approach is very time-consuming and requires considerable amounts of chemical cost and human efforts. Systematic optimization of the formulation was followed instead of the OFAT approach by employing the quality by design (QbD)-based formulation by design (FbD) as per the ICH Q8 (R2) guideline. In the FbD approach, one can define the quality target product profile (QTPP) and response variable (critical quality attributes (CQAs)) and identify the influence of independent variables (critical material attributes (CMAs) and critical process parameters (CPPs)) on CQAs [121]. A Box-Wilson central composite design (CCD) was employed to generate a second-order polynomial equation for the CQAs in RSM [89]. Compared to face-centered CCDs ($\alpha = 1$), near-rotatable or rotatable CCDs ($\alpha = 1.414$) provide decreased prediction error and improved valuation of curvature (quadratic) effects. Compared to Box–Behnken design (BBD), the CCD offers a wide design space due to the inclusion of axial points, in which the influence of various factors at five different levels on the response can be easily analyzed. The rotatable CCD model was widely explored for response surface analysis and optimization. [90, 122]. Table 6. 2 shows the levels of the evaluated factors (CMAs and CPP) and the CQA. The composition of 20 trial batches with their CQA (saturation solubility of PIP) is shown in Table 6. 3.

Table 6. 2 Coded levels, real values for each factor under experiment, and CQA

Screened factors (CMAs & CPP) and responses (CQAs)	**Levels**				
	Coded Values				
	-1.681	**-1**	**0**	**+1**	**+1.681**
Independent variables (CMA & CPP)	Real values				
Soluplus®: PLFEE (X_1, w:w)	0.636	2	4	6	7.363
Tween® 80: PLFEE (X_2, w:w)	0.131	0.2	0.3	0.4	0.468
Sonication time (X_3, min)	19.773	30	45	60	70.226
Dependent variables (CQAs)	Goal				
Saturation solubility of PIP (Y, mg/mL)	To maximize				

CQA: critical quality attributes; CMAs: critical material attributes and CPP: critical process parameter

Table 6. 3 Central composite design (CCD)-based trial formulation batches with respective CQA

Batches	Independent variables (CMAs & CPP)						Response/CQA or Y (mg/mL)
	Coded values			Actual values			
	X_1 (w:w)	X_2 (w:w)	X_3 (min)	X_1 (w:w)	X_2 (w:w)	X_3 (min)	
1	+1	+1	-1	6	0.4	30	5.379±0.021
2	0	0	0	4	0.3	45	4.784±0.034
3	0	0	+1.681	4	0.3	70.226	5.196±0.017
4	-1.681	0	0	0.636	0.3	45	3.661±0.012
5	0	+1.681	0	4	0.468	45	5.732±0.123
6	0	-1.681	0	4	0.131	45	4.998±0.032
7	0	0	0	4	0.3	45	4.922±0.033
8	+1	-1	+1	6	0.2	60	5.285±0.031
9	0	0	-1.681	4	0.3	19.773	4.895±0.011
10	0	0	0	4	0.3	45	4.710±0.045
11	-1	-1	-1	2	0.2	30	4.303±0.036
12	-1	+1	+1	2	0.4	60	4.723±0.054
13	-1	-1	+1	2	0.2	60	4.463±0.153
14	0	0	0	4	0.3	45	4.733±0.205
15	-1	+1	-1	2	0.4	30	4.705±0.035
16	+1.681	0	0	7.363	0.3	45	5.169±0.081
17	+1	+1	+1	6	0.4	60	5.828±0.168
18	0	0	0	4	0.3	45	4.703±0.218
19	0	0	0	4	0.3	45	4.733±0.038
20	+1	-1	-1	6	0.2	30	4.728±0.073

Results were represented as mean ± SD (n = 3)

The statistical model fit summary is represented in Table 6. 4. The higher R^2 values reflect the better significance of the experimental model [87]. The cubic model was found to possess a higher R^2 value (0.991) compared to other models. However, the sequential p-value was found to be high ($p>0.05$), reflecting the model's insignificance. Hence, the cubic model was found to be aliased. The quadratic model produced the highest adjusted and predicted R^2 values for response (Y) over the liner, 2FI, and cubic models (Table 6. 4). The software suggested the quadratic model as the best-fit model to describe the experimental design based upon a high model R^2 value (0.9854), an acceptable difference (<0.2) between adjusted and predicted R^2 values, and a high lack of fit value (>0.05). The R^2 value of 0.9854 in the quadratic model signifies that 98.5% of the data can be explained, analyzed, and examined through this model. From the model summary statistics (Table 6. 4), the quadratic model comes out best since it exhibited low standard deviation ("Std. Dev."), high "R-squared" values, and a low "Predicted Residual Sum of Squares" (PRESS). Hence, the effect of various variables on the saturation solubility of PIP in SDs can be best explained, analyzed, and interpreted by the quadratic model using the quadratic equation.

Table 6. 4 Results of model fit summary and model summary statistics

Fit summary report						
Source (Models)	R^2 value	Sequential p-value	Lack of Fit p-value	Adjusted R^2	Predicted R^2	
Linear	0.718	0.0001	0.0032	0.66514	0.5056	
2FI	0.747	0.6895	0.0021	0.63041	0.5225	
Quadratic	0.985	<0.0001	0.5444	0.97227	0.9364	Suggested
Cubic	0.991	0.4064	0.5987	0.97415	0.8822	Aliased
Model summary statistics						
Source	Std. Dev.	R^2	Adjusted R^2	Predicted R^2	PRESS	
Linear	0.2791	0.7180	0.6651	0.5056	2.1865	
2FI	0.2933	0.7471	0.6304	0.5225	2.1116	
Quadratic	0.0803	0.9854	0.9723	0.9364	0.2812	Suggested
Cubic	0.0775	0.9918	0.9742	0.8823	0.5207	Aliased

2FI: two-factor interaction model

Statistical analysis was executed using the analysis of variance (ANOVA) program in the Design-Expert software, and the results are shown in Table 6. 5. At a 95% level of confidence, the overall model p-value (i.e., 0.0001<0.05) for Y indicates the significance of the model and a good fit with the statistical results [87]. Except for the term X_2X_3, the p values for all model terms were found to be <0.05, reflecting the appropriateness of the model for response surface analysis. In the case of many insignificant model terms, the model reduction approach may improve the model predictability. The "Lack of Fit Tests" compares residual error with pure error from replicated design points. The lack of fit p-value (0.5444) was found to be non-significant (p>0.05), which is a primary requirement for such studies. This non-significant lack of fit p-value represents the ability of the model to fit the data properly to the model equation [122]. The adequate precision value represents the signal-to-noise ratio, and a value greater than 4 is necessary [89]. As per the utilized rotatable

CCD model, the obtained adequate precision value was found to be 37.2901, reflecting the attainment of adequate precision. Hence this model can be utilized to explore the design space to find out the optimized SDs formula.

Table 6. 5 ANOVA for quadratic model and fit statistics

ANOVA						
Source	**Sum of Squares**	**df**	**Mean Square**	**F-value**	**p-value**	
Model	4.3582	9	0.4842	75.03	<0.0001	significant
X_1	2.2665	1	2.27	351.20	<0.0001	
X_2	0.6994	1	0.6995	108.39	<0.0001	
X_3	0.2095	1	0.2096	32.47	0.0002	
$X_1 X_2$	0.0353	1	0.0354	5.48	0.0413	
$X_1 X_3$	0.0856	1	0.0856	13.27	0.0045	
$X_2 X_3$	0.0077	1	0.0078	1.20	0.2987	
X_1^2	0.2394	1	0.2394	37.10	0.0001	
X_2^2	0.6177	1	0.6178	95.73	<0.0001	
X_3^2	0.1274	1	0.1274	19.74	0.0012	
Residual	0.0645	10	0.0065			
Lack of Fit	0.0305	5	0.0061	0.9004	0.5444	not significant
Pure Error	0.0339	5	0.0068			
Cor Total	4.4227	19				
Fit statistics						
Standard deviation (SD)	Mean	C.V (%)	R^2	Adjusted R^2	Predicted R^2	Adequate precision
0.0803	4.88	1.65	0.9854	0.9723	0.9364	37.2901

X_1= Soluplus®: PLFEE w/w, X_2 = Tween® 80: PLFEE w/w, X_3 = sonication time

Diagnostic plots (Figure 6. 5, Figure 6. 6, and Figure 6. 7) allow the investigation of the goodness of fit of the proposed model. The linearity in the "normal plot of residual," optimum lambda value in the "Box-Cox plot," linearity in the "actual v/s

predicted plot," constant range of residuals in the "externally studentized residual v/s predicted plot," randomly scatter within the control limits in the "externally studentized residual v/s run plot," and "residual v/s factor plot" represents the goodness of fit of the proposed model. The projected model polynomial coded quadratic equation (Equation 6.19) was used to make predictions about the response (saturation solubility) for given levels of each factor. This equation identifies the relative impact of the factors by comparing the factor coefficients. The values and signs of the coefficients associated with each factor reflect the magnitude and direction of the effect of the independent variables on response, respectively [87].

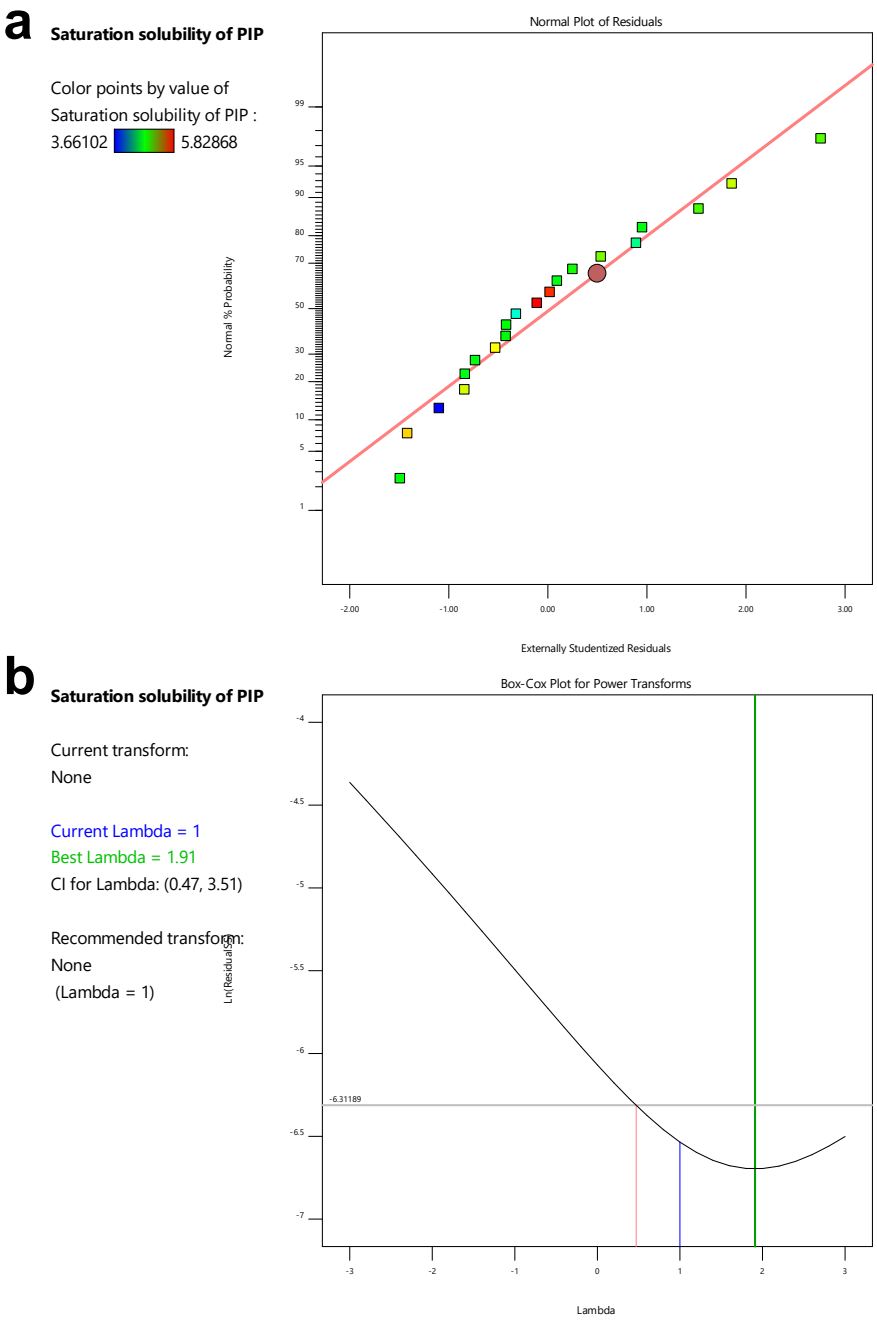

Figure 6. 5 Diagnostic plots and perturbation plot (a) normal plot of residuals and (b) Box-Cox plot

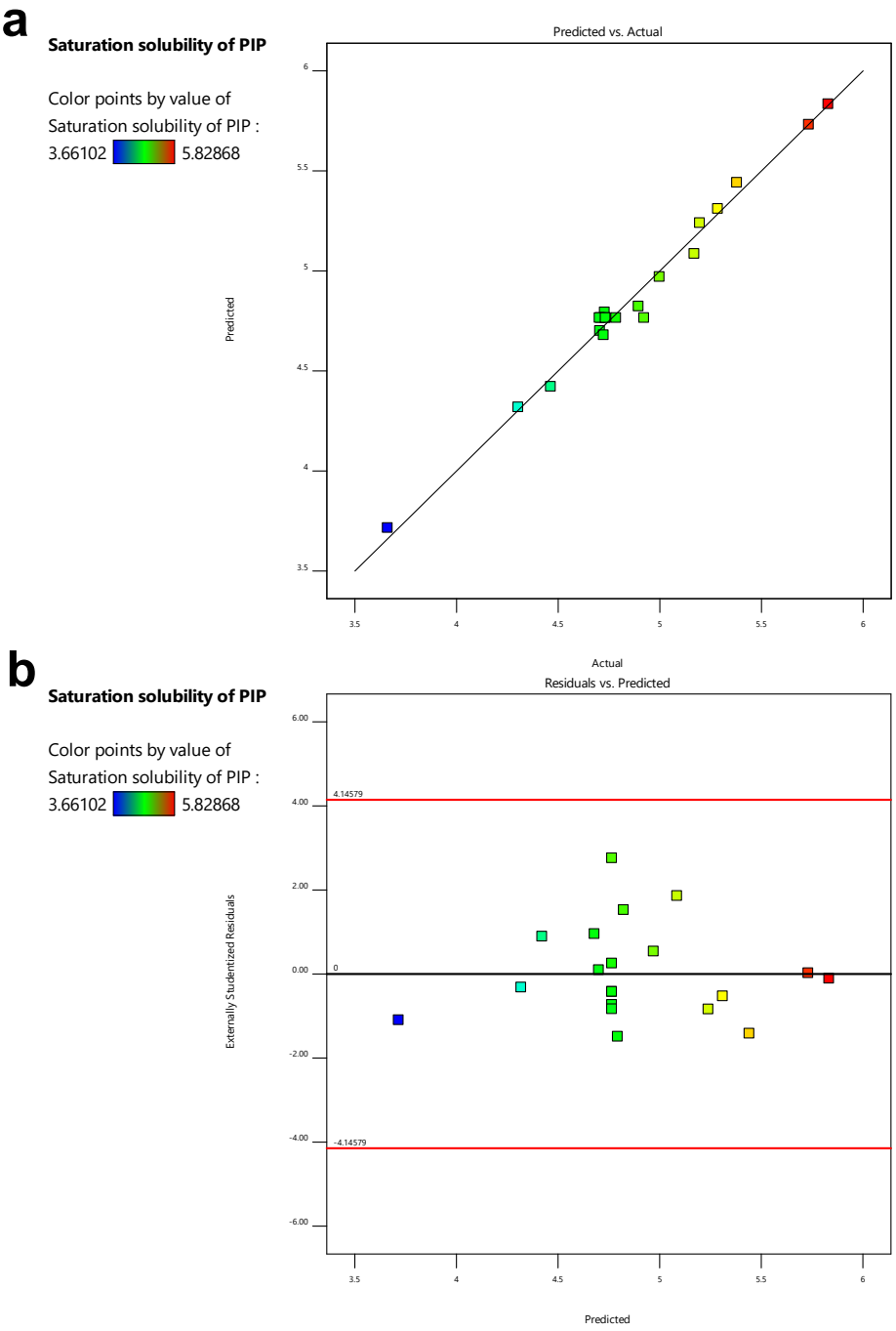

Figure 6. 6 Diagnostic plots and perturbation plot (a) predicted vs. actual plot and (b) residual vs. predicted plot

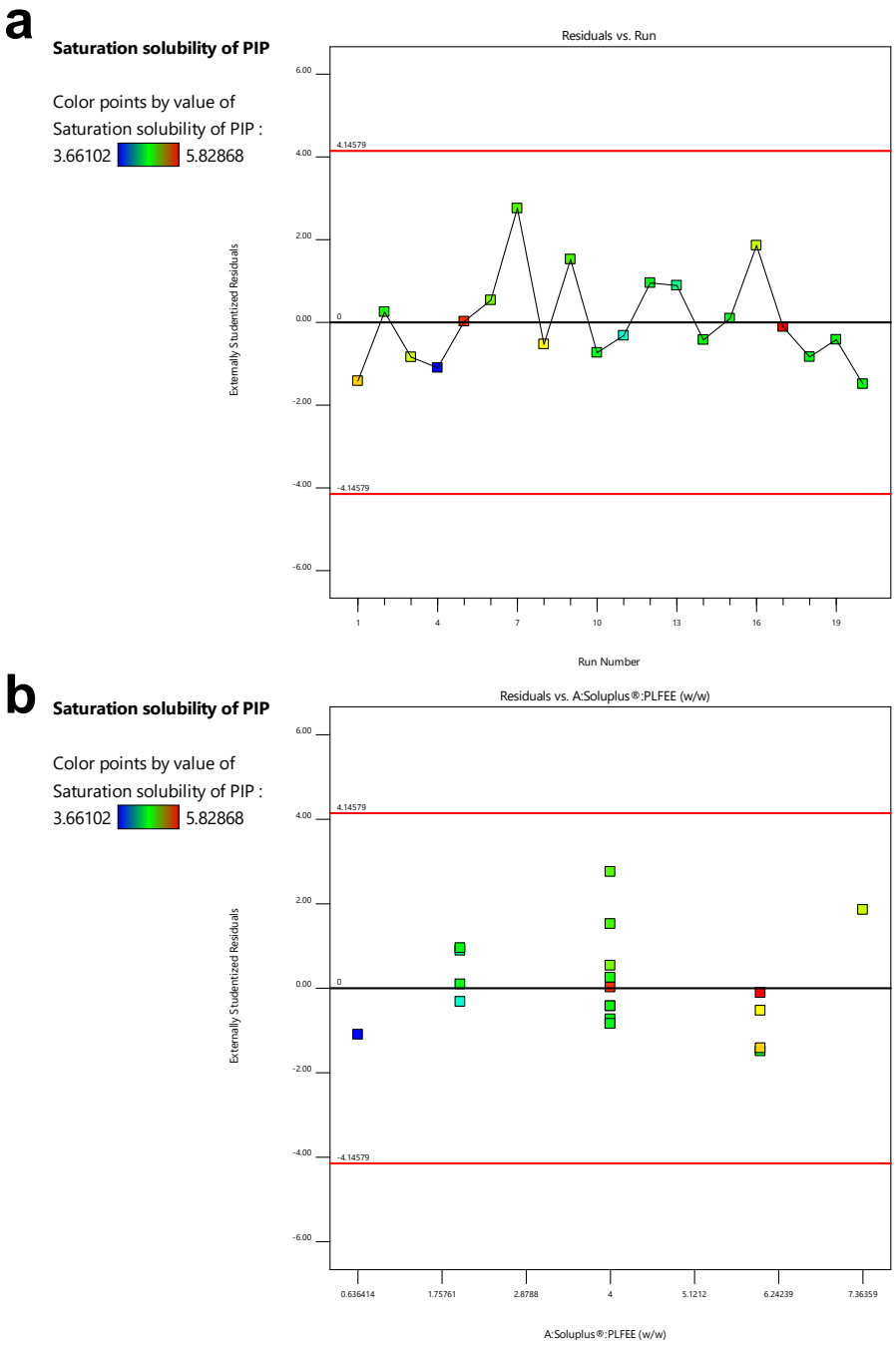

Figure 6. 7 Diagnostic plots and perturbation plot (a) residual vs. run and (b) residual vs. factor plot

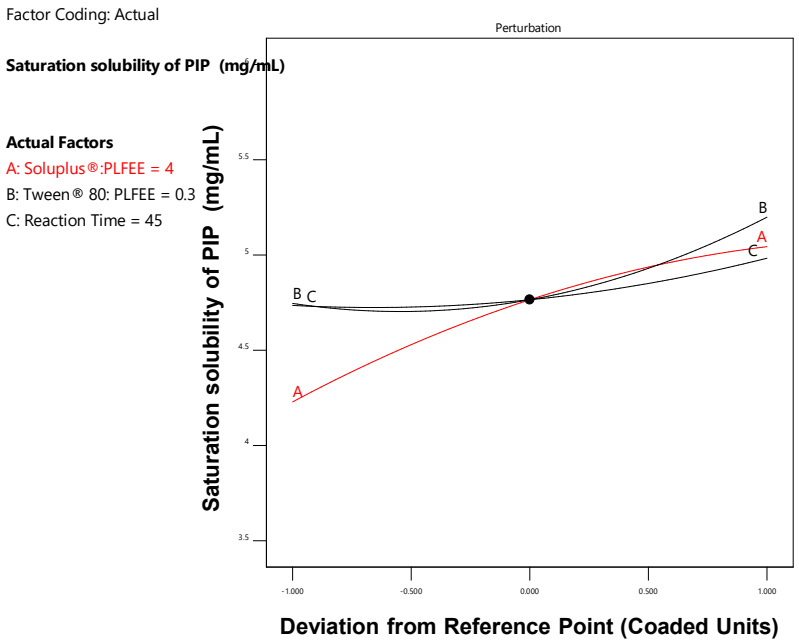

Figure 6. 8 Perturbation plot for saturation solubility of PIP

Model coded equation

$$Saturation\ solubility\ of\ PIP = 0.7148 + 0.0611\ X_1 + 0.0339\ X_2 + 0.0186\ X_3 + 0.0100\ X_1X_2 + 0.0155\ X_1X_3 - 0.0047\ X_2X_3 - 0.0193\ X_1^2 + 0.0311\ X_2^2 + 0.0141\ X_3^2 \qquad (6.19)$$

The coefficients with a positive sign demonstrate a positive impact (synergistic effect) on the response (Y), whereas the negative sign demonstrates a negative impact (inverse effect) on the response [87, 89, 90]. The significance of the quadratic polynomial model was assessed by using ANOVA data (Table 6. 5). For any of the terms (main, interaction, or quadratic) in the model, a large "F" value and a small "P" value directed a more significant effect on the response (Y) [89]. The linear variable (X_1) displayed the largest and most significant ($P<0.05$) effect on the saturation solubility of the SDs, whereas the other two variables (X_2 and X_3) showed slightly lesser effects on Y due to comparatively small "F" value and larger "P" value. Except for X_2X_3, all the interaction terms and the quadratic terms (X_1^2, X_2^2, and X_3^2) displayed

a significant effect on Y. The perturbation plot (Figure 6. 8) revealed a steep slope for X_1 compared to other factors (X_2 and X_3), signifying the greater effect of X_1 on the saturation solubility of PIP. The saturation solubility of PIP was found to be increased rapidly when the factor X_1 moved from -1 to +1.

The relationship among the factors (X_1, X_2, and X_3) and response (Y) was further inferred from the 3D response surface plots and 2D contour plots (Figure 6. 9). Increasing the ratio of Soluplus® to PLFEE (X_1) significantly increased the saturation solubility (Y) of PIP ($p<0.05$). Similar results of increased solubility with an increase in polymer concentrations were previously reported by various authors [87, 92, 123]. The solubility enhancement by Soluplus® can be ascribed to the micellar solubilization behavior of Soluplus® as described under the phase solubility section. The micelle population increased with an increase in the concentration of Soluplus® owing to the improvement of PIP solubility [92]. Similarly, the Y was found to be increased with increasing the Tween® 80 to PLFEE ratio (X_2). The enhanced solubility is attributed to the amphiphilic property of Tween® 80, which solubilizes the PIP through micellar solubilization [112]. The higher amount of X_1 and X_2 causes more amorphous modification of the PLFEE and ultimately enhances the saturation solubility. Further, due to the amphiphilic property of both CMs, they reduce the interfacial tension, improve the wettability of PIP in a concentration-dependent manner and ultimately enhance the saturation solubility. The saturation solubility of PIP was found to be increased with increasing the sonication time. The prolonged sonication time allows better molecular interactions among the PIP (in PLFEE) and CMs (Soluplus® + Tween® 80), causes more amorphous modification, and ultimately enhances the saturation solubility.

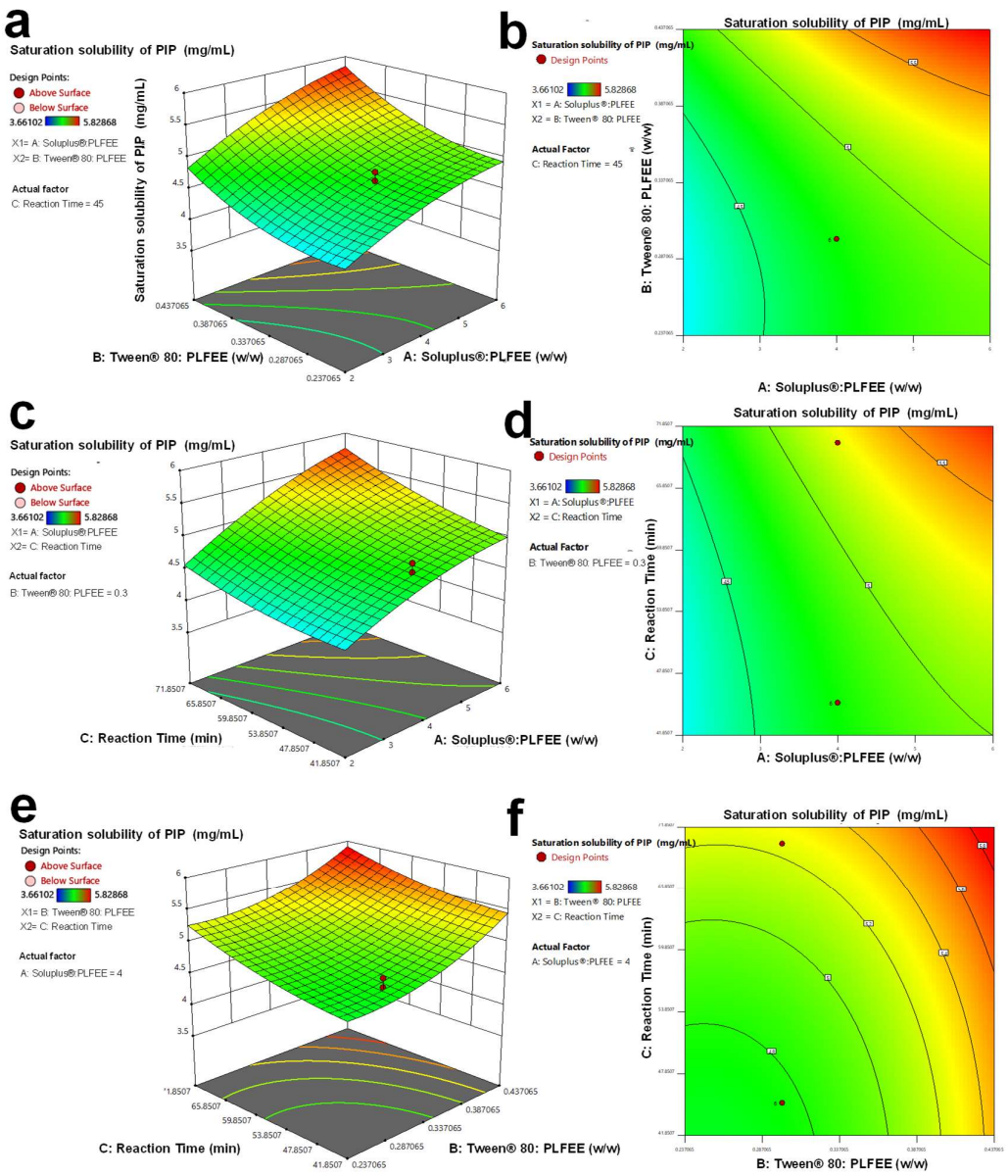

Figure 6. 9 Three-dimensional response surface plots and corresponding counterplots for saturation solubility (a and b) effect of factor X_1 and X_2, considering factor X_3 constant (c and d) effect of factor X_1 and X_3, considering factor X_2 constant, and (e and f) effect of factor X_3 and X_2, considering factor X_1 constant

6.4.3.2 Optimization of formulation

The numerical and graphical optimization techniques with the desirability approach were utilized to develop an optimized formulation with the desired responses. To obtain an optimized formula from design expert software, the target (range of dependent variables) is set as indicated in Figure 6. 10a. The optimal values of

formulation variables producing the highest overall desirability function, D = 1 were obtained via a numerical and graphical optimization process. The composition of the software-suggested optimized SD (Figure 6. 10b) was 5.989 w/w of Soluplus®: PLFEE (X_1), 0.399 w/w of Tween® 80: PLFEE (X_2), and 59.974 min sonication time (X_3), which would show saturation solubility of 5.829 mg/mL. The overlay plot as a function of the change in X_1, X_2, at constant X_3 value was shown in Figure 6. 10c. From the overlay plot, the desired region for constraining variables was identified inside the yellow design space. The flag mark in the yellow zone indicates the optimized batch.

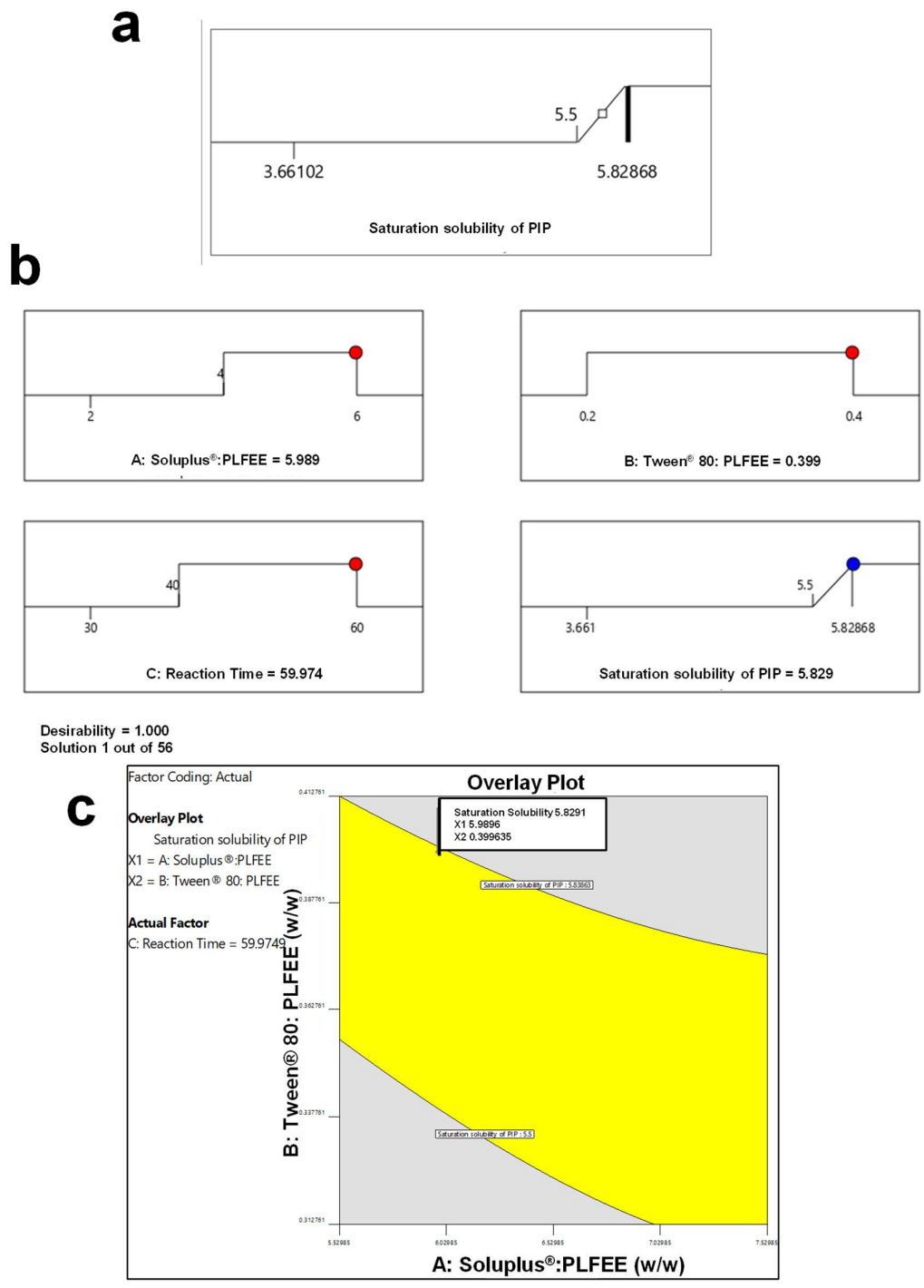

Figure 6. 10 Constrains and solutions to achieve CQA (a) criteria for achieving maximum saturation solubility and (b) one of the software-generated solutions out of 56 solutions, and (c) overlay plot as a function of change in X_1 and X_2, considering X_3 constant

6.4.3.3 Checkpoint analysis (validation of method)

The experimental and predicted values of Y were 5.672 ± 0.023 (n = 5) and 5.829 mg/mL, respectively. The percentage prediction error (% Bias) for the checkpoint batch was found to be -2.693%, which was <5%, validating the authenticity of predictive capacity and accuracy of the design model [87, 90].

6.4.4 Characterizations of optimized solid dispersion (SD)

6.4.4.1 Drug content and content uniformity

The drug content of SD with respect to PIP was found to be 98.079 ± 0.231%. The variation of the PIP content among the sampled specimens from different locations of SD powder was found to be negligible (% RSD <2%). This indicates the content uniformity of the SD, i.e., the PLFEE is uniformly distributed throughout the CMs to form amorphous SD without apparent phase separation. Such good content uniformity is ascribed to the molecular level mixing of PLFEE with the CMs in the organic solvent during sonication and rotary-based continuous evaporation during the formulation of SD that will offer dosing uniformity.

6.4.4.2 Percent yield

The % yield of SD was found to be 98.231 ± 0.245%. The rotary vacuum evaporation-based method allows the evaporation of organic solvent without loss of formulation as the entire process occurs in a single round bottom flask. Due to the round structure of the flask, a very small quantity of SD remains on its wall, which leads to a slight decrease in the overall yield.

6.4.4.3 Micromeritics Properties

The bulk density and tapped density of SD were found to be 0.283 ± 0.024 g/mL and 0.347 ± 0.025 g/mL, respectively. The angle of repose, CI, and HR values represent

the flowability of the powder. The CI of a powder is a measure of bridge strength or potential powder arch and stability, whereas the HR is related to inter-particulate friction [124]. The obtained angle of repose, CI, and HR were found to be 36.623 ± 0.543°, 18.443 ± 0.051%, and 1.226 ± 0.016, respectively, suggesting fair flow property of SD powder [124]. The flow property can be enhanced further by utilizing glidants or lubricants.

6.4.4.4 X-ray diffraction (XRD)

XRD is widely used for investigating the molecular order of solid dispersion [19]. The XRD results of standardized PLFEE, Soluplus®, Tween® 80, PM, and optimized SD were shown in Figure 6. 11. The PLFEE showed sharp diffraction patterns at 2θ of 12.606°, 14.658°, 19.644°, 21.86°, 24.097°, 25.984°, 31.562°, 37.768°, and 41.231° which is superimposable with the peaks for PIP [125-129]; reflecting its crystallinity nature. Soluplus® showed halo diffraction patterns with diffused peaks which are well consistent with reported XRD reports, representing its amorphous nature [92, 118, 130, 131]. Tween® 80 exhibited halo diffractions and diffused peaks, reflecting its amorphous nature. The PM retained the diffraction peaks of PLFEE at 14.811°, 19.88°, 21.976°, 25.751°, and 41.756° with low intensity and broad peaks of CMs, signifying no alteration in the crystallinity of PLFEE. However, the decreased diffraction intensity of PLFEE in PM is due to the higher proportion of Soluplus®. Such results of decreased diffraction intensity of drugs in the presence of a higher proportion of polymers were reported elsewhere [119]. The X-ray diffractogram of the SD presented a typical halo pattern similar to Soluplus® and Tween® 80 with the nonappearance of the characteristic peaks of PLFEE, signifying the completely amorphous form of PLFEE in the SD. The result reflects that the PLFEE is molecularly dispersed in the CMs of SD [132]. Crystalline material possesses strong crystal lattice

energy, which leads to low aqueous solubility [92]. Therefore, any strategy that results in lower crystal lattice energy or disrupts the crystallinity would improve the water solubility of the drug [92]. SD is an effective formulation strategy to disrupt the crystallinity of the drug partially or totally, resulting in a significant enhancement of solubility. As hydrophilic carriers, Soluplus® and Tween® 80 have been verified to lose the crystallinity of drugs, producing amorphous solid dispersions with improved drug wetting, solubility, and dissolution [92, 106, 107, 114, 118]. In solvent evaporation techniques, after the complete evaporation of the solvent, the drug candidate is ultimately frozen in the carrier matrix without creating a crystal lattice (producing a disordered amorphous state) [114]. The molecular interaction among the PLFEE and CMs (Soluplus® and Tween® 80) could successfully change the crystal form of the PLFEE into an amorphous state.

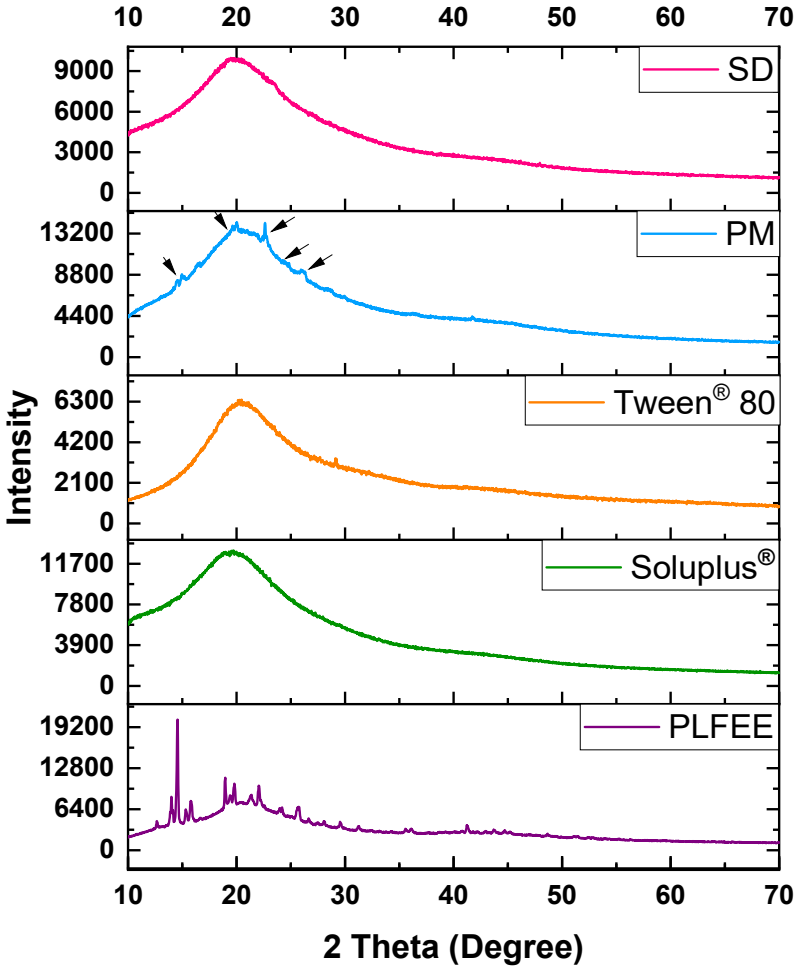

Figure 6. 11 XRD diffractograms of optimized SD and formulation components (PLFEE, Soluplus®, Tween® 80, and PM)

6.4.4.5 Differential scanning calorimetry (DSC)

The DSC study was executed to analyze the thermal behaviors of standardized PLFEE, Soluplus®, PM, and optimized SD (Figure 6. 12). The PLFEE exhibited a sharp endothermic peak at 121.059° C, signifying its crystallinity, attributed to the melting of numerous phytoconstituents. Soluplus® exhibited a broad endothermic peak at 69.567°C corresponding to its glass transition temperature (Tg), representing its amorphous nature [92, 133, 134]. The PM showed both the characteristic endothermic peaks of PLFEE at ~ 121.215°C and CMs at 68.897°C. However, the decreased intensity and slightly broader endotherm of PLFEE are due to a higher proportion of

CMs (dilution effect). The presence of two distinct endotherms in the PM reveals the phase separation state in which the crystalline PLFEE and amorphous CMs co-exist in their original state. In contrast, the thermograms of SD did not display the endothermic peak of PLFEE, signifying a complete transition of crystalline extract into its amorphous state. Similar results have been reported previously [92, 115, 118, 134]. The thermogram of SD displayed a broad endothermic peak at 50.239°C, which is completely different from PLFEE, Soluplus®, and PM. The Tg of Soluplus® was shifted towards its lower temperature (50.239°C), indicating an interaction between PLFEE and CMs. Analogous results of solid dispersion using Soluplus® were reported previously [114, 115]. The drug and CMs remain dispersed at a molecular level in an amorphous solid solution, resulting in a conversion to an amorphous product that displays a single Tg [19]. The SD displayed a single Tg, demonstrating the amorphous and homogeneous form due to the complete miscibility of the PLFEE in the CMs [19]. The obtained Tg of SD was below the corresponding Tg of polymer and above 40°C, which was anticipated to be stable when stored at room temperature [115]. According to the Boyer-Beaman rule, a drug candidate that demonstrates good glass-forming possessions has Tg/Tm (in Kelvin) value higher than 0.67 (i.e., as per the rule of $2/3^{rds}$) to produce solid dispersions [130]. Therefore, with a Tg/Tm value of 0.869 K, PLFEE is anticipated to be able to produce solid dispersion.

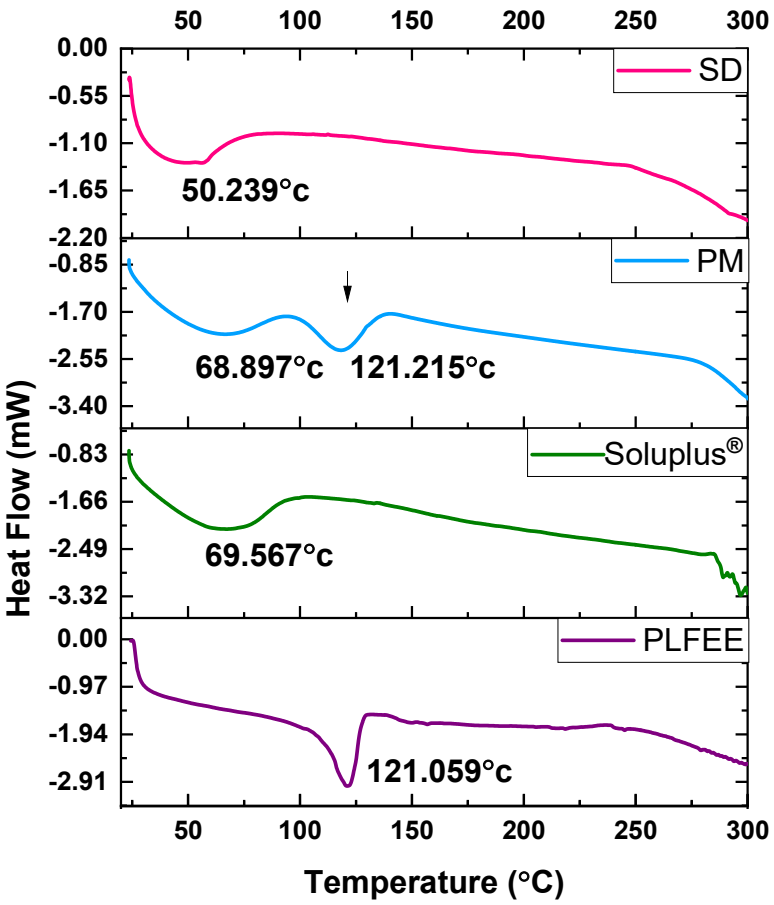

Figure 6. 12 DSC thermograms of PLFEE, Soluplus®, PM, and optimized SD

6.4.4.6 Thermogravimetric analysis (TGA)

TGA was carried out to investigate the thermal degradation pattern of formulation components and formulation. The % weight loss of samples during linear heating from 10°C to 800°C was shown in Figure 6. 13. The PLFEE displayed two-step degradation patterns, with the initiation of weight loss at ~201.978°C, representing its thermal stability up to this temperature. Further, a significant weight loss of 64.206% from 201.978°C to 384.392°C and 17.36% from 384.392°C to 800°C was noticed. Soluplus® showed a four-step degradation pattern, with the first 1.221% loss of weight at 300.78°C due to the evaporation of moisture [135]. Apart from this, no potential degradation was observed up to 300.78°C, demonstrating the thermal stability of

Soluplus® up to this temperature. Similar TGA data of Soluplus® was reported previously [135, 136]. Further, a continuous weight loss of 21.961% between 300.78°C to 355.183°C, 67.97% between 355.183°C to 464°C, and 7.508% between 464°C to 800°C were due to its degradation. PM displayed a steps degradation pattern that is almost identical to that of Soluplus® due to its higher proportion. The initial weight loss of 1.723% is ascribed to moisture loss, followed by stepwise weight loss of 22.958% from 294.53°C to 347.603°C, 66.621% from 347.603°C to 461.761°C, and 7.504 from 461.76°C to 800°C. The SD displayed initial weight loss of 1.324% at 205°C due to moisture loss followed by continuous weight loss of 22.93% from 205°C to 344.03°C, 60.891% from 344.03°C to 467.335°C, and 13.985% from 467.335 to 800°C. The % weight loss of SD in various steps is different from others, reflecting the existence of an entirely new phase other than PM.

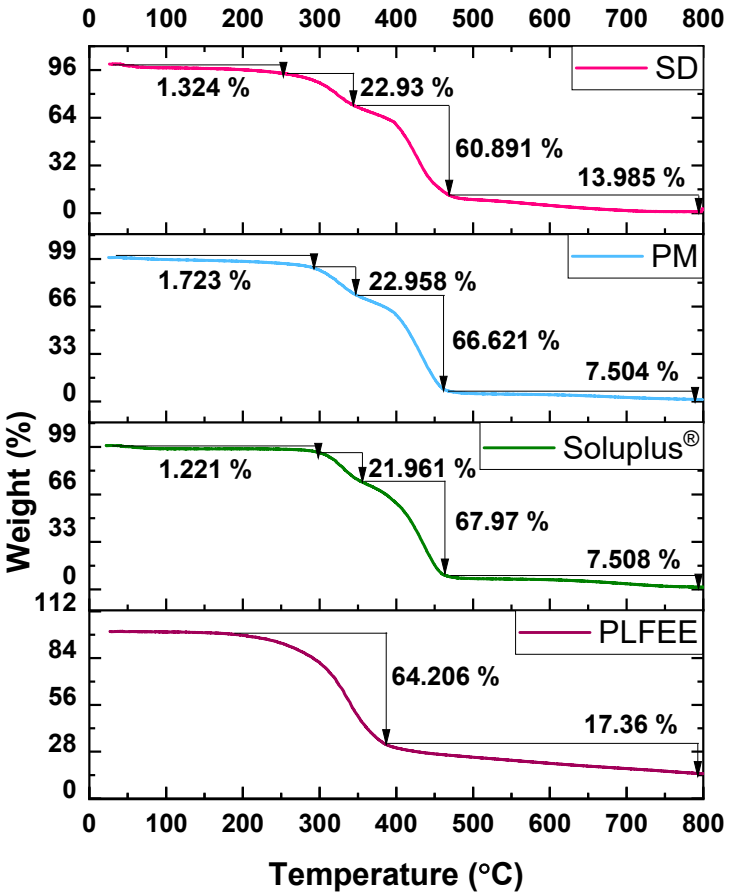

Figure 6. 13 TGA thermograms of PLFEE, Soluplus®, PM, and optimized SD

6.4.4.7 Attenuated total reflectance-Fourier transform infrared spectroscopy (ATR-FTIR)

FTIR is a non-destructive vibrational spectroscopic technique for the investigation of the chemical bonds, composition of the drug, and drug-excipient interactions. When various formulation components are mixed at a molecular level, it creates alterations in the oscillating dipole of the molecules. Such alterations are reflected in terms of the frequency, intensity, and bandwidth of the interacting groups [115]. The results of ATR-FTIR were shown in Figure 6. 14. The standardized PLFEE showed the aromatic C-H stretching at 2928.865 cm^{-1}, aliphatic C-H stretching of methylenedioxy group at 2855.822 cm^{-1}, carbonyl stretching of -C=O-N= at 1635.45 cm^{-1}, C=C asymmetric stretching of aliphatic diene at 1612.843 cm^{-1}, aromatic C=C stretching of benzene

ring 1444.887 cm^{-1}, asymmetrical stretching of =C-O-C at 1246.541 cm^{-1}, symmetrical stretching of =C-O-C at 1036.838 cm^{-1}, C–H bending for trans -CH=CH- at 999.256 cm^{-1}, C-O stretching of methylenedioxy group at 929.315 cm^{-1}. All the assigned peaks of standardized PLFEE are in accordance with the reported data of PIP due to its relatively higher amount in the extract [19, 137]. The bands at 2928.865 cm^{-1}, 1635.483 cm^{-1}, 1612.843 cm^{-1}, 1444.887 cm^{-1}, and 929.315 cm^{-1} were also contributed by structurally similar constituents like piperlongumine, piperlonguminine, and pellitorine. Peaks at 1720.038 cm^{-1} were ascribed to -C=O stretching of the aldehydic or conjugated ester group. The peak at 1273.941 cm^{-1} was ascribed to aromatic -C-N stretching, 1071.567 cm^{-1} was ascribed to an alcoholic -C-O stretching or -C-N stretch of aliphatic amine or -C-O stretch of ester, or -C-O-C stretch of dialkyl ether group, and peak at 742.544 cm^{-1} was ascribed to bending of the aromatic out-of-plane ring. Soluplus® exhibited a strong broad peak at 3411.878 cm^{-1} (alcoholic -O-H stretching of hydrophilic polyethylene glycol subunits), 2929.03 cm^{-1}, and 2860.94 cm^{-1} (aliphatic -C-H stretching), 1730.609 cm^{-1} (-C=O stretching of the ester group of polyvinyl acetate), 1612.82 cm^{-1} (amidic -C=O stretching of polyvinyl caprolactam), 1443.76 cm^{-1} (-C-H bending), and peaks from 1241.05 cm^{-1} to 1025.87 cm^{-1} (-C-O stretching of alcohol or ester or ether groups) [92, 114, 130, 131, 134]. Tween®80 showed a broad peak at 3506.26 cm^{-1} for an alcoholic -O-H stretching, 2921.93 cm^{-1} for asymmetric stretching of -C-H group, 2857.44 cm^{-1} for the symmetric stretching of the -C-H group, and 1734.92 cm^{-1} for -C=O stretching of ester group [138]. The peak at 1646.11 cm^{-1} was ascribed to C=O stretching of the amide group, 1456.133 cm^{-1}, and 1349.24 cm^{-1} were ascribed to -C-H bending of alkane. Peaks from 1296 cm^{-1} to 1093.5 cm^{-1} were ascribed to C-O stretch alcohols, esters, or ethers.

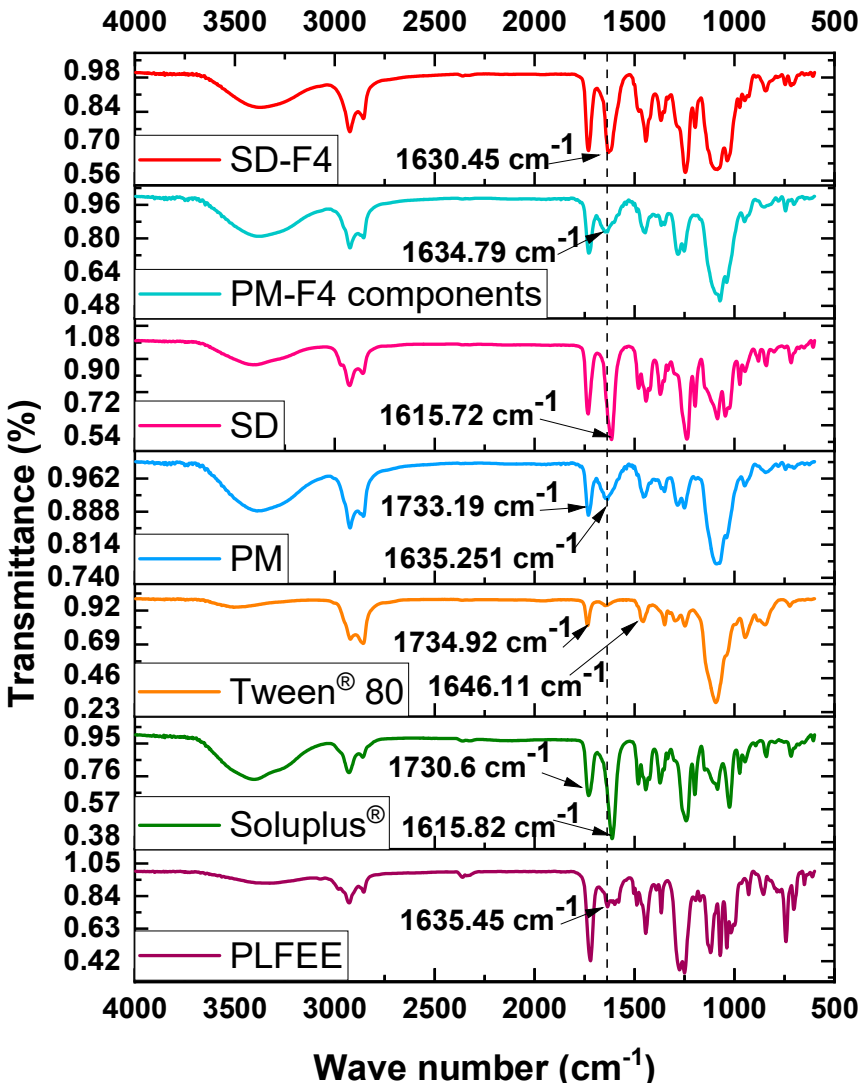

Figure 6. 14 ATR-FTIR results of SD, PLFEE, Soluplus®, Tween® 80, PM, optimized SD, PM of formulation F4, and SD F4

PM showed a strong broad peak at 3378.362 cm^{-1} for an alcoholic -O-H stretching, 2924.278 cm^{-1}, and 2857.564 cm^{-1} for aliphatic -C-H stretching, 1733.196 cm^{-1} for -C=O stretching of the ester group, 1636.81 cm^{-1} for carbonyl stretching of the amide group, 1455.65 cm^{-1} and 1349.92 cm^{-1} for C-H bending of alkane groups, 1284.765 cm^{-1} to 1093.5 cm^{-1} were ascribed to C–O stretch alcohols, esters, or ethers. The FTIR of the physical mixture (PM-F4 components) was recorded to investigate the dilution effect by CMs. A similar FTIR fingerprint was obtained as that of PM. However, the

spectral intensity of PLFEE peaks was found to be increased due to the presence of a lower proportion of CMs in the PM-F4 compared to PM. The spectra of PM and PM-F4 are the superposition of Soluplus®, Tween®80, and PLFEE, representing the chemical compatibility among the used excipients and standardized plant extract [114].

The SD showed a broad vibrational peak at 3413.43 cm^{-1} for an alcoholic -O-H stretching, 2926.99 cm^{-1} and 2858.85 cm^{-1} for aliphatic -C-H stretching, a sharp peak at 1733.378 cm^{-1} for -C=O stretching of the ester group, 1616.873 cm^{-1} for -C=O stretching of the amide group, 1444.22 cm^{-1} for -C-H bending, peaks from 1238.94 cm^{-1} to 1044.79 cm^{-1} for -C-O stretching of alcohol or ester or ether groups. The characteristic peak of PLFEE at 1636 cm^{-1} was found to have disappeared in SD. The spectra of optimized SD showed the predominance of the characteristic peaks of Soluplus®, which might be due to its higher proportion in the formulation. However, in the case of PM, the characteristic peak of PLFEE at 1636 cm^{-1} was retained even at a higher proportion of CMs, which did not support the disappearance of characteristic peaks of PLFEE in SD due to a higher proportion of CMs. The predominance of the characteristic peaks of Soluplus® and the disappearance of the characteristic peak of PLFEE is possibly due to the molecular level trapping of PLFEE inside the CM matrix of SD [139]. A similar result was also observed with SDs of atorvastatin calcium with Soluplus®, where the spectra of SDs lacked characteristics spectrum of atorvastatin calcium and displayed the characteristic peaks of Soluplus® [85]. To elucidate further, the spectra of SD-F4 (containing a lower amount of CMs) were recorded. The intensities of Soluplus® peaks were found to be decreased in SD-F4 due to its lower proportion compared to SD. However, the shifting of characteristic carbonyl stretching (-C=O-N=) band of PLFEE occurred from 1635.66 cm^{-1} to a lower wave number

(1630.45 cm^{-1}). The minute shifting of the carbonyl stretching band in formulations may be ascribed to the possible hydrogen bonding between the -C=O of PLFEE and the hydroxyl group of CMs (Soluplus® + Tween®80). Similar H-bonding between PIP and sorbitol and PEG in the case of solid dispersion was reported previously [19]. There is a slight shifting of the -C=O band in SD-F4, representing partial molecular level interaction of PLFEE and CMs due to a lower proportion of CMs. While witnessing the -C=O stretching band in the physical mixtures (PM-F4 and PM), it could be observed that there was no substantial change in the stretching frequency in the PMs due to the deficiency of interaction among the PLFEE and the CMs. However, in the case of SD, due to the complete molecular interaction and bonding among PLFEE and CMs, the characteristic peaks of PLFEE were found to have disappeared. A similar result of the disappearance of characteristic peaks of darunavir in the SDs with Kolliphor TPGS was reported previously [117]. The polar groups of PIP (PLFEE), such as carbonyl, piperidine ring N, and methylene deoxy, can form a hydrogen bond with the CMs [19]. Such interactions via H-bonding offer molecular level dispersion of the drug in the 3-dimensional network of CMs, hinder the molecular mobility of the drug and hinder phase separation/recrystallization, thus anticipated to offer long-term physical stability to the solid dispersion [19, 25]. Additionally, the drug-CM interaction also provides improved drug solubility and maintenance of a greater degree of supersaturation [25].

6.4.4.8 HPTLC

The compatibility of the extract (mainly PIP and PLGN) with the formulation excipient was also verified by the HPTLC method. The fingerprints of the developed plate are shown in Figure 6. 15a-c. Out of various mobile phases, toluene: ethyl acetate (6:4 v/v) offered the best results at retardation factor (Rf) of 0.39 ± 0.003 for PIP and

0.456 ± 0.0047 for PLGN. The Rf value of PIP and PLGN in the extract (PLFEE) was found to be 0.39 ± 0.0005 and 0.45 ± 0.004, respectively, representing the integrity of PIP and PLGN in the extract. The PM and SD showed the Rf value of PIP (0.39 ± 0.002) and PLGN (0.456 ± 0.0035), which were close to the value obtained for pure components and extract. The fingerprints of the developed plate under 254 nm, 366 nm, and visible light were shown in Fig. 5a-c. The fingerprints (under 245 nm and 366 nm) reflected the presence of chromatographic bands for pure PIP and PLGN in PLFEE, PM, and SD, representing their integrity in the extract, physical mixture, and formulation. Thus, the PLFEE is compatible with the used excipients of the solid dispersion system.

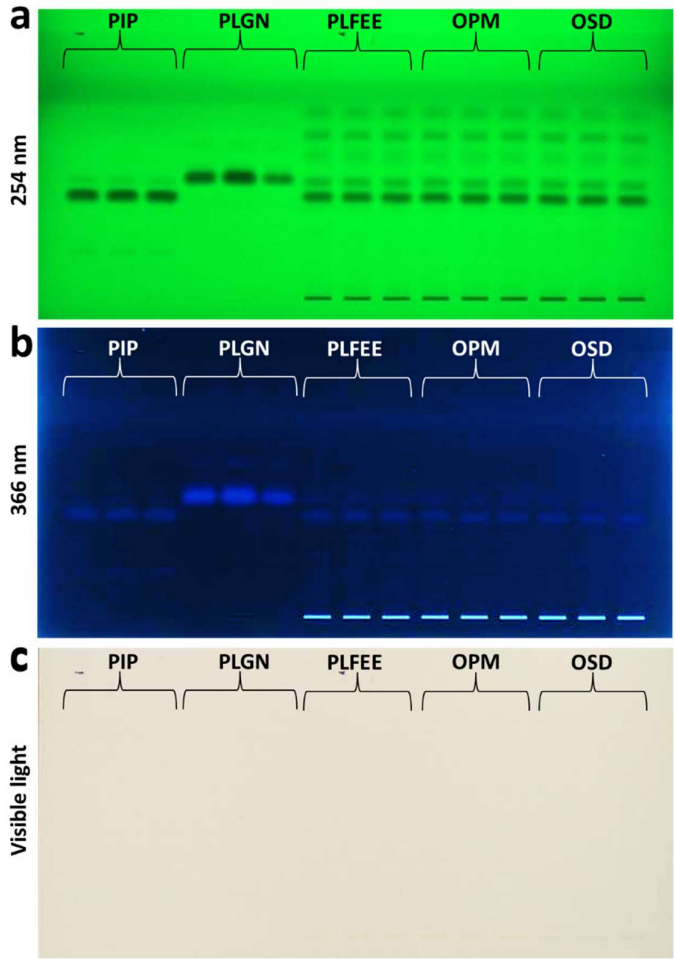

Figure 6. 15 HPTLC fingerprints of PIP, PLGN, PLFEE, PM, and SD (a) fingerprint under 254 nm, (b) fingerprint under 366 nm, and (c) fingerprint under visible light

6.4.4.9 Contact angle

The contact angle was measured to investigate the wettability of PLFEE and SD. The lower the contact angle between the drop of water and the film of solid, the better the wettability [140]. Improved wettability offers enhanced solubility and dissolution. The contact angle (θ) of 0° represents complete wetting, whereas a "θ" of 180° represents no wetting [141]. A contact angle below 65° represents hydrophilicity, and a value higher than 65° represents hydrophobicity [142]. Although the θ can be altered in various solutions, water was frequently used as a wetting solution in such measurements [141, 142]. The mean contact angle (θ_M) against each measurement

(step number) for PLFEE and optimized SD was shown in Figure 6. 16a. The SD film showed a very low contact angle (θ = 17.04° ± 1.27, Figure 6. 16b) and nearly 4.18-fold lesser compared to PLFEE (θ = 71.34° ± 0.913, Figure 6. 16c). The SD was found to be hydrophilic, whereas the PLFEE showed hydrophobicity. The lower θ value of SD may be ascribed to the presence of CMs, their porous structure, and their amorphous nature compared to PLFEE. The CMs used in SD are amphiphilic, which reduces the interfacial tension and, ultimately, the θ value.

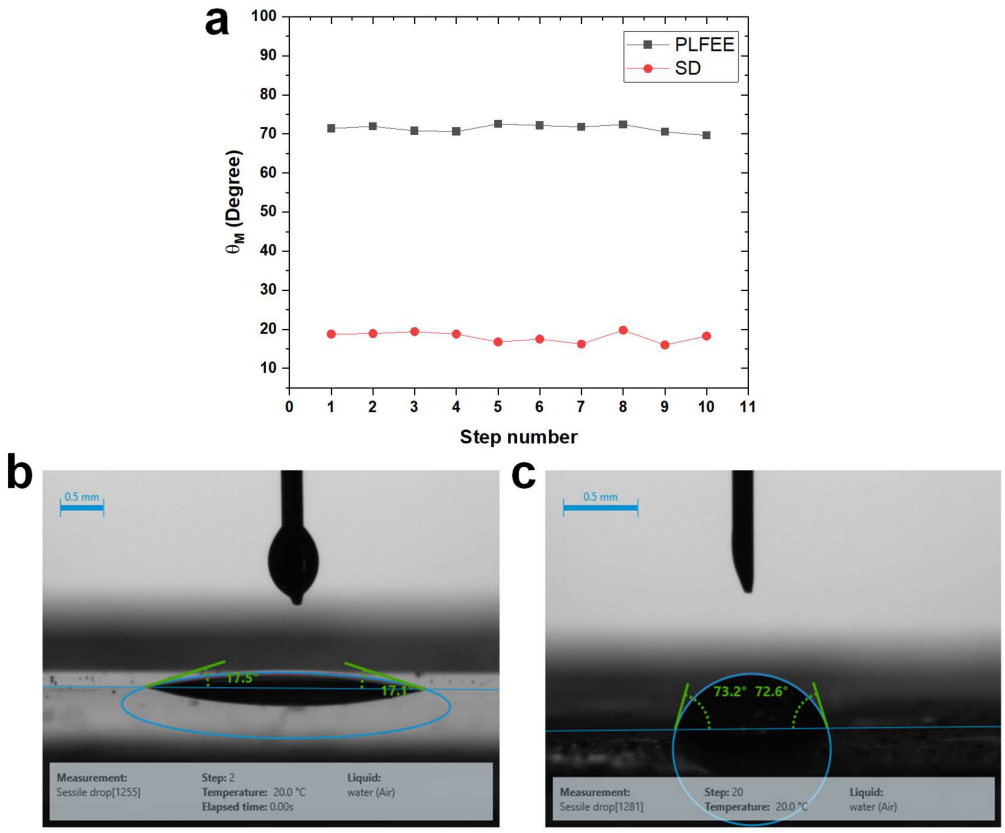

Figure 6. 16 Contact angle measurements (a) mean contact angle (θ_M) of 10 individual droplets, (b) contact angle of the water droplet on SD film, and (c) contact angle of the water droplet on PLFEE film

6.4.4.10 HRSEM

The HRSEM photomicrographs were shown in Figure 6. 17. The PLFEE showed irregular surface morphology (Figure 6. 17a). The Soluplus® showed roughly spherical structures with irregular surface morphology (Figure 6. 17b). The PM showed agglomerated particles of Soluplus® and PLFEE with irregular surface morphology (Figure 6. 17c). The Tween®80 was not distinguished in PM due to its liquid nature which is uniformly coated over the surface of Soluplus® and PLFEE particles. The SD showed irregular particles (Figure 6. 17d). The individual surface properties of formulation components were not observed in SD due to the complete molecular interaction among PLFEE and CMs owing to the creation of new surface morphology during solvent evaporation. The ethanolic solutions of PLFEE and SD were dried on a glass slide and observed after 14 days for possible crystal growth. The dried PLFEE on the glass slide (Figure 6. 17e) showed crystalline blocks representing the phenomenon of natural crystal growth. In contrast, the SD dried on the glass slide appeared as a smooth surface without any crystallinity (Figure 6. 17f), representing the retention of amorphous property and inhibition of nucleation and crystal growth during storage.

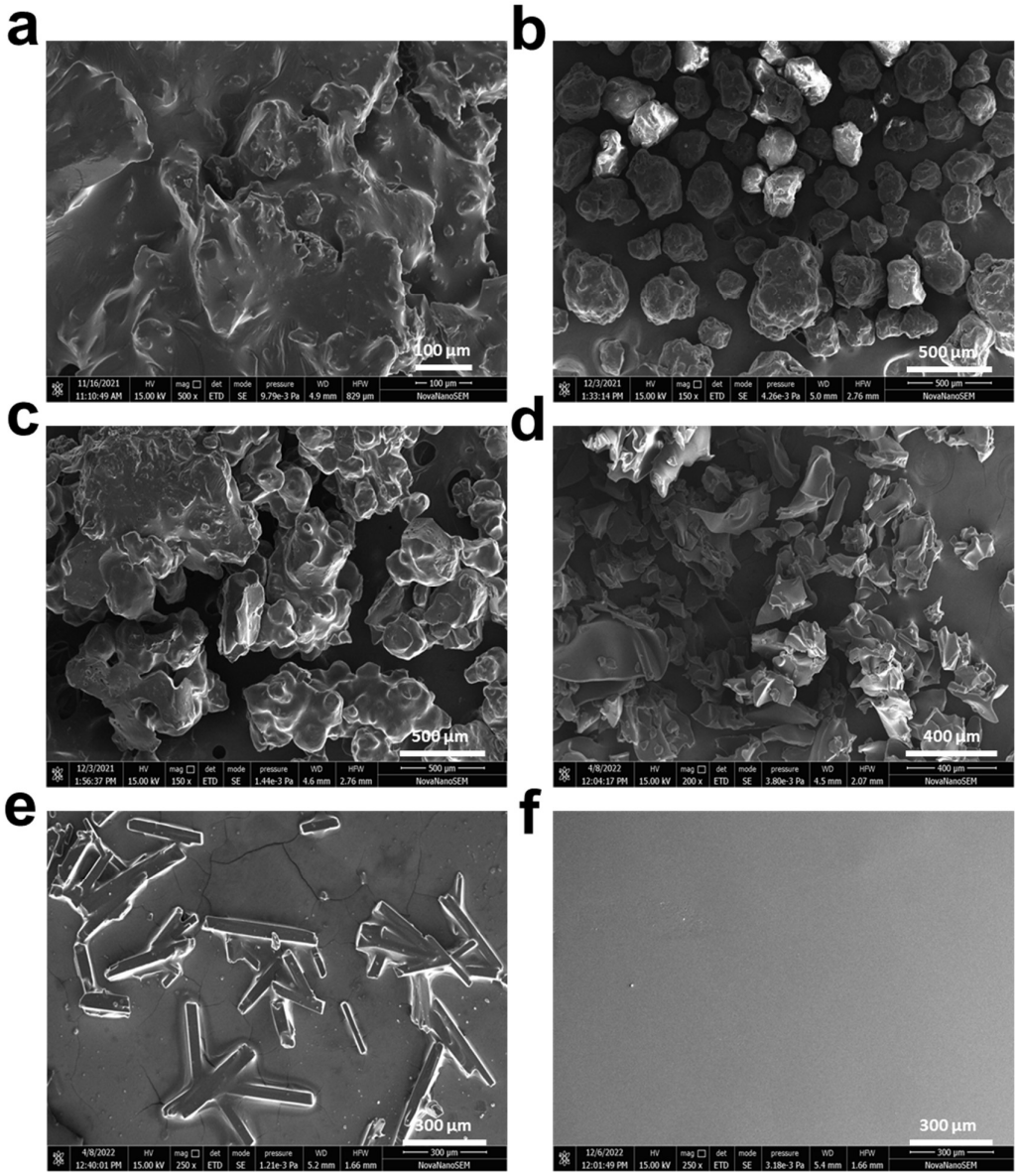

Figure 6. 17 HRSEM results of (a) PLFEE, (b) Soluplus®, (c) PM, (d) SD, (e) PLFEE dried on a slide, and (f) SD dried on a slide

6.4.4.11 PLM

Crystalline materials are optically anisotropic and possess optical birefringence properties. In contrast, amorphous materials (optically isotropic) do not show any birefringence and were observed as a black background. The PLM results of PLFEE, Soluplus®, PM, and SD at 10X magnification are shown in Figure 6. 18. The photomicrographs of the PLFEE demonstrated intense birefringence, reflecting their

crystalline nature. The Soluplus® showed no birefringence due to its amorphous nature. The PM showed optical birefringence, representing the retention of crystallinity of PLFEE in PM. In contrast, the SD exhibited no birefringence, suggesting the complete amorphous conversion of crystalline PLFEE in the solid dispersion. The results of PLM are in accordance with the XRD and DSC results.

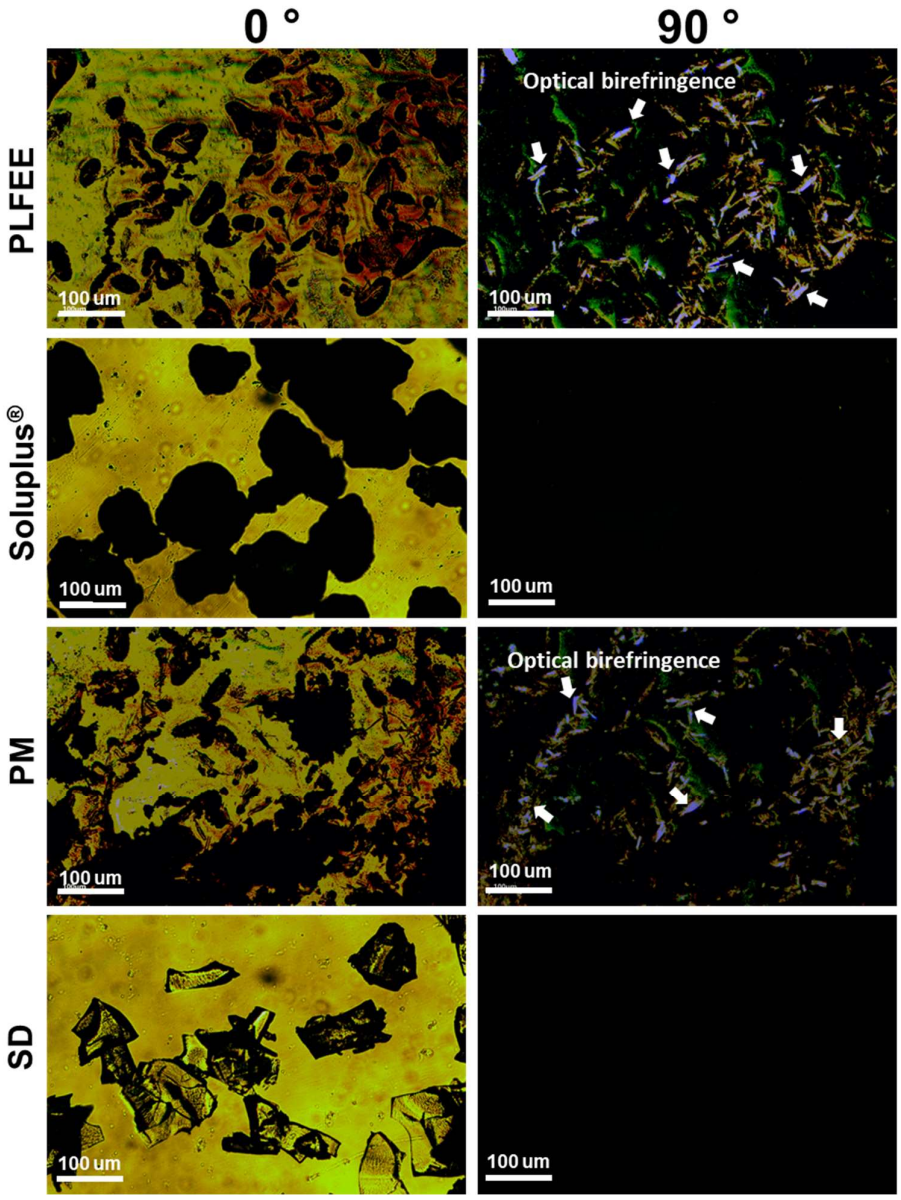

Figure 6. 18 PLM photomicrographs of PLFEE, Soluplus®, PM, and SD at 10X magnification

6.4.4.12 Moisture content analysis

The moisture content of optimized SD measured by the moisture analyzer was found to be 1.124 ± 0.254%, which is in accordance with the initial weight loss of 1.324% obtained from the TGA result. A very low amount of moisture in SD may be due to the adsorption of atmospheric moisture during the handling of the sample. The moisture content values of 1.3-5% were reported with SD systems [143, 144]. High moisture content negatively affects the physical stability of SD. The presence of excess moisture can plasticize the system and further reduce the T_g of SD [144].

6.4.4.13 *In-vitro* dissolution and release kinetics

Poor dissolution is a major rate-limiting step in the oral absorption and bioavailability of poorly aqueous soluble candidates from a solid formulation. Hence, it is of utmost importance to improve the dissolution rate of poorly aqueous soluble drugs to achieve maximum bioavailability and therapeutic efficacy. To assess the impact of CMs, the dissolution pattern of PIP from PLFEE, PM, and SD was studied and compared. The *in-vitro* dissolution profiles of PLFEE, PM, and SD in pH 1.2 are shown in Figure 6. 19. The release of PIP from PLFEE, PM, and SD at 2 h was found to be 10.851 ± 3.845%, 29.867 ± 3.5983%, and 87.383 ± 3.546%, respectively. The PLFEE showed low dissolution owing to its poor aqueous solubility, wettability, and high crystallinity. The dissolution of PIP in the case of PM and SD was found to be significantly ($p<0.05$) enhanced compared to the PLFEE. The SD attained saturation at 6 h. The SD maintains the supersaturation for up to 24 h without any precipitation or decrease in dissolution.

The PM showed improved dissolution compared to the PLFEE and decreased dissolution compared to the SD. The hydrophilic CMs present in the PM possess the surfactant property, which decreases the interfacial tension, causes wetting of the insoluble PIP, solubilizes through micellar solubilization, and ultimately enhances the

saturation solubility. However, the PM is a simple physical mixture of PLFEE and CMs, which did not achieve molecular level interaction, retain the drugs in their original size, and possess crystallinity, hence possess comparatively low dissolution than that of SD. In contrast, the SD is a molecular mixture in which size reduction and amorphous modification occur. The enhanced solubility and dissolution of PIP in SD than PM and PLFEE are ascribed to particle size reduction, reduction of diffusion layer thickness due to smaller particle size, increased surface area, increased wetting, decreased interfacial tension, amorphous modification, inhibition of nucleation or crystal growth, and micellar solubilization [19, 92, 111, 114].

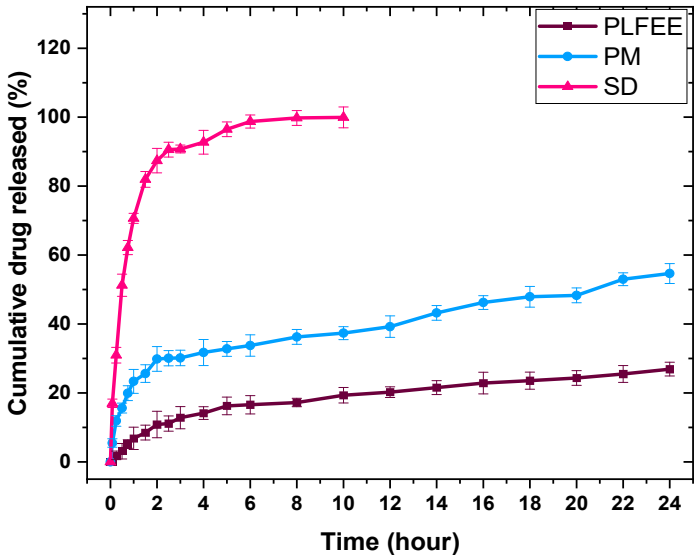

Figure 6. 19 *In-vitro* dissolution study of PLFEE, PM, and optimized SD in pH 1.2. Each analysis was carried out in triplicate, and the results were represented as mean ± standard deviation.

The self-assembling behavior of CMs (i.e., Soluplus® and Tween® 80) produces micelles during dissolution and enhances the solubility of PIP through micellar solubilization. The hypothesized diagram of micellar solubilization by SD is shown in Figure 6. 20. The improved dissolution of SD was further explained through the ‘‘spring and parachute’’ phenomenon. During the dissolution of optimized SD,

supersaturation (spring) was achieved, which was found to be maintained for a longer time (parachute), thereby providing a higher amount of dissolved drug for drug absorption. In SDs, drug candidates are mostly existing as amorphous forms dispersed within the CMs at the molecular level [111]. During exposure to the dissolution media, the drug candidate dissolves with excipients and creates a supersaturated solution [111]. Owing to the highly energetic amorphous form of the drug in a supersaturated solution, there exists a thermodynamic driving force that permits them to undergo nucleation and crystal growth [111]. However, the CMs in the SDs retain the drug in the metastable amorphous state, inhibit the nucleation and crystal growth and maintain the supersaturation for a prolonged time, and ultimately improve the dissolution [19, 25, 111].

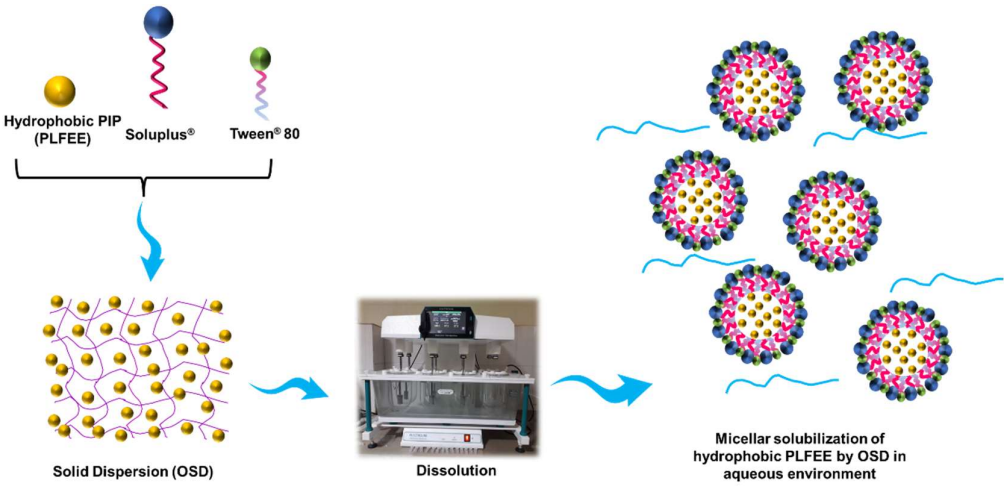

Figure 6. 20 The hypothesized diagram of the micelles of OSD during dissolution

The dissolution data of SD in pH 1.2 was fitted to various kinetic models, and the correlation coefficient (R^2) was estimated for comparison. Table 6. 6 represents dissolution rate constants (K_0, K_1, K_H, K_{kp}, and K_{HC}), correlation coefficients (R^2), and release exponents (n) of various mathematical kinetic models. The data of SD showed the greatest correlation with the Korsmeyer-Peppas model due to the higher R^2 value

(0.916). The goodness of fit of the dissolution behavior of various SDs with the Korsmeyer-Peppas model has been reported by various authors [90, 145, 146]. The mechanism of release was investigated from the Korsmeyer-Peppas model by fitting 60% of the initial dissolution data. The "n" values of <0.45, 0.46-0.88, 0.89, and >0.89 represent Fickian diffusion, anomalous diffusion, case II transport, and supercase II transport, respectively [90]. The SD showed anomalous diffusion (n = 0.6) in pH 1.2, representing that the mechanism of PIP release was predominantly diffusion-controlled.

Table 6. 6 Kinetics of drug release in pH 1.2 up to 24 h

Zero order		**First order**		**Higuchi Model**		**Korsmeyer-Peppas model**		**Hixson-Crowell model**	
K_0	R^2	K_1	R^2	K_H	R^2	K_{kp}	R^2	K_{HC}	R^2
11.274	0.65	0.769	0.904	35.911	0.835	59.156	**0.916**	0.247	0.548

K_0: zero-order release constant, K_1: first order rate constant, K_H: Higuchi dissolution constant, K_{kp}: Korsmeyer release rate constant, K_{HC}: Hixson-Crowell rate constant, n: drug release exponent or diffusional exponent, and R^2: Correlation coefficient

6.4.4.14 Hydrodynamic vesicle size, size distribution, and zeta potential

The average hydrodynamic particle size (Z_{avg}) of SD during dissolution in pH 1.2 was found to be 88.1 ± 2.315 nm (Figure 6. 21a). The SD during dissolution is suspected to form micelle in dissolution media, which could enhance the solubility of PLFEE (mainly the PIP) through a micellar solubilization mechanism. The PDI is a measure of homogeneity of particle size distribution, which varies from 0 to 1 (perfectly uniform to highly polydisperse). Values smaller than 0.1 represents a nearly homogeneous monodispersed sample, and value between 0.1 and 0.2 represents a population with a relatively narrow size distribution, whereas values larger than 0.3 indicates a polydisperse/ heterogenous sample having broad particle size distribution [89]. The formed micelles in pH 1.2 at 37°C were found to be heterogenous, having

a PDI of 0.304 ± 0.01 (Figure 6. 21a). The width of the correlogram and the middle point of the fall represents the PDI and size of vesicles, respectively (Figure 6. 21b).

The zeta potential (ζ) is an indication of colloidal stability. The ζ values from ± 0-10 mV indicate highly unstable, ± 10-20 mV indicate relatively stable, ± 20-30 mV indicate moderately stable, and values greater than ± 30 mV represent high colloidal stability [96]. The value of zeta potential was found to be 0.894 ± 0.123 mV in pH 1.2 (Figure 6. 21c). The phase plot (Figure 6. 21d) showed an irregular pattern due to very low ζ value. Such low ζ value, nanometric Z_{avg}, and PDI of Soluplus® micelle were reported elsewhere [109].

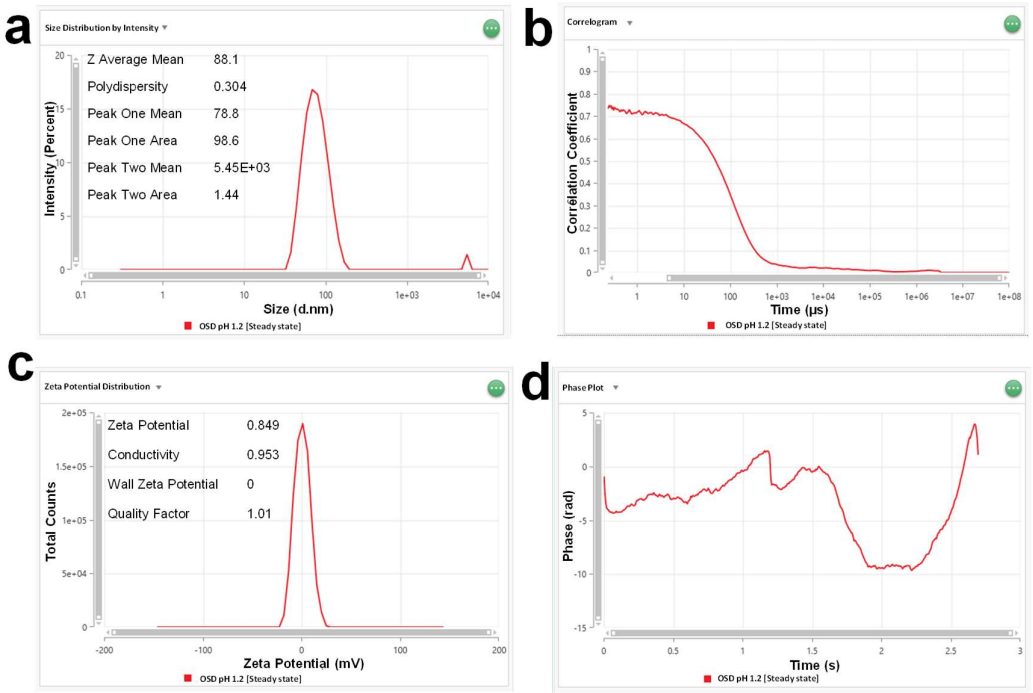

Figure 6. 21 Hydrodynamic particle size, polydispersity index, and zeta potential on formed micelles during dissolution (a) Z_{avg}, (b) correlogram, (c) ζ, and (d) phase plot

6.4.4.15 HRTEM and SAED analysis

The HRTEM results of SD in pH 1.2 at 0.5 µm (Figure 6. 22a) and 200 nm scale (Figure 6. 22b) revealed the spherical-shaped nano micellar structure with smooth

surface morphology, having a mean micelle size (average size of 17 micelles) of 85.116 ± 14.13 nm. The high standard deviation is due to the heterogeneity of the produced micelles. The size distribution chart revealed that most of the micelles were within the range of 80 nm to 90 nm (Inset Figure 6. 22c). The SAED results (Figure 6. 22d) displayed a diffused ring pattern, implying the retention of the amorphous form of the SD in pH 1.2.

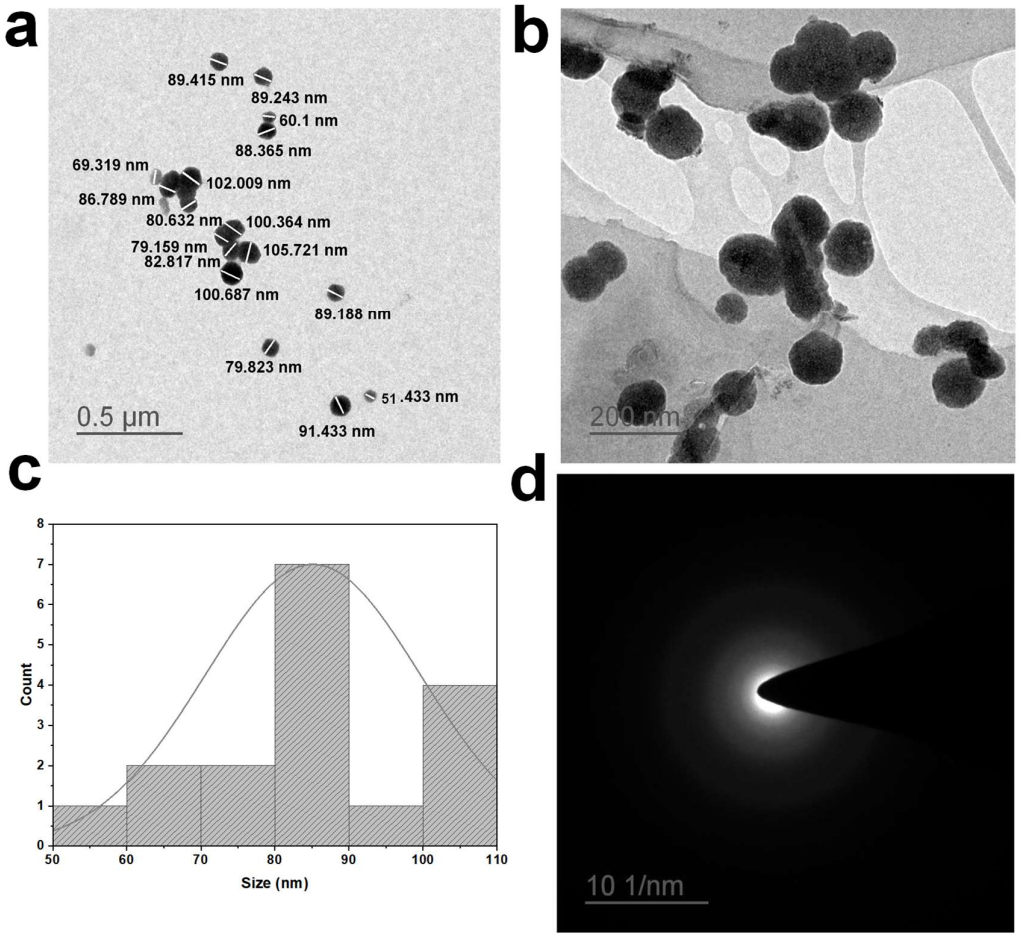

Figure 6. 22 HRTEM and SAED results of produced micelles in pH 1.2 dissolution media (a) HRTEM photomicrograph of micelles at 0.5 µM scale, (b) size distribution, (c) HRTEM photomicrograph of micelles at 200 nm scale, and (f) SAED pattern

6.4.4.16 Stability Study

When the SD containing hard-gelatin capsules were warped in double-layer aluminum foils and tested under accelerated (40 ± 2°C and 75 ± 5% RH) stability conditions, the

physical appearance, drug content (97.879 ± 1.57%) and saturation solubility (5.813 ± 0.034 mg/mL) remained unchanged. The XRD, DSC, TGA, and ATR-FTIR outcomes of the accelerated stability study are represented in Figure 6. 23.

The XRD (Figure 6. 23a) and DSC results (Figure 6. 23b) revealed the retention of the amorphous nature of the SD throughout the stability study in all stability conditions. The % weight loss of SD with respect to the temperature observed through TGA analysis remained unaltered, revealing the retention of thermal property (Figure 6. 23c). The characteristic vibrational peaks of SD (Figure 6. 23d) observed at various time points were found to be retained throughout the stability study without shifting or disappearance of important peaks, signifying the retention of its chemical integrity. The stability of solid dispersions is always troublesome owing to the aging problem. However, the SD showed excellent stability in terms of physical appearance, drug content, saturation solubility, crystallinity, thermal behavior, and chemical composition.

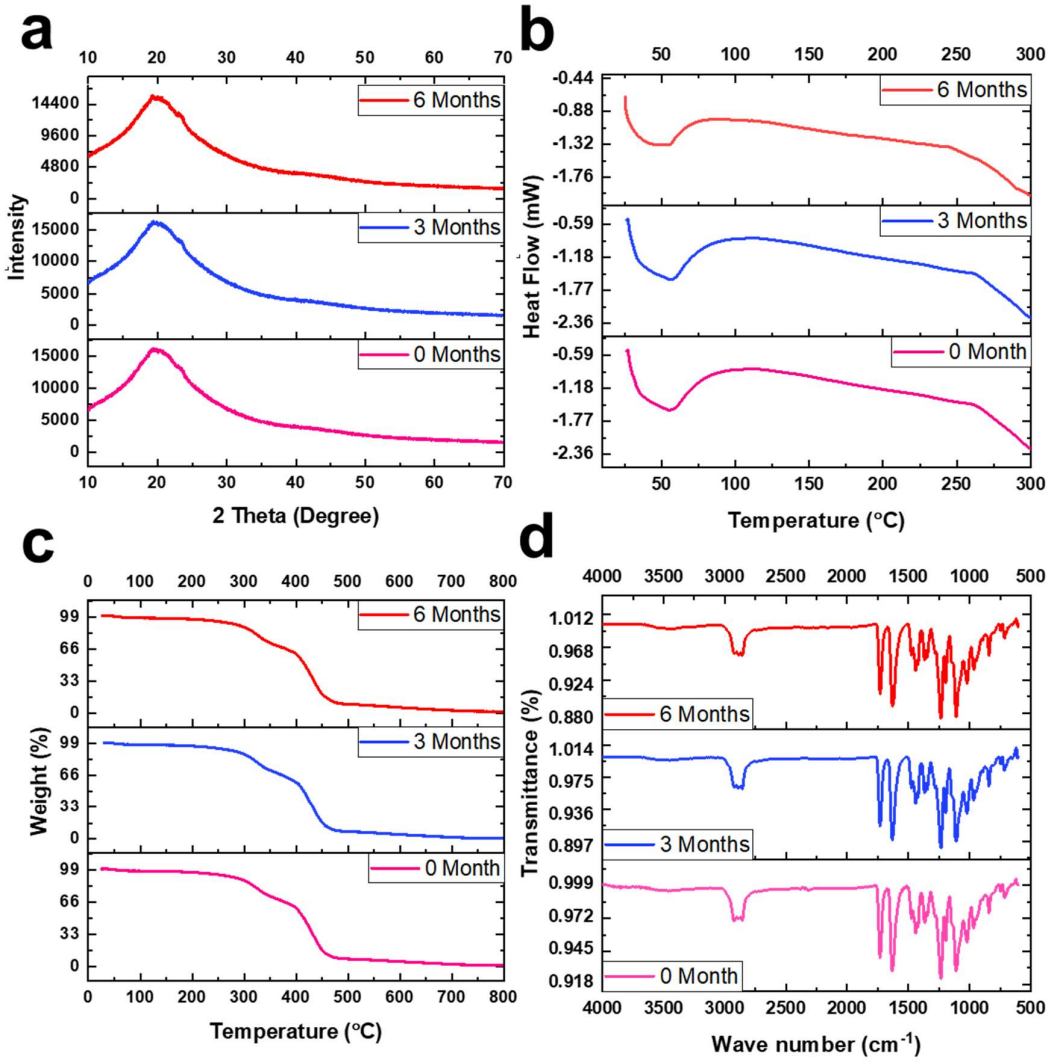

Figure 6. 23 Accelerated stability study of optimized SD up to 6 months at an interval of 3 months (a) XRD, (b) DSC, (c) TGA, and (d) ATR-FTIR

6.4.5 *In-vitro* cytotoxicity

B16F10 melanoma cell line was used as the cancerous cell line, and the human embryonic kidney cell line (HEK 293) was chosen as a non-cancerous (normal) cell line for cytotoxicity comparison. The cytotoxicity results of PLFEE suspension, PLFEE solution, optimized SD, and DTIC against B16F10 and HEK293 after 24 h are presented in Figure 6. 24a-f. The optimized SD showed improved dose-dependent cytotoxicity against B16F10 cells compared to PLFEE suspension and PLFEE solution (Figure 6. 24a). The standard anticancer drug, DTIC also demonstrated dose-

dependent cytotoxicity against B16F10 cells (Figure 6. 24b). The log concentration of PLFEE suspension, PLFEE solution, optimized SD v/s % cell viability of B16F10 were presented in Figure 6. 24c. The calculated IC_{50} values of PLFEE suspension, PLFEE solution, optimized SD against B16F10 were found to be 516.51 ± 3.286 (R^2 = 0.978), 87.41 ± 2.149 (R^2 = 0.998), and 57.25 ± 2.396 µg/mL (R^2 = 0.985), respectively. The tested negative control (placebo SD and 0.2 % DMSO) did not show any cytotoxicity to the B16F10 cell line (data not shown), indicating the cytotoxicity is only for the standardized PLFEE and DTIC. The estimated IC_{50} value as per non-linear regression analysis (Figure 6. 24d) for DTIC was found to be 29.22 ± 2.172 µg/mL (R^2 = 0.978). The tested PLFEE suspension, PLFEE solution, optimized SD, and DTIC showed no cytotoxicity towards the normal HEK 293 cell line (Figure 6. 24e and Figure 6. 24f). Such outcomes represent their selective cytotoxicity towards cancer cells without harming the normal cells.

Thus, the important outcomes of the study were that the cytotoxicity of optimized SD against B16F10 melanoma cells was found to be significantly higher ($p<0.05$) than PLFEE suspension and PLFEE solution (Figure 6. 24c). The optimized SD improved the cytotoxicity activity of the standardized PLFEE. The higher cytotoxicity of SD might be ascribed to its high cell uptake and partitioning into the cells. During the *in-vitro* assay, the free PLFEE (suspension) diffuses throughout the intracellular environment via the passive diffusion mechanism. Due to the limited solubility and therefore, the low concentrations of PLFEE in the surrounding media, low cellular uptake occurred, leading to low cytotoxicity. In contrast, the PLFEE solution (in 0.2 % DMSO) showed improved cytotoxicity due to relatively higher concentration in the local media and better diffusion. In the case of optimized SD, it not only improved the solubility in the surrounding media but also improved the partitioning/ membrane

permeability into the cell due to the micellar formation (as observed previously). The micellar property is contributed by the amphiphilic Soluplus® and Tween®80. The outcome of the cytotoxicity study is in accordance with the reported outcomes of curcumin SD compared to a neat drug, where the authors found improved cytotoxicity of curcumin SD against human glioblastoma (U-87 MG) and breast cancer (MCF-7) cell lines [147]. In recent work, curcumin SD also showed improved *in-vitro* cytotoxicity against colorectal adenocarcinoma cells (SW480) compared to pure curcumin [148]. In another work, the SD of curcumin also demonstrated improved cytotoxicity against human breast cancer cell line (MDA-MB-23) than that of unformulated curcumin [149].

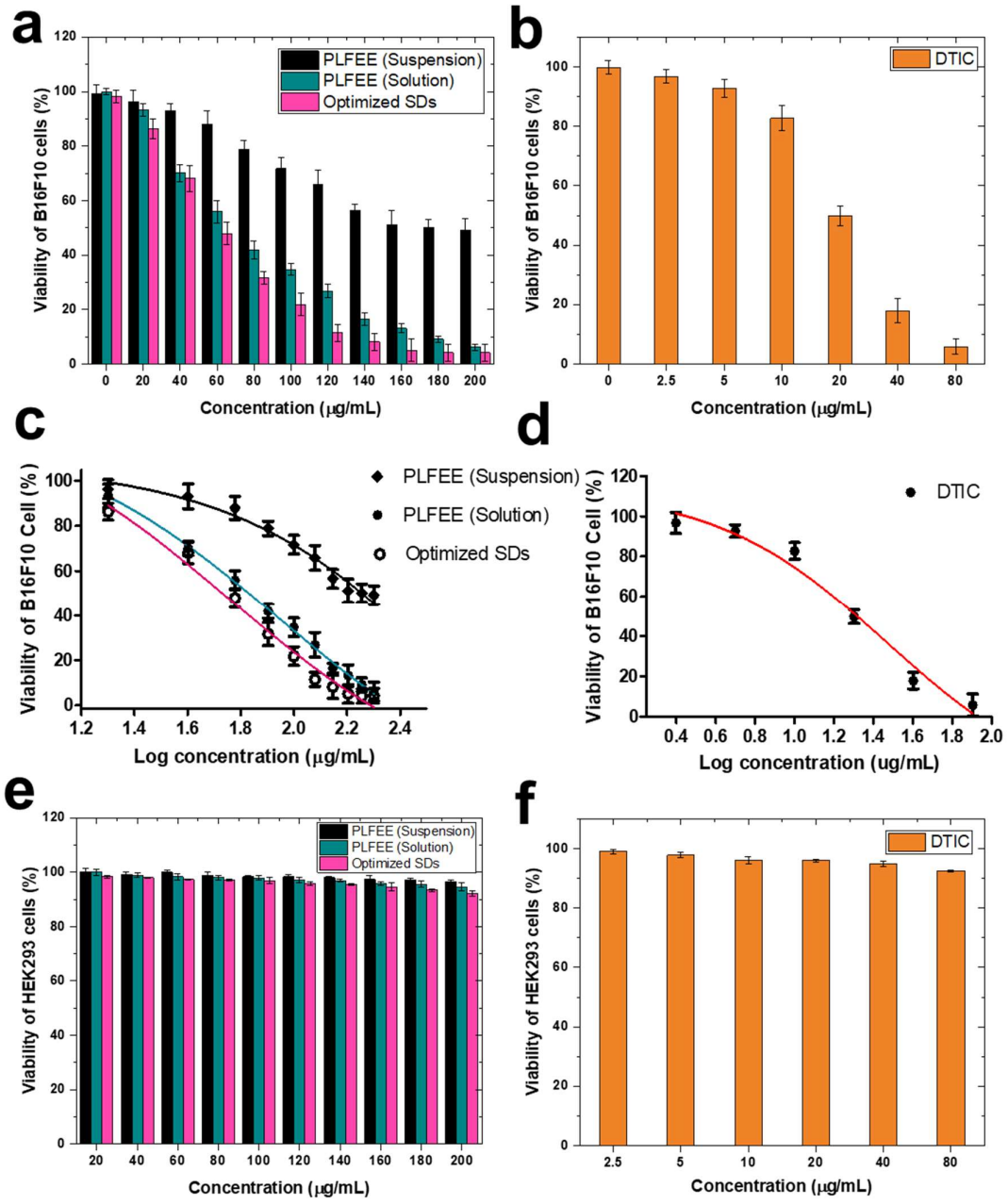

Figure 6. 24 Cytotoxicity studies (a) cytotoxicity of PLFEE suspension, PLFEE solution, and optimized SD against B16F10 after 24 h, (b) cytotoxicity of DTIC against B16F10 after 24 h, (c) log (concentration) of PLFEE suspension, PLFEE solution, and optimized SD v/s viability (%) of B16F10 after 24 h, (d) log (concentration) of DTIC v/s viability (%) of B16F10 after 24 h, (e) cytotoxicity of PLFEE suspension, PLFEE solution, and optimized SD against HEK 293 cells after 24 h, and (f) cytotoxicity of DTIC against HEK293 after 24 h. Each data point represents the mean ± SD of three independent experiments.

6.4.6 Cell migration assay (*in-vitro* wound healing assay)

The photomicrographs of *in-vitro* cell migration assay are represented in Figure 6. 25a, and the % cell migration is represented in Figure 6. 25b. After 12 h, the control group (without any treatment) showed 83.886 ± 3.425 % of wound area occupied (% migration) by the cells, and after 24 h, it showed complete migration, representing rapid cell migration. In contrast, the standardized PLFEE showed 50.791 ± 2.143 % and 80.075 ± 2.124 % of the wound areas occupied by cells at 12 and 24 h, respectively. Further, the optimized SD showed a relatively low migration area of 41.276 ± 2.843 % and 60.316 ± 2.378 % at 12 and 24 h, respectively, indicating suppression of cell motility. The standardized PLFEE and optimized SD significantly ($p<0.05$) inhibited the motility of B16F10 cells compared to the control group at 12 and 24 h (Figure 6. 25b). Further, the optimized SD also significantly inhibited the % of cell migration compared to the standardized PLFEE (Figure 6. 25b). The B16F10 is a highly metastatic variant of murine melanoma cell line, which rapidly migrate towards the wound area and occupied 100 % area after 24h. The standardized PLFEE possesses the inherent cytotoxic activity, hence inhibiting the migration of the cells up to a certain extent (relatively low wound area occupied by cells). The optimized SD has significantly higher inhibitory action, which is ascribed to the improved solubility in media partitioning/ membrane permeability into the cell due to the micellar formation.

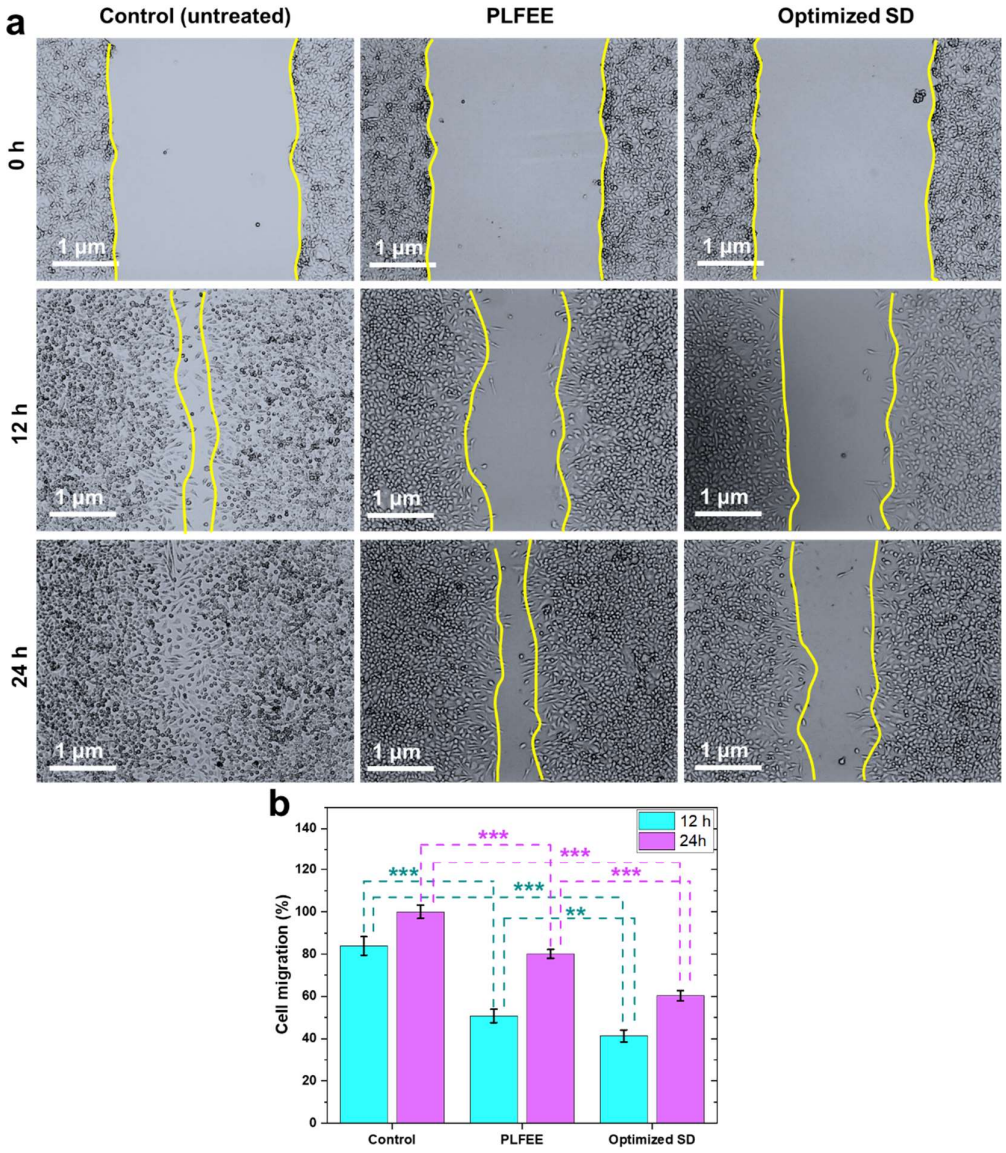

Figure 6. 25 *In-vitro* cell migration assay (a) inhibitory effect of PLFEE and optimized SD on the motility of B16F10 cells and (b) percentage cell migration in the presence of PLFEE and optimized SD. Each data point represents the mean ± SD of three independent experiments. The statistical analysis was carried out using one-way ANOVA followed by Tukey's multiple comparison test at $p<0.05$

6.4.7 *In-vivo* oral bioavailability

6.4.7.1 Bioanalytical HPLC Method for quantitative estimation of Piperine (PIP) in plasma

Based upon our previous observation of PIP having easily identifiable sharp peak with retention time within 10 min at 80:20 v/v methanol and water as mobile phase, the same mobile phase was tried to develop the HPLC chromatogram of p-DMAB as IS in the presence of PIP extracted from plasma samples. Very sharp and well-distinct chromatograms of PIP and IS (Figure 6. 26a) were observed with the selected mobile phase at Rt of 7.02 ± 0.062 and 4.113 ± 0.026 min, respectively. The absorption maxima (λmax) obtained from DAD spectra of PIP (Figure 6. 26b) and p-DMAB were found to be 342 and 346 nm, respectively (Figure 6. 26c), confirming the identity of PIP and p-DMAB [78]. The two-dimensional (2-D) and three-dimensional (3-D) chromatograms (Figure 6. 26d and Figure 6. 26e) confirmed the absence of any peaks around the elution time of PIP or p-DMAB. However, very minute bands around Rt of 2-3 Min were due to the blank plasma and mobile phase, in which intensity is very low and found to be decreased upon gradual increasing the concentration of the analyte.

6.4.7.1.1 Validation of bioanalytical HPLC method

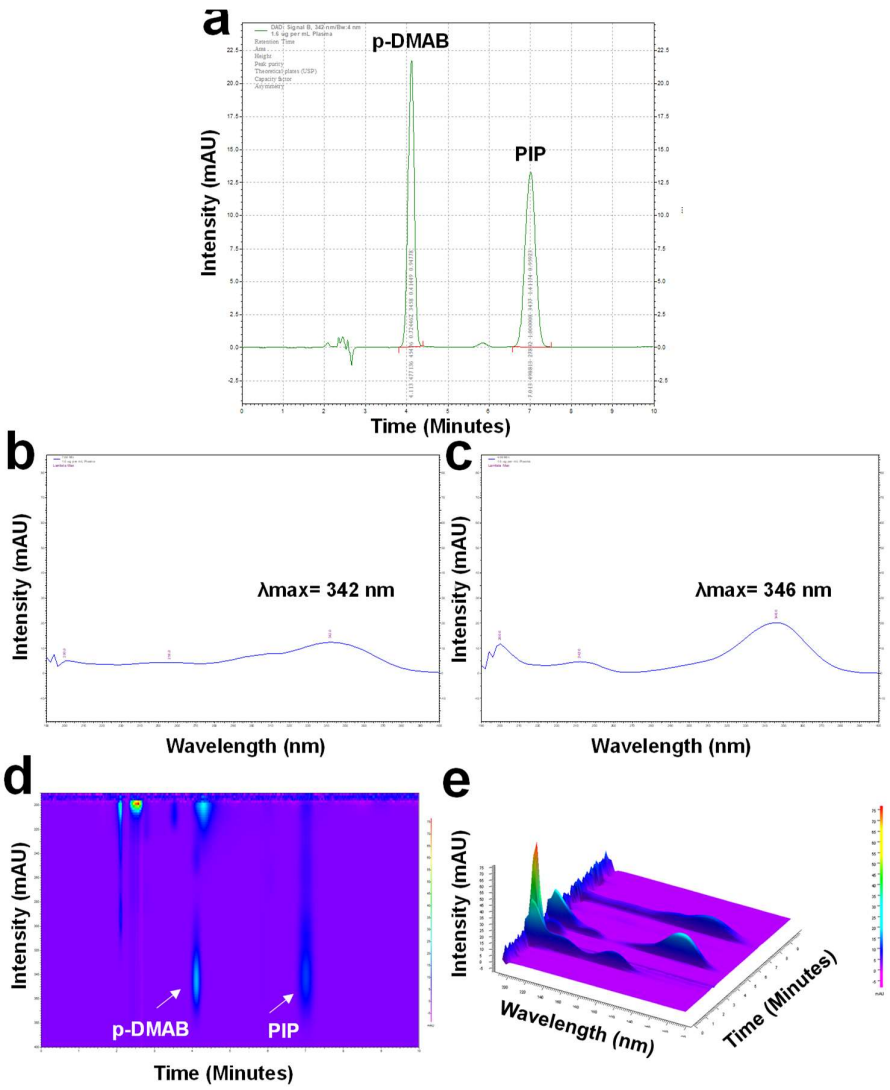

Figure 6. 26 Chromatograms of PIP (1.6 µg/mL) and p-DMAB (1 µg/mL) in mobile phase methanol and water (80:20 v/v) (a) chromatogram of PIP (Rt = 7.02 ± 0.062 min) and p-DMAB (Rt = 4.113 ± 0.026 min) at wavelength 342 nm, (b) DAD absorption spectrum of PIP having λmax = 342 nm (c) DAD absorption spectrum of p-DMAB having λmax = 346 nm, (d) 2-D contour chromatogram of PIP and p-DMAB, and (e) 3-D chromatogram of PIP and p-DMAB

6.4.7.1.2 Linearity and range

The average area ratio (Area of PIP: Area of IS) of three repetitive measurements plotted against respective concentrations were presented in Figure 6. 27a. A linear relationship was obtained between the selected concentrations of PIP (0.05 to 25.6

µg/mL) and the chromatographic area ratio (at 342 nm) with correlation coefficients (r^2 = 0.999) and regression equation y = 0.67195 x – 0.04527 (n = 3).

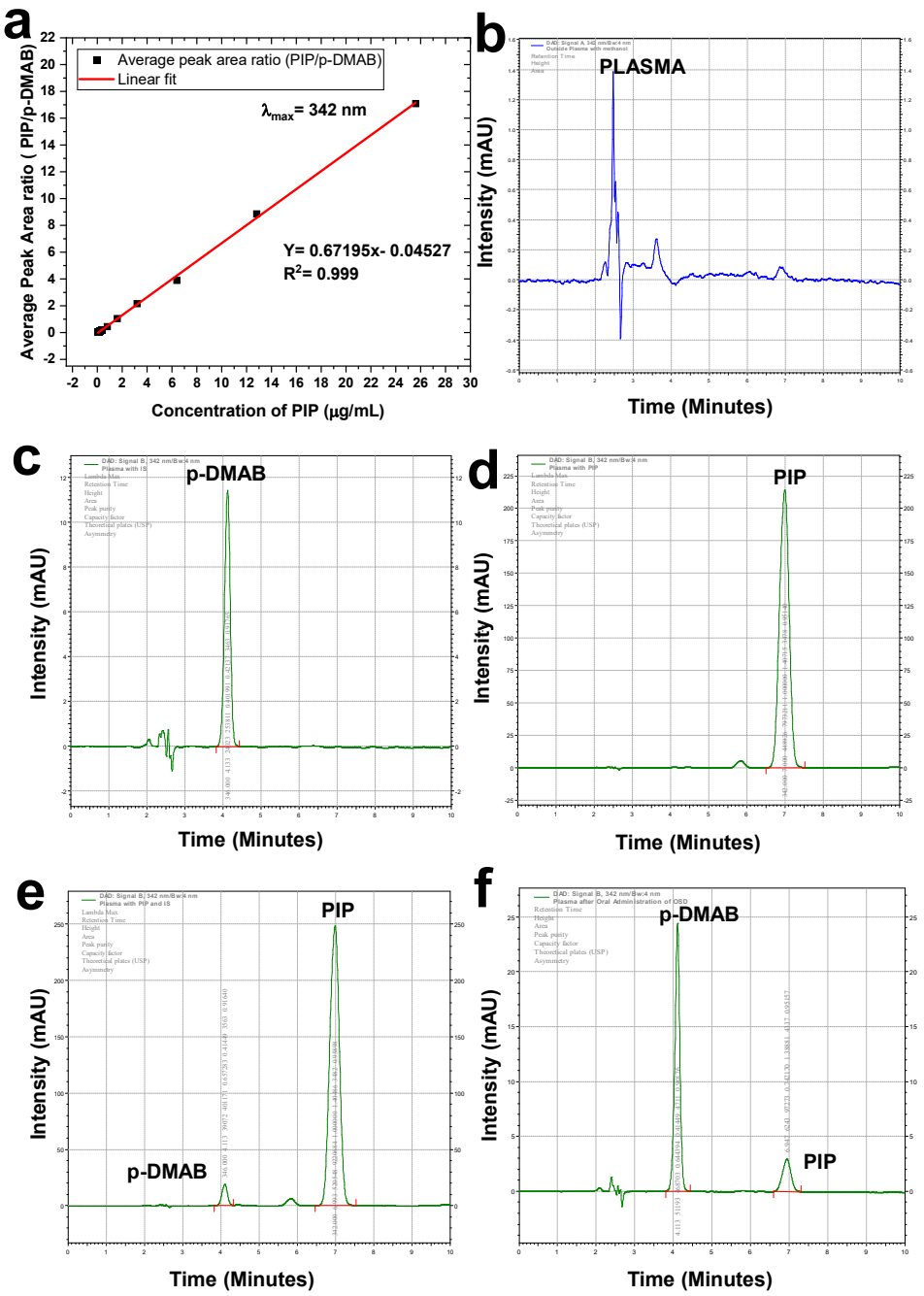

Figure 6. 27 Calibration curve and selectivity study (a) calibration curve of PIP in plasma at wavelength 342 nm with p-DMAB as IS, (b) HPLC chromatograms of blank rat plasma, (c) plasma spiked with p-DMAB (0.354 µg/mL), (d) plasma spiked with PIP (25.6 µg/mL), (e) plasma spiked with p-DMAB (1 µg/mL) and PIP (25.6 µg/mL), and (f) extracted plasma sample after oral administration of optimized solid dispersion (OSD) with the p-DMAB (1 µg/mL) as internal standard

6.4.7.1.3 Selectivity

The selectivity of the HPLC method was verified for examining the endogenous interference or matrix effects of plasma components with the analyte. The selectivity of the HPLC method towards the analyte and IS is shown in Figure 6. 27b-f. The blank plasma showed a less intense peak around 2 to 3 min (Figure 6. 27b). The absence of any interfering plasma peak at the retention time of IS (Rt = 4.113 ± 0.026 min) and analyte (Rt = 7.02 ± 0.062 min) reflected the selectivity of the developed HPLC method (Figure 6. 27c, Figure 6. 27d, and Figure 6. 27e) [78]. The extracted plasma (Figure 6. 27f) after oral administration of PLFEE also showed the two distinguished peaks of p-DMAB (spiked) and PIP, which is very far from the plasma matrix peak. The detection of PIP and IS by HPLC was highly selective, with no interferences of the plasma matrix components.

6.4.7.1.4 Accuracy

The closeness of theoretical and experimental values indicates the accuracy of the analytical method. The results of the accuracy of PIP evaluated in terms of % RE were represented in Table 6. 7. The % RE values are within the acceptance limit (<20%) prescribed as per the FDA guideline.

Table 6. 7 Accuracy studies of the developed HPLC method for estimation of PIP in plasma (n = 3)

Level (%)	**PIP spiked concentration or actual value (µg/mL)**	**Experimental concentration or observed value (µg/mL)**	**% RE**
Low	0.1	0.106 ± 0.005	6
Medium	1.6	1.59 ± 0.047	-0.625
High	25.6	25.742 ± 0.053	0.554

6.4.7.1.5 Precision

Precision represents the closeness among a series of readings obtained from multiple samples of the same homogeneous sample under specified analytical conditions. In the present study, the repeatability and intermediate precision (intra-day and inter-day) studies were performed to study the precision of the HPLC method for different concentrations (0.1, 1.6, and 25.6 µg/mL) of working standard solution. The results of the precision study are summarized in Table 6. 8. The % RSD values obtained from the repeatability study were below 20%, which fulfilled the acceptance criteria and showed a high degree of precision of the developed HPLC method for quantitative analysis of PIP in plasma [99, 150].

Table 6. 8 Precision results of the developed HPLC method for quantification of PIP in plasma

Concentration of PIP (µg/mL)	**Obtained area ratio ± SD (mAU)**		**RSD (%)**	
1.6	1.0481 ± 0.002		0.196	
Concentration of PIP (µg/mL)	**Intra-day (at an interval of 6 h)**		**Inter-day (Day1-Day3)**	
	Obtained area ratio ± SD (mAU)	**RSD (%)**	**Obtained area ratio ± SD (mAU)**	**RSD (%)**
0.1	0.02888 ± 0.0004	1.548	0.02878 ± 0.0005	1.953
1.6	1.04619 ± 0.001	0.102	1.05021 ± 0.006	0.571
25.6	17.1522 ± 0.245	1.433	17.1193 ± 0.2024	1.182

6.4.7.1.6 Sensitivity (LLOD and LLOQ)

The LLOQ is the lowest concentration of the tested analyte, producing a signal-to-noise ratio of 10:1, at which the accuracy and precision are less than 20% [150, 151]. The LLOD and LLOQ values of the developed method for the quantification of PIP in plasma were found to be 0.031 and 0.095 µg/mL, respectively. The lower value of LOD and LOQ represents a good sensitivity of the analytical method for analysis of PIP in plasma, even at very low concentrations.

6.4.7.1.7 Percent extraction recovery (PER)

The PER represents the extraction ability of the used organic solvent in the developed method for extraction of analyte and IS. As per the FDA guideline, the PER need not be 100%, but the extent of the recovery of an analyte and of the used IS should be reproducible and consistent [99]. The mean PER of PIP and IS from the plasma were found to be 93.023 ± 1.1529 to 94.935 ± 0.045% and 97.05 ± 1.6385%, respectively (Table 6. 9). The consistent and high PER values demonstrated the suitability of the used method for the extraction of analytes from plasma and their quantification through the developed HPLC method.

Table 6. 9 Percent extraction recovery (PER) of PIP and p-DMAB through the developed HPLC method (n = 3)

Level (%)	**PIP spiked concentration or actual value (µg/mL)**	**PER ± SD (%) (n = 3)**
Low	0.1	93.023 ± 1.1529
Medium	1.6	94.162 ± 0.25
High	25.6	94.935 ± 0.045
	IS spiked concentration or actual concentration (µg/mL)	PER ± SD (%) (n = 6)
	0.67	97.05 ± 1.6385

6.4.7.1.8 Robustness and Ruggedness

The developed HPLC method showed the lower % RSD values (<2%) of peak area ratio and retention time (Table 6. 10) under deliberate changes in the chromatographic condition, confirming the robustness of the developed HPLC method for the estimation of PIP in plasma.

Table 6. 10 Robustness and ruggedness study of developed HPLC method for estimation of PIP (1.6 µg/mL) in rat plasma

Parameters	Variations made	Area ratio ± SD (mAU)	RSD (%)	Retention time (Rt) ± SD (min)	RSD (%)
Wavelength (nm)	340	1.058 ± 0.007	0.711	7.08 ± 0.024	0.352
	342	1.032 ± 0.006	0.603	7.08 ± 0.024	0.352
	344	1.016 ± 0.004	0.579	7.06 ± 0.013	0.303
Run Time (min)	8	1.034 ± 0.003	0.342	7.074 ± 0.024	0.347
	10	1.0328 ± 0.006	0.603	7.08 ± 0.024	0.352
	12	1.0279 ± 0.002	0.273	7.033 ± 0.033	0.483
Flow rate (mL/ min)	0.8	1.035 ± 0.001	0.099	8.811 ± 0.002	0.032
	1	1.032 ± 0.007	0.682	7.08 ± 0.024	0.352
	1.2	1.042 ± 0.008	0.855	5.877 ± 0.013	0.23
Mobile phase composition (Methanol: Water) (v/v)	78:22	1.034 ± 0.007	0.686	7.853 ± 0.032	0.418
	80:20	1.038 ± 0.004	0.441	7.08 ± 0.024	0.352
	82:18	1.035 ± 0.006	0.633	6.29 ± 0.008	0.129

6.4.7.1.9 System Suitability

The system suitability checks the specificity and validity of the developed analytical method. The % RSD of different validation parameters, such as retention time (Rt), peak area, number of theoretical plates, peak purity, tailing factor, and capacity factor, was estimated for system suitability analysis (Table 6. 11). The % RSD of all examined parameters was within the permissible limits (<2%) [78]. The number of theoretical plates (N>2000) and tailing factor (<2) were within the acceptable limit [78].

The peak purity of PIP was found to be 0.992 ± 0.007, which is close to a unit, representing a high degree of purity [152]. The capacity factor (K^1) represents the degree of interaction of the analyte with the stationary phase in the column. A capacity factor of zero indicates no interaction, whereas a capacity factor >1 indicates a certain degree of interaction with the stationary phase. Ideally, a capacity factor of an analyte varies from 1-5. A higher value of capacity factor (>20) indicates a greater degree of

interaction of analytes with the stationary phase, which leads to prolongation of elution time. The K^1 value for estimation of PIP was found to be within the optimal range, thus requiring less run time (10 min) for its analysis in the plasma sample. The system suitability results disclose the suitability of the developed HPLC system for quantitative analysis of PIP in rat plasma.

Table 6. 11 System suitability study of developed HPLC method for analysis of PIP (12 μg/mL) in rat plasma (n = 6)

Parameters	**Average Value ± SD**	**RSD (%)**
Peak area ratio (mAU)	1.048 ± 0.002	0.196
Retention time (Rt)	7.041 ± 0.022	0.323
Number of theoretical plates	3179.667 ± 18.292	0.576
Peak purity	0.992 ± 0.007	0.707
Tailing factor (Asymmetry)	0.969 ± 0.004	0.515
Capacity factor (k^1)	1.413 ± 0.001	0.073

6.4.7.1.10 Stability test

The stability study results demonstrated no significant difference ($p<0.05$) in the concentration of the analyte (PIP) between the initial value and the value at the end of each stability study (Table 6. 12) at high, medium, and low concentrations. The % RE of PIP in rat plasma between the initial concentrations and the concentrations after three freeze-thaw cycles or long-term stability was less than the acceptance criteria (% RE< ± 15.0%) as per FDA guidelines [99]. The stability results reflected the chemical stability of the analyte in the plasma matrix.

Table 6. 12 Stability study reports of analyzed QC samples (n = 3)

PIP spiked concentration or actual value (µg/mL)	Concentration (µg/mL)			RE (%)	
	Initial (fresh) (Mean ± SD)	After 3 freeze-thaw cycle (Mean ± SD)	After 30 days in -20° C (Mean ± SD)	RE (%) between initial and freeze-thaw stability	RE (%) between initial and long-term stability
0.1	0.11 ± 0.0006	0.112 ± 0.003	0.106 ± 0.002	2.343	-3.255
1.6	1.624 ± 0.001	1.603 ± 0.008	1.49 ± 0.122	-1.273	-9.011
25.6	25.593 ± 0.366	25.668 ± 0.394	25.121 ± 0.49	0.292	-1.879

6.4.7.2 Bioavailability study

The quantitative estimation of PIP in plasma following the oral administration of PLFEE, PM, and SD was done using the validated HPLC method. Mean plasma concentration-time profiles of PIP after oral administration of PLFEE, PM, and optimized SD are presented in Figure 6. 28, and the pharmacokinetic (PK) parameters are summarized in Table 6. 13. Compared to the PLFEE, the plasma concentration of PIP was found to be increased following oral administration of SD and PM. One-way ANOVA followed by post hoc Tukey test was applied to validate significant differences between the mean C_{max} and AUC_{0-t} obtained for PLFEE, PM, and SD. Differences were considered significant at $p<0.05$. A significant improvement of C_{max} was obtained for SD (3.278 ± 0.301 µg/mL, $p <0.01$) and PM (2.013 ± 0.069 µg/mL, $p<0.05$) compared to PLFEE (1.482 ± 0.235 µg/mL). The C_{max} values of SD and PM are found to be approximately 2.211 and 1.358-fold higher than that of the PLFEE, respectively. The area under the curve from time 0 to 24 h (AUC_{0-t}) of SD (27.001 ± 2.875 µg/mL*h) was found to be significantly higher ($p<0.01$) than that of PLFEE (14.304 ± 1.365 µg/mL*h). The PM also showed a significant improvement ($p<0.05$)

of AUC_{0-t} (19.286 ± 2.438 µg/mL*h) compared to PLFEE. The time to reach peak plasma concentration (T_{max}) of PLFEE, PM, and SD was found to be 4 h. The MRT_{0-t} of PLFEE and PM were found to be 6.770 ± 0.116 h and 6.483 ± 0.126 h, respectively. The MRT_{0-t} of SD (6.377 ± 0.134 h) was found to be decreased compared to PLFEE, and PM, demonstrating rapid elimination of SD. The relative bioavailability (F_{rel}) of SD and PM were found to be 188.765% and 134.829%, respectively, compared to the PLFEE and are approximately 1.888-fold and 1.348-fold higher than that of neat PLFEE. Dissolution is the rate-limiting step in the oral bioavailability of poorly soluble phytoconstituents, so a small elevation of dissolution rate can enhance oral bioavailability. The findings of the bioavailability study aligned with the results of the *in-vitro* dissolution study, demonstrating that SD provided a noticeable enhancement of dissolution rate compared with crystalline PLFEE and PM. The PM is a simple physical mixture in which the PLFEE still exists in its crystalline form. However, due to the presence of hydrophilic CMs in PM, the dissolution and the bioavailability were found to be slightly improved. Moreover, the PK parameters and plasma drug-time profile clearly showed a significant increase in C_{max}, AUC_{0-t}, and F_{rel} of the PIP by the prepared SD. The improved oral bioavailability of SD might be accounted to the following factors: (i) enhanced solubility and dissolution due to amorphous conversion, highly porous structure, increased wetting, and micellar solubilization; (ii) maintenance of supersaturation and prevention of nuclear growth/ precipitation by the CMs (surfactant and polymer); and (iii) improved permeability owing to the amphiphilic behavior of CMs.

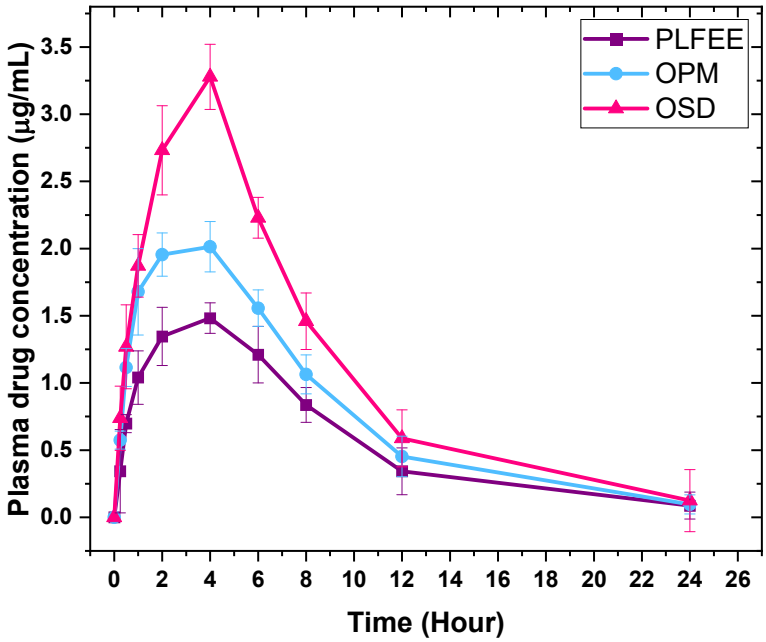

Figure 6. 28 Plasma drug concentration-time profile after oral administration of PLFEE, PM, and SD each equivalent to 62.83 mg/kg of PIP in female SD rats (n = 5, Mean ± SD)

Table 6. 13 Pharmacokinetic (PK) parameters of PIP following single oral administration of PLFEE, PM, and optimized SD (n = 5, Mean ± SD)

PK parameters	Unit	PLFEE	PM	Optimized SD
C_{max}	µg/mL	1.482 ± 0.235	2.013 ± 0.069*	3.278 ± 0.301**
T_{max}	h	4	4	4
AUC $_{0-t}$	µg/mL*h	14.304 ± 1.365	19.286 ± 2.438*	27.001 ± 2.875**
AUC $_{0-\infty}$	µg/mL*h	14.906 ± 2.73	19.912 ± 2.072	27.765 ± 1.946
$t_{1/2}$	h	4.788 ± 0.363	4.506 ± 0.334	4.259 ± 0.517
K_{el}	1/h	0.144 ± 0.005	0.153 ± 0.004	0.162 ± 0.002
MRT $_{0-t}$	h	6.770 ± 0.116	6.483 ± 0.126	6.377 ± 0.134
MRT $_{0-\infty}$	h	7.745 ± 0.29	7.239 ± 0.367	7.031 ± 0.6
Vz/F	(mg/kg)/(µg/mL)	29.116 ± 1.687	20.512 ± 2.816	13.905 ± 0.528
CL/F	(mg/kg)/(µg/mL)/h	4.214 ± 0.097	3.155 ± 0.123	2.262 ± 0.156
F_{rel}	%	-	134.829	188.765

C_{max}: peak plasma concentration, T_{max}: time to reach peak plasma concentration, AUC_{0-t}: area under the plasma drug concentration-time curve from time 0-24 h, $AUC_{0-\infty}$: area under the plasma drug concentration-time curve from time 0 to infinity h, $t_{1/2}$: elimination half-life, K_{el}: elimination rate constant, MRT_{0-t}: mean residence time from time 0-24 h, $MRT_{0-\infty}$: mean residence time from time 0 to infinity h, V_z/F: apparent volume of distribution, CL/F: apparent systemic clearance following an extravascular (e.v.) administration, and F_{rel}: relative bioavailability; *$p<0.05$ and **$p<0.01$ when compared with rats administered with PLFEE

6.4.8 Acute oral toxicity study

The study was performed as per OECD 425 guidelines, and the toxicity was reported based on survival or death, decrease in body weight, behavioral alterations, biochemical parameters, hematological parameters, and histopathology. At all doses of standardized PLFEE, rapid movement and disagreeable behavior of animals were observed, which is due to its pungent principle. At the dose of 2000 mg/kg, tremors after 2 h and mortality within 24-48 h were observed. In contrast, no tremors or mortality was found at the dose of 550 mg/kg and lower doses at 48 h. The surviving mice (administered with 550 mg/kg) were further observed for 14 days. No death of animals was observed in the case of the 550 mg/kg group after 14 days. A statistically insignificant difference ($p<0.05$) was noticed between the body weight of the PLFEE (550 mg/kg) treated C57BL/6 group (21.786 ± 1.423 g) and the vehicle control C57BL/6 group (21.273 ± 1.123 g) on the 15^{th} day. The initial body weight was found to be slightly increased in both cases, which is due to the normal physiological growth of the body. The biochemical (Table 6. 14) and hematological parameters (Table 6. 15) of the PLFEE (550 mg/kg) treated C57BL/6 group and vehicle control C57BL/6 group, studied after 14 days, reflected a non-significant difference ($p<0.05$).

All the histological interpretations are based on the photomicrographs and observations from six replicate sections of each specimen. Figure 6. 29 represents the comparative histopathology of various vital organs of vehicle-treated and 550 mg/kg standardized PLFEE-treated C57BL/6 mice. The histology of vehicle-treated mice and PLFEE-treated mice showed branching myocytes (BM) of the heart, glomerulus (G) of the kidney, central vein (CV) of the liver; bronchioles (B) of the lungs, red pulp (RP) and white pulp (WP) of the spleen. The result is similar to the reported histopathological observations on mice [153]. The photomicrographs of vital organs

showed no sign of abnormality or significant variances in histology between the two groups, representing the nontoxic nature of standardized PLFEE at the dose of 550 mg/kg and suggesting possible pre-clinical applications.

The overall results revealed no sign of toxicity in the C57BL/6 animals after the administration of 550 mg/kg of standardized PLFEE. The calculated LD_{50} value (provided by the AOT425statpgm software) of PLFEE against C57BL/6 mice was 1098 mg/kg at a 95% level of confidence.

Table 6. 14 Biochemical parameters of vehicle control C57BL/6 group and PLFEE (550 mg/kg) treated C57BL/6 group.

Serum biochemical parameters	**Vehicle control C57BL/6 group**	**PLFEE (550 mg/kg) treated C57BL/6 group**
Urea (mg/mL)	43.66 ± 3.456	42.86 ± 4.578
Creatinine (mg/dL)	0.23 ± 0.02	0.35 ± 0.01
ALP (U/L)	45.88 ± 2.154	41.18 ± 3.216
SGOT (U/L)	140.9 ± 0.231	138.6 ± 0.324
SGPT (U/L)	33.95 ± 4.217	36.25 ± 3.218
Total Cholesterol (mg/dL)	93.97 ± 2.746	91.95 ± 3.147
Triglyceride (mg/dL)	108.4 ± 3.473	103.87 ± 4.126
Total protein (g/dL)	7.147 ± 0.289	6.9675 ± 0.345
Glucose (mg/dL)	215 ± 11.246	223 ± 7.243

ALP: alkaline phosphatase, SGOT: serum glutamic-oxaloacetic transaminase, SGPT: serum glutamic pyruvic transaminase Data are represented as Mean ± SD. Students t-test was performed at $P<0.05$ using GraphPad Prism 5 (GraphPad Software, Inc., San Diego, California).

Table 6. 15 Hematological parameters of vehicle control C57BL/6 group and PLFEE (550 mg/kg) treated C57BL/6 group

Hematological parameters	**Vehicle control C57BL/6 group**	**PLFEE (550 mg/kg) treated C57BL/6 group**
Hemoglobin (gm/dL)	12.9 ± 2.873	13.2 ± 3.146
TLC/ WBC (*10^3/μL)	3.7 ± 0.623	4.4 ± 0.437
Neutrophils (%)	37 ± 3.423	34 ± 2.474
Lymphocytes (%)	54 ± 7.543	58 ± 5.758
Eosinophils (%)	2 ± 0.816	3 ± 0.671
Monocytes (%)	7 ± 1.247	5 ± 2.546
Basophils (%)	0	0
TRBCs (×10^6/ μL)	9.78 ± 0.316	9.36 ± 0.243
PCV (%) or HCT (%)	39.8 ± 5.126	42.2 ± 6.498
MCV (fL)	46.0 ± 4.983	45.1 ± 5.457
MCH (pg)	11.2 ± 4.457	14.6 ± 3.471
MCHC (g/dL)	33.3 ± 5.124	32.4 ± 7.778
RDW (%)	16.8 ± 2.146	14.245 ± 3.694
Platelet (×10^5/ μL)	5.55 ± 0.249	5.16 ± 0.312

TLC: total leucocyte count, WBC: white blood cells, TRBCs: total red blood cell counts, PCV: packed cell volume or HCT: hematocrit test, MCV: mean corpuscular volume, MCH: mean corpuscular haemoglobin, MCHC: mean corpuscular haemoglobin concentration, RDW: red cell distribution width; Data are represented as Mean ± SD. Students t-test was performed at $p<0.05$ using GraphPad Prism 5 (GraphPad Software, Inc., San Diego, California).

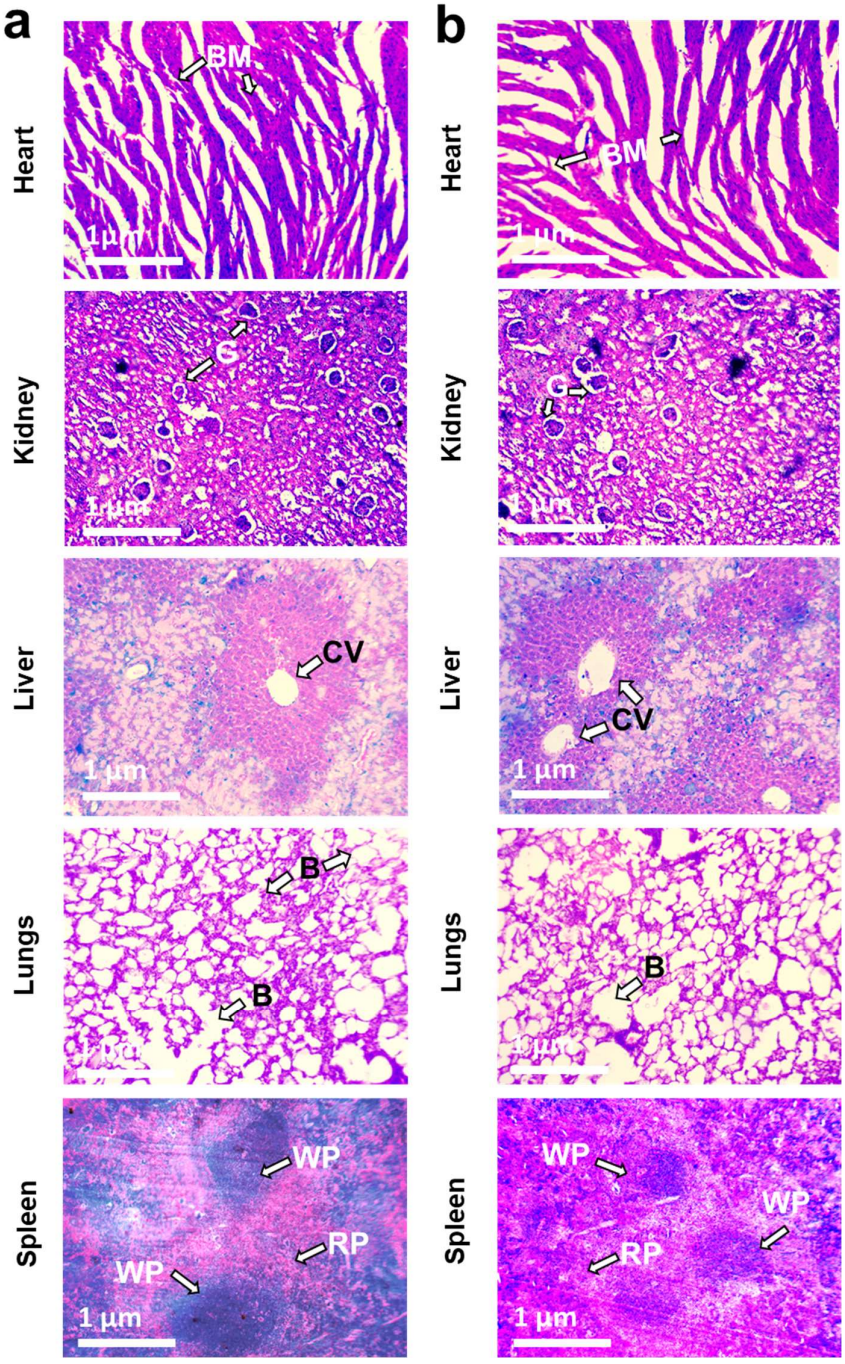

Figure 6. 29 Histopathology study of heart, kidney, liver, lungs, and spleen of (a) vehicle control C57BL/6 group and (b) PLFEE (550 mg/kg) treated C57BL/6 group at 10X magnification for acute oral toxicity assessment. BM: branching myocytes; G: glomerulus; CV: central vein; B: bronchioles: RP: red pulp; and WP: white pulp. The histopathological observations were obtained from the vital organs of the vehicle control C57BL/6 group and PLFEE (550 mg/kg) treated C57BL/6 group, each comprising 4 animals/group. The histological photomicrographs and descriptions are based on the histology of six replicate organ sections of each organ.

6.4.9 *In-vivo* anticancer activity against melanoma

After investigation and confirmation of improved solubility, *in-vitro* dissolution profile, *in-vivo* oral bioavailability, and *in-vitro* cytotoxicity against melanoma (B16F10) cell line of PLFEE, the *in-vivo* anticancer activity of optimized SDs were evaluated and compared with standardized PLFEE.

The *in-vivo* syngeneic experimental tumor model was established by subcutaneous implantation of highly metastatic B16F10 murine cancer cells to the C57BL/6 mice. This model allows the interaction of melanoma cells with T-cells and B-cells, thus possessing an advantage over the xenografts model in which immunosuppressed mice were used [47]. The treatments were started 8 days after the tumor induction and continued up to the 30^{th} day. The body weight and tumor volume were evaluated throughout the treatment period.

In most of the previous studies [154, 155], tumor regression studies were performed for up to 30 days. Further, we have also noticed slight rupture and oozing of fluid at the surface of solid tumor after 35 days in our pilot studies, which may give incorrect regression data. Considering the above factors, we have decided to conduct our main study for 30 days.

The dose of the standardized PLFEE (200 mg/kg b.wt.) was selected based on our pilot studies on tumor regression studies, where we have obtained statistically significant tumor regression outcomes. The dose of DTIC (5 mg/kg i.p. every 2 days) was selected based on the reported literature [103].

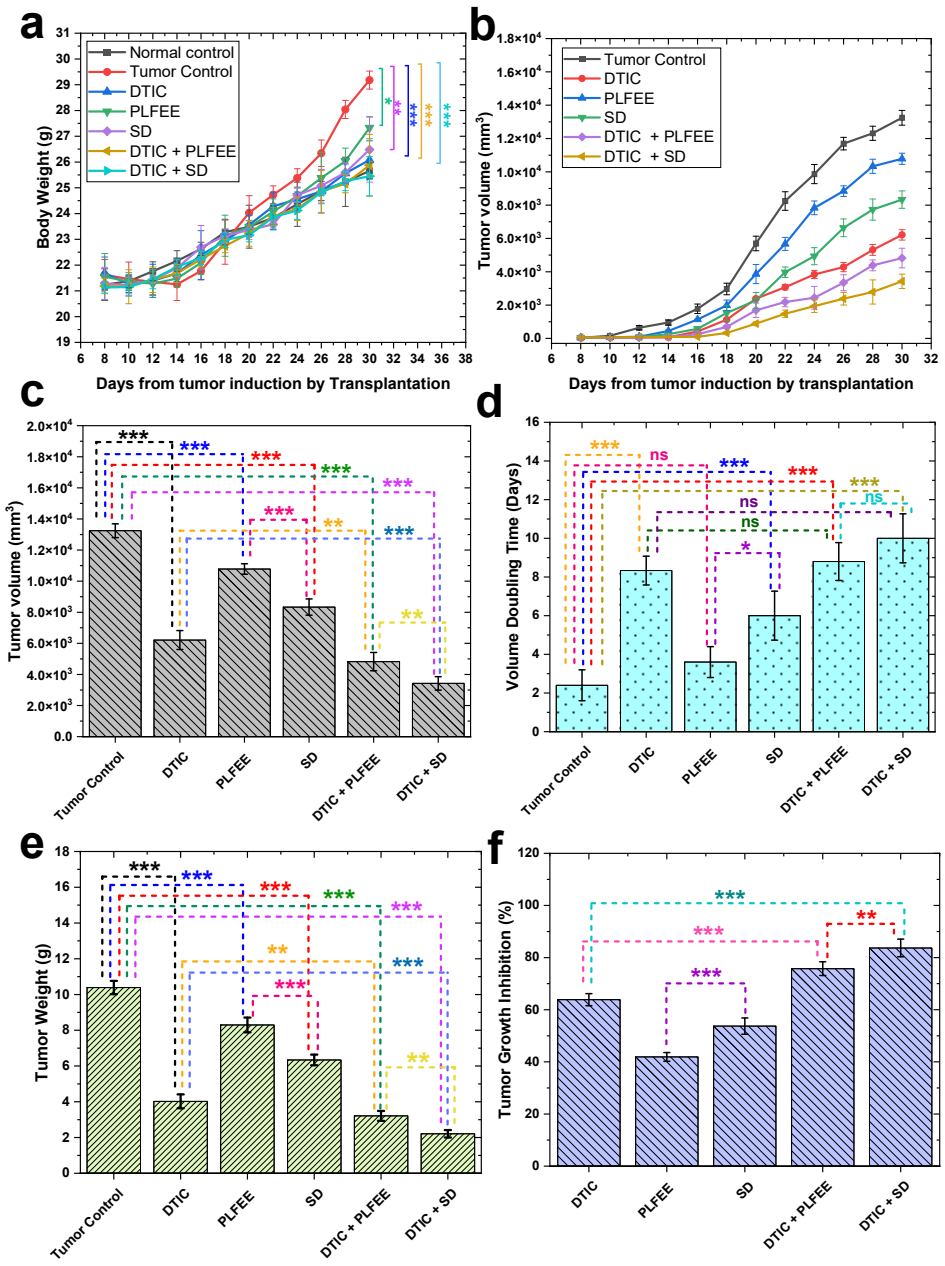

Figure 6. 30 Tumor regression analysis (a) changes in body weight, (b) tumor volume at an interval of two days after developed palpable tumor, (c) tumor volume at the end of dosing (30th day), (d) tumor volume doubling time (VDT) of various group, (e) tumor weight at 30th day, (f) percent tumor growth inhibition (% TGI) of various groups at 30th day. The asterisk marks (*) represent the level of significance at $p<0.05$ in all cases. The statistical analysis for the oral bioavailability and tumor regression analysis was performed using one-way ANOVA followed by Tukey's multiple comparison test at $p<0.05$ using GraphPad Prism 5 (GraphPad Software, Inc., San Diego, California).

The changes in the body weight during the study were recorded to monitor the *in-vivo* tumor growth. The normal control group showed a gradual increase in body weight up to the 30th day. The tumor control group showed an initial loss of body weight followed by faster weight gain than the treated groups and normal control group due to uncontrolled tumor growth (Figure 6. 30a). The body weight of all treated groups was found to be significantly lower ($p<0.05$) than that of the "tumor control group" due to the treatment effects.

The results of tumor volume of C57BL/6 mice of various groups (untreated and treated) during the treatment period and at the end of the study were shown in Figure 6. 30b and Figure 6. 30c, respectively. The "tumor control group" represented a higher overall TV than the treated groups Figure 6. 30b. The calculated TV was in the order of "tumor control group" > "PLFEE group" > "SD group" > "DTIC group" > "DTIC + PLFEE" > "DTIC + SD" group (Figure 6. 30c). A significant decrease ($p<0.05$) in the tumor volume was noticed in the treated group compared to the tumor control group (vehicle-treated) on the 30th day of tumor induction. The standardized PLFEE alone significantly reduced ($p<0.05$) the TV compared to the tumor control group. Further, the optimized SD significantly decreased ($p<0.05$) the TV compared to the tumor control group and test PLFEE group. The marked reduction of TV in the case of optimized SD was due to the improved absorption and greater bioavailability of the hydrophobic phytoconstituents compared to the neat PLFEE. In the case of the standard drug group, the DTIC exhibited a significant reduction ($p<0.05$) of the tumor volume compared to the tumor control group. When the standardized PLFEE was used as an adjuvant to the DTIC, a significant reduction ($p<0.05$) of the TV was noticed compared to the DTIC alone and tumor control group on the 30th day. Further, in the case of the "DTIC + SD" treated group, a remarked decrease and significant reduction

($p<0.05$) of TV were found compared to the "DTIC + PLFEE" group, ascribed to the improved bioavailability of phytoconstituents when administered in the form of SD.

The VDT (in days) of various treatment groups was found to be increased compared to the "tumor control" group due to the treatment effects (Figure 6. 30d). The "PLFEE group" showed a non-significant difference in the VDT compared to the "tumor control" group. The VDT value in the case of the optimized "SD group" was found to be significantly higher ($p<0.05$) than that of the PLFEE-treated and tumor-control group. The "DTIC group" demonstrated a significant improvement in the VDT ($p<0.05$) compared to the "tumor control." A significant prolongation of the VDT ($p<0.05$) was noticed in the case of "DTIC + PLFEE group" compared to the "tumor control group". However, at a 95% level of significance, a non-significant difference in the VDT was noticed between the "DTIC + PLFEE" group and the DTIC group. The "DTIC + SD group" demonstrated a significant lengthening of the VDT ($p<0.05$) compared to the "tumor control group," but a non-significant difference in the VDT was observed between "DTIC + SD group" and "DTIC + PLFEE" group. At a 95 % level of significance, all the treatment groups showed prolongation of VDT compared to the "tumor control" group. However, some non-significant differences in the VDT among various treatment groups are due to the uncontrolled rapid cell proliferation at the beginning of the tumor progression. During the study, it was observed that most of the tumors attained double their initial volume within 8±1 days. So, among some of the treatments, a statistical significance difference was not established.

The results of isolated tumor weight at the end of the study were represented in Figure 6. 30e. The tumor control group showed the highest tumor weight. In contrast, all the treatment groups showed a significantly lower ($p<0.05$) tumor weight. The tumor

weight in the case of the standardized "PLFEE group" was found to be significantly reduced ($p<0.05$) compared to the "tumor control group." Further, the optimized SD significantly decreased ($p<0.05$) the tumor weight compared to the standardized "PLFEE group" and "tumor control group" due to its improved absorption and greater bioavailability compared to the neat PLFEE. In the case of the DTIC-treated group, a significant loss ($p<0.05$) of the tumor weight was noticed compared to the "tumor control group." The "DTIC + PLFEE group" further decreased the tumor weight compared to the DTIC alone and "tumor control group" on the 30^{th} day. Further, in the case of the "DTIC + SD" treated group, a significant loss of tumor weight ($p<0.05$) was observed compared to the "DTIC + PLFEE" group and "tumor control group." Hence, the optimized SD can be used as an effective adjuvant therapy with DTIC than standardized PLFEE.

The % TGI was found to be significantly increased ($p<0.05$) in the case of treated groups compared to the tumor control group (Figure 6. 30f). Except for PLFEE (% TGI = 41.89774 ± 1.684%), all the treatment groups showed a TGI of more than 50%. A % TGI of >50% was considered to be meaningful [104]. The SD-treated group showed a significant improvement ($p<0.05$) of % TGI compared to the PLFEE-treated group. The "DTIC + PLFEE" group demonstrated a significant improvement of % TGI compared to the standard drug (DTIC) alone, representing the efficiency of adjuvant therapy. Further, the "DTIC + SD" group showed a significant enhancement of % TGI compared to the "DTIC + PLFEE" group, representing the higher efficacy of adjuvant therapy when the PLFEE is administered as an SD form. The photograph of representative tumors from each group on the 30^{th} day is shown in Figure 6. 31a.

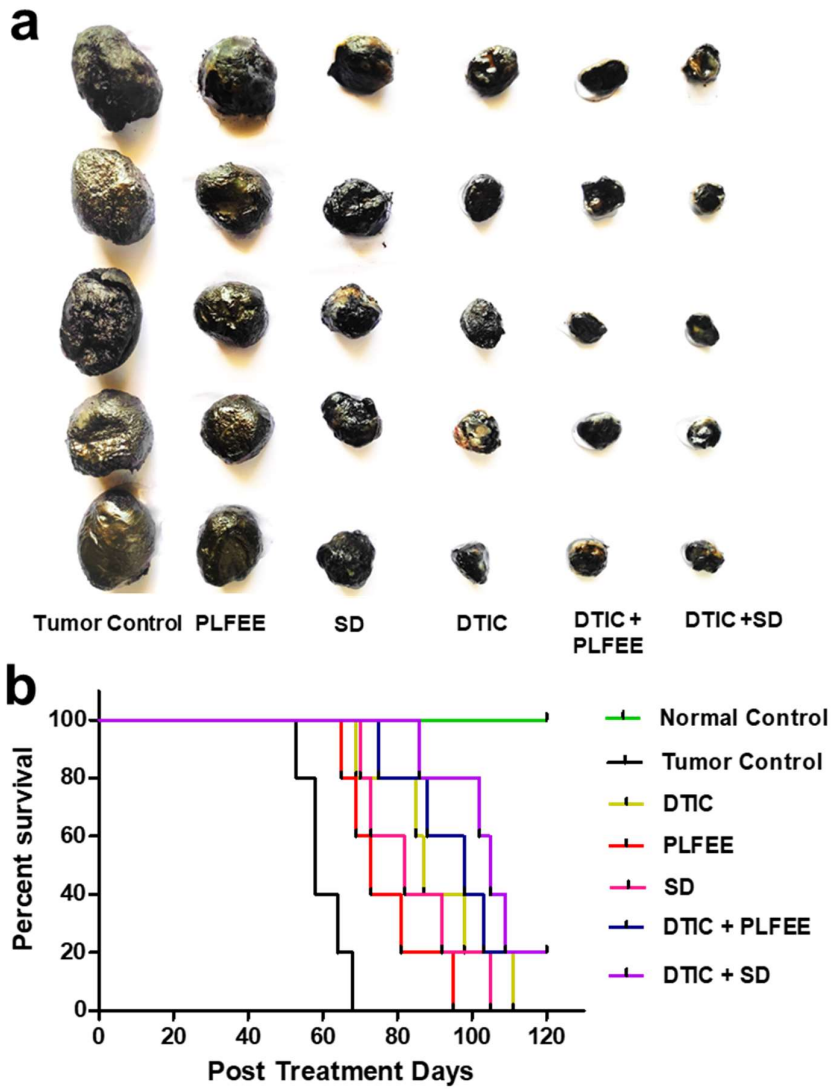

Figure 6. 31 Tumor photograph and survival plot (a) photograph of representative tumors from each group on the 30th day and (b) Kaplan-Meier survival plot.

The life span of treated groups was found to increase compared to the "tumor control" group. The results of the percent survivorship of various groups were graphically represented as a Kaplan-Meier survival plot (Figure 6. 31b). The % ILS were DTIC: 49.501%, PLFEE: 27.242%, SD: 40.211%, DTIC + PLFEE: 60.797%, and DTIC + SD: 68.438%. An increase in the life span by 25% or more over that of tumor control was regarded as effective antitumor activity [104]. The % ILS in the case of SD was found to be higher than that of the "PLFEE group". The PLFEE with the DTIC showed

an improvement of % ILS compared to the DTIC alone. Further, an increase in the % ILS has been noticed in the "DTIC + SD" group compared to the "DTIC + PLFEE" group. Overall, the *in-vivo* study revealed the stronger antitumor activity of SD compared to standardized PLFEE. The improved efficacy of the standard anticancer drug (DTIC) was noticed during the use of PLFEE as adjuvant therapy. A further enhancement of DTIC activity was observed during the use of SD as adjuvant therapy instead of PLFEE.

6.4.9.1 Histopathology of tumor

The histopathological results of skin, skin over the tumor, and tumor tissues from C57BL/6 mice of various groups were represented in Figure 6. 32. The histology of healthy skin (Figure 6. 32a) showed distinct layers of epidermis, dermis, and hypodermis, representing the normal architecture. In contrast, the histology of skin over melanoma (Figure 6. 32b) showed ruptured architecture with the presence of live tumor cells. The tumor control group showed a higher population of live tumor cells (LTC) (Figure 6. 32c). In contrast, all the treatment groups significantly reduced LTC population (Figure 6. 32d-h). The group administered with standardized PLFEE showed few necrotic regions (NR) with a reduction of LTC. The SD-treated group showed a marked reduction of LTC with a relatively higher population of NR. The DTIC alone showed a pronounced decrease in the LTC population as an antineoplastic drug. Further, a marked reduction of the LTC was observed in the case of the "DTIC + PLFEE" group with a relatively higher NR. The "DTIC + SD" group showed a very low population of LTC and more NR compared to the "DTIC + PLFEE" group. The overall result reflected the higher antitumor activity of SD compared to the neat PLFEE. Further, SD as an adjuvant medication will enhance the activity of DTIC for melanoma therapy.

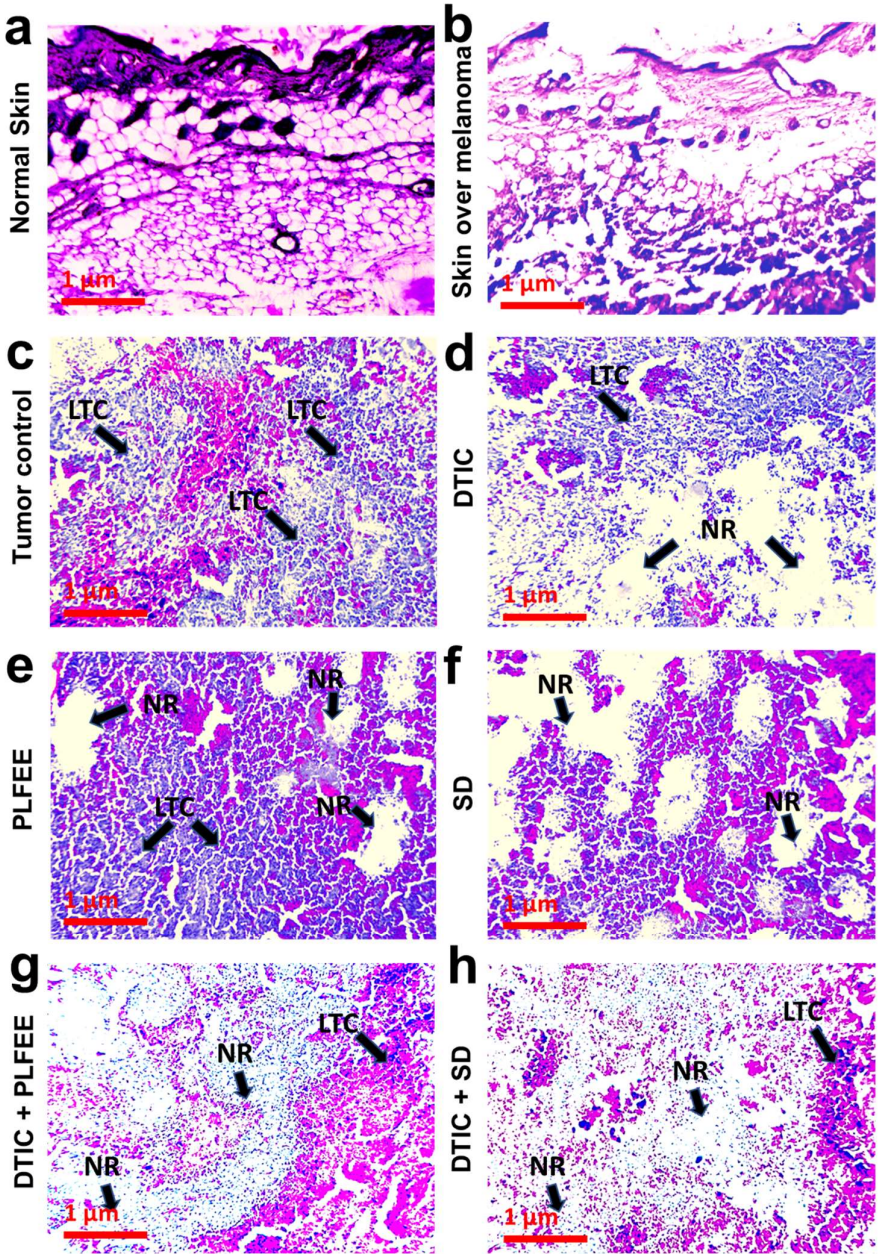

Figure 6. 32 Histopathology study of skin and melanoma tumor: histology of (a) normal skin, (b) skin over melanoma tumor, (c) tumor control, (d) tumor of DTIC treated, (e) tumor of PLFEE treated, (f) tumor of SD treated, (g) tumor of DTIC + PLFEE treated, and (h) tumor of DTIC + SD treated group. NR: necrotic region; LTC: live tumor cell. The histopathological observations were obtained from the skin and tumors of each animal from seven different groups (5 animals/group). All the histological interpretations are based on the photomicrographs and observations from six replicate sections of each specimen.

Numerous plant extracts and phytoconstituents have been reported for melanoma therapy for their ability to suppress melanoma through the regulation of oxidative status, modulation of immunity, correction of disordered replication and induction of apoptosis, and prevention of invasion, angiogenesis, and metastasis [2, 10]. Cancer cells utilize multiple mechanisms for their development, progression, invasion, angiogenesis, and metastasis. Hence, it is rational to use plant extract or fraction (containing numerous phytoconstituents) that may act synergistically in a multi-targeting manner rather than a single constituent or drug molecule.

The extract of *Piper longum* fruit and its constituents have shown their anticancer activity against melanoma. The PIP was reported to inhibit transcription factors, such as CREB, AP-1, NF- kβ, and proinflammatory cytokines expression (IL-6, IL-1β, GM-CSF, and TNF-α) in B16F10 (melanoma) cells [12]. It was also reported to cause G1 phase arrest and apoptosis induction in B16F0 and SK MEL 28 melanoma cells through activation of checkpoint kinase-1 (Chk1). Mainly, the generation of ROS by PIP in melanoma cells is involved in inducing G1 cell cycle arrest through the activation of Chk1 [13]. Further, the PIP was also studied for inhibition of lung metastasis in the B16F10 cell-induced tumor model in C57BL/6 mice [14]. The compound piperlongumine was reported to produce cytotoxicity against A375, A875, and B16F10 and induce apoptosis via reactive oxygen species-mediated disruption of mitochondria [15]. The PLGN was also reported to suppress melanogenesis via the downregulation of tyrosinase expression in the melanin synthesis pathway [16], and inhibition of melanogenesis seems a rational adjuvant approach for the treatment of metastatic melanoma [17]. The 70% ethanolic extract of *Piper longum* fruit also demonstrated *in-vitro* and *in-vivo* antiangiogenic activities via inhibition of VEGF, tumor-directed capillary formation, and inhibition of proinflammatory cytokines [18].

The investigated standardized PLFEE demonstrated *in-vitro* cytotoxicity against B16F10 cells without affecting normal HEK 293 cell line (Fig.8). The standardized PLFEE alone showed significant ($p<0.05$) *in-vivo* anticancer activity with tumor regression outcomes compared to the vehicle-treated tumor control group on the 30th day of tumor induction. The therapeutic activity of standardized PLFEE (dose of 200 mg/kg) is attributed to the aforementioned reported anticancer mechanisms [12-16, 18]. The administered oral dose of 200 mg/kg of PLFEE was fixed as per the pilot studies. The optimized SD showed improved *in-vivo* tumor regression results compared to unformulated standardized PLFEE. The significantly higher ($p<0.05$) *in-vivo* anticancer activity of SD is ascribed to its improved dissolution, oral absorption, and bioavailability. Further, the micelles generated from SD may be passively targeted to the tumor microenvironment by the enhanced permeation and retention (EPR) effect, resulting in improved anticancer activity.

The standard anticancer drug, DTIC, exhibited a significant ($p<0.05$) tumor regression outcome compared to the tumor control group, standardized PLFEE, and SD group. DTIC is the only Food and Drug Administration (FDA) approved first-line chemotherapeutic drug for melanoma therapy, which is a strong alkylating agent. Its anticancer activity is ascribed to the destruction of cancer cells by adding an alkyl group to their DNA [156]. When the standardized PLFEE was used as an adjuvant to the DTIC, significant ($p<0.05$) tumor regression outcomes were observed compared to the DTIC alone and tumor control group on the 30th day. The synergistic anticancer activity of DTIC with the PLFEE is ascribed to the additive inherent anticancer activity of the contained phytoconstituents in PLFEE and the alkylating property of DTIC. The major bioactive phytoconstituent, PIP, was reported to act as an herbal bioenhancer that increases the bioavailability of drugs by promoting (i) rapid absorption of drugs

or (ii) by inhibiting the enzymatic drug metabolism. It is also a potent inhibitor of the P-glycoprotein (P-gp) efflux pump and principal metabolizing enzyme CYP3A4 [157]. ATP-binding cassette (ABC) transporters (mainly the P-gp) are expressed at membranes of cancer cells that induce multidrug resistance. Relatively minor improvements in drug resistance are sufficient to render treatment ineffective in cancer cells. The use of P-gp inhibitors with chemotherapeutic drugs has been previously verified to overcome multidrug resistance [157, 158]. Many of the phytochemicals, including PIP, quercetin, naringin, genistein, sinomenine, curcumin, allicin, capsaicin, and glycyrrhizin have been reported to act as herbal bioenhancers [157, 159]. The DTIC was reported to be effluxed by the P-gp pump [160]; thus, its inhibition by the PIP contained in the standardized PLFEE might be responsible for synergistic anticancer activity. DTIC is a prodrug, which catalytic activation by liver cytochromes P450 enzymes (mainly by CYP1A1, CYP1A2, and CYP2E1) is required for anticancer activity [161]. However, PIP is reported to possess an inhibitory effect on the principal metabolizing enzyme CYP3A4 [157]. Thus, the metabolic inhibition by the PIP may not contribute to improved anticancer activity. Hence, the improved anticancer activity of DTIC when administered with PLFEE might be attributed to the inherent anticancer activity of the standardized PLFEE and the P-gp efflux inhibition. Further, in the case of the "DTIC + SD" treated group, a significant ($p<0.05$) anticancer activity was found compared to the "DTIC + PLFEE" group, ascribed to the improved bioavailability of phytoconstituents when administered in the form of SD.

6.5 Conclusions

Due to the limited aqueous solubility of the phytoconstituents in the PLFEE, the 4th generation solid dispersion was developed with the use of Soluplus® and Tween® 80. The solvent evaporation by rotary vacuum evaporation was utilized for the development of solid dispersion and optimized by the QbD approach. The RSM was used to analyze the influence of various factors on saturation solubility as a response. The numerical and graphical optimization was carried out, and the outcomes of the software-suggested formula were validated by formulating and analyzing the response. The SD showed amorphous properties with good drug content, content uniformity, wettability, and low moisture content. The ATR-FTIR and HPTLC results revealed the absence of any incompatibility among the extract and the excipients of the SD. The HR-SEM revealed the homogeneous irregular morphology of SD. The *in-vitro* dissolution study revealed the improved dissolution profile of SD compared to the physical mixture (PM) and PLFEE. The DLS and HRTEM results of the dissolution sample revealed the formation of micelle during the dissolution, resulting in micellar solubilization and improved dissolution. The stability study revealed the prolonged maintenance of physicochemical and pharmaceutical properties without any alterations. The *in-vivo* oral bioavailability result of SD reflected a significant ($p<0.05$) improvement of bioavailability (C_{max} and AUC) compared to neat extract and PM. The acute oral toxicity study (OECD 425) via hematological, biochemical, and histopathological observations revealed the nontoxic nature of the standardized PLFEE at the chosen dose. The effect of SD was studied in the syngeneic transplantation model in melanoma (B16F10) bearing C57BL/6 mice. The results of the tumor regression study revealed improved therapeutic activity of SD compared to neat PLFEE. Further, the SD also improved the anticancer activity of DTIC as an

adjuvant therapy. The overall result revealed the potential of developed PLFEE contained SD for melanoma cancer therapy either alone or as an adjuvant therapy with DTIC.

6.6 Summary points

- *P. longum* extract has shown its treatment potential against melanoma.
- Due to the limited aqueous solubility of the phytoconstituents in the PLFEE, the 4th generation solid dispersion was developed with the use of Soluplus® and Tween® 80 via solvent evaporation method utilizing Quality-by-Design (QbD) approach.
- Central Composite Design (CCD)-based response surface methodology was used in order to analyze the influence of various factors on saturation solubility as a response.
- The numerical and graphical optimization was carried out by Design-Expert® software, and the outcomes of the software-suggested formula were validated by formulating and analyzing the response.
- The optimized SD showed amorphous properties with good drug content, content uniformity, wettability, and low moisture content.
- The ATR-FTIR and HPTLC results revealed the absence of any incompatibility among the extract and the excipients of the SD.
- The HR-SEM revealed the homogeneous irregular morphology of SD.
- The *in-vitro* dissolution study revealed the improved dissolution profile of SD compared to the physical mixture (PM) and PLFEE.
- The DLS and HRTEM results of the dissolution sample revealed the formation of micelle during the dissolution, resulting in micellar solubilization and improved dissolution.
- The accelerated stability study revealed the prolonged maintenance of physicochemical and pharmaceutical properties without any alterations.
- The optimized SD showed improved dose-dependent cytotoxicity against B16F10 cells compared to PLFEE suspension & PLFEE solution and showed no cytotoxicity towards the noncancerous healthy

HEK 293 cell line, reflecting selective cytotoxicity to the cancerous cell.

- The optimized SD significantly ($p<0.05$) inhibited the motility of B16F10 cells compared to the control and standardized PLFEE group at 12 and 24 h.
- The *in-vivo* oral bioavailability result of SD reflected a significant ($p<0.05$) improvement of bioavailability (C_{max} and AUC) compared to neat extract and PM.
- The acute oral toxicity study (OECD 425) via hematological, biochemical, and histopathological observations revealed the nontoxic nature of the standardized PLFEE at the chosen dose.
- The results of the tumor regression study in the syngeneic transplantation melanoma model (in C57BL/6 female mice) revealed improved therapeutic activity of SD compared to neat PLFEE.
- Further, the SD also improved the anticancer activity of DTIC as an adjuvant therapy.
- The overall result revealed the potential of developed PLFEE contained SD for melanoma cancer therapy either alone or as an adjuvant therapy with DTIC.